

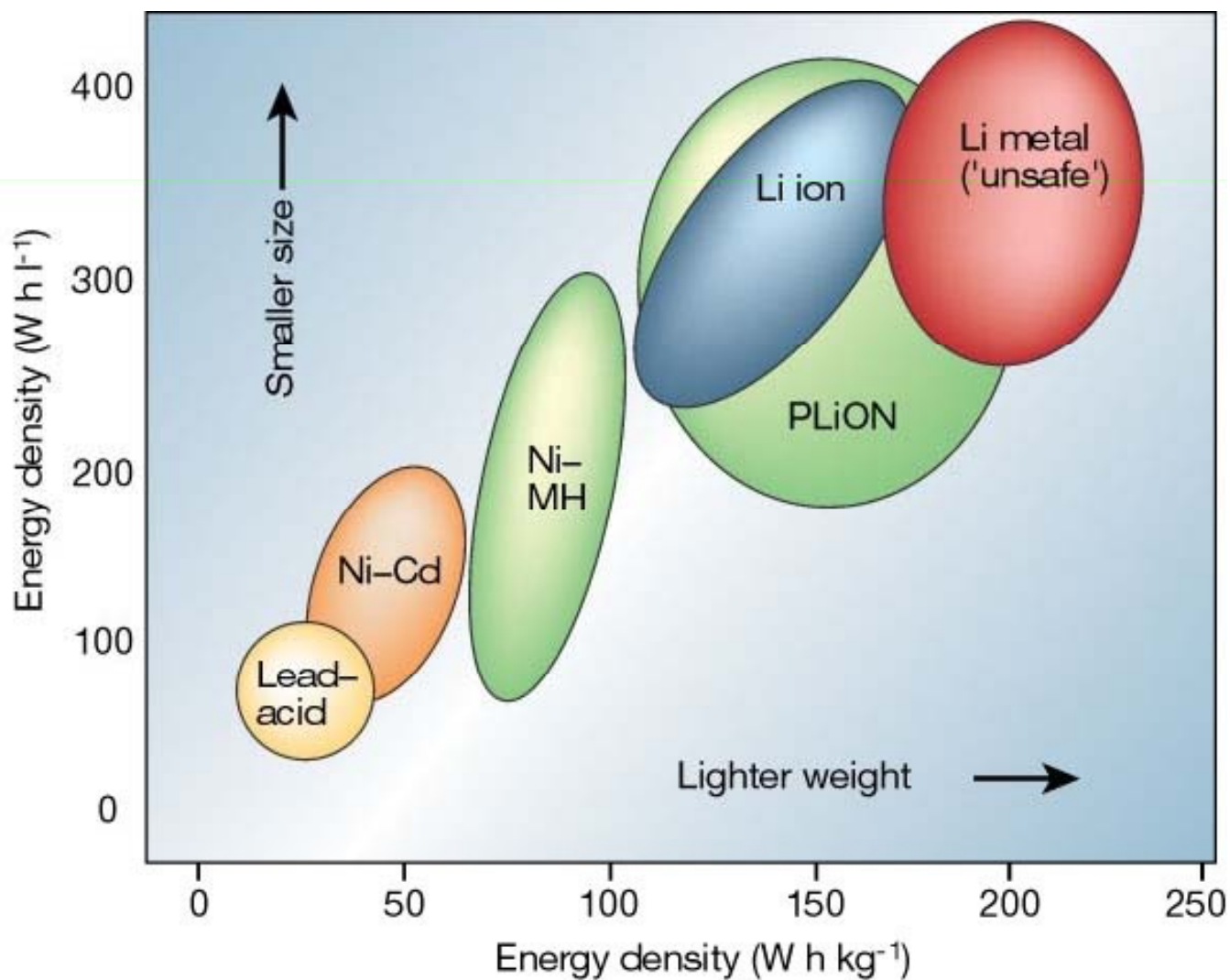
Li-Ion Battery

Byungwoo Park

**Department of Materials Science and Engineering
Seoul National University**

<http://bp.snu.ac.kr>

Rechargeable Batteries



J.-M. Tarascon's group, *Nature* (2001)

Applications of Advanced Li-Ion Battery



PMP



**Laptop
Computer**



**Mobile
Phone**



**MP3
Player**



**Portable
Game**



Digital Camera

High-Power Applications



**Hybrid Electric Vehicles
(HEV)**

Toyota Prius HEV



**Power
Tools**

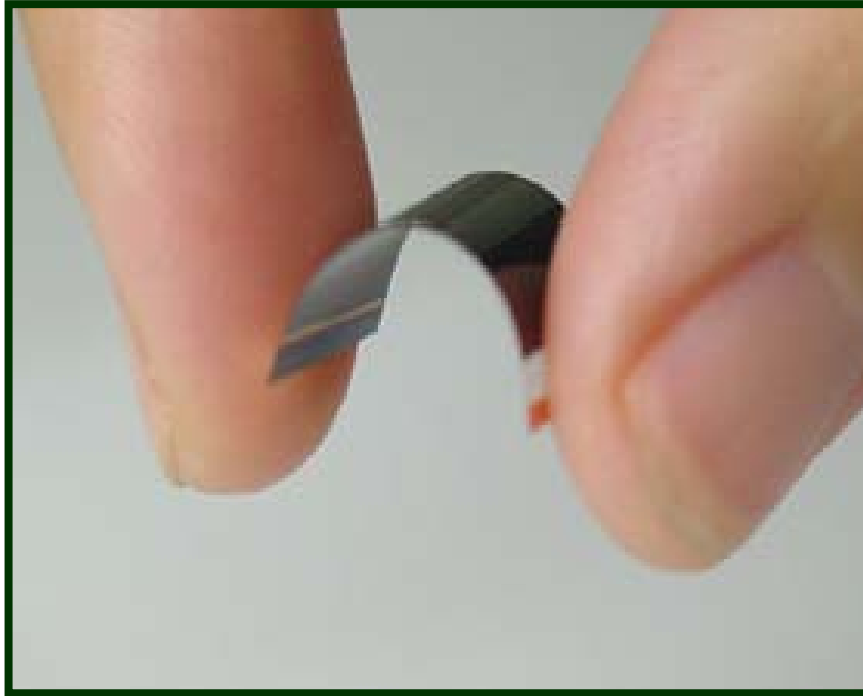
Makita



E-Motorcycle

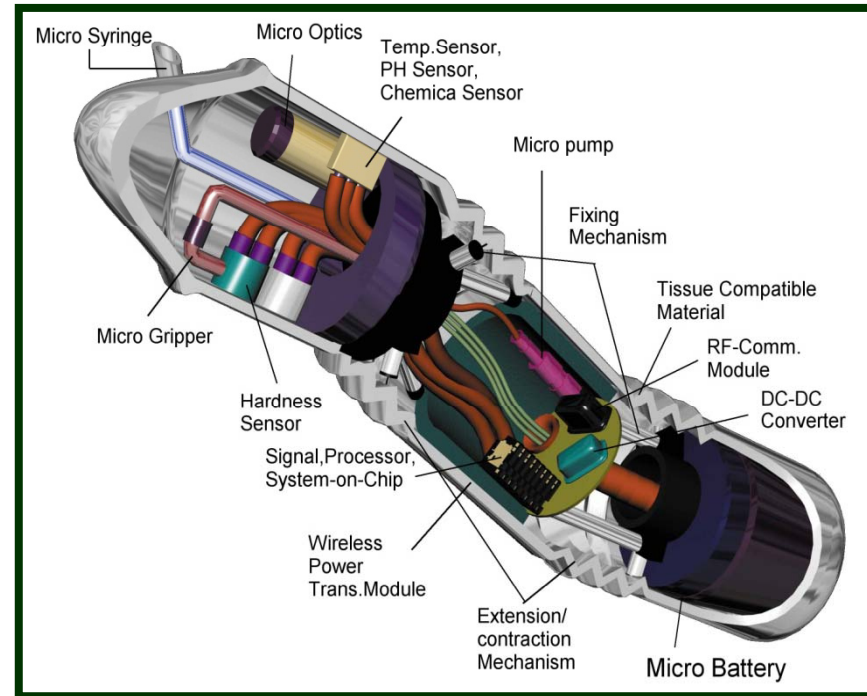
Greenwit

Thin-Film Battery



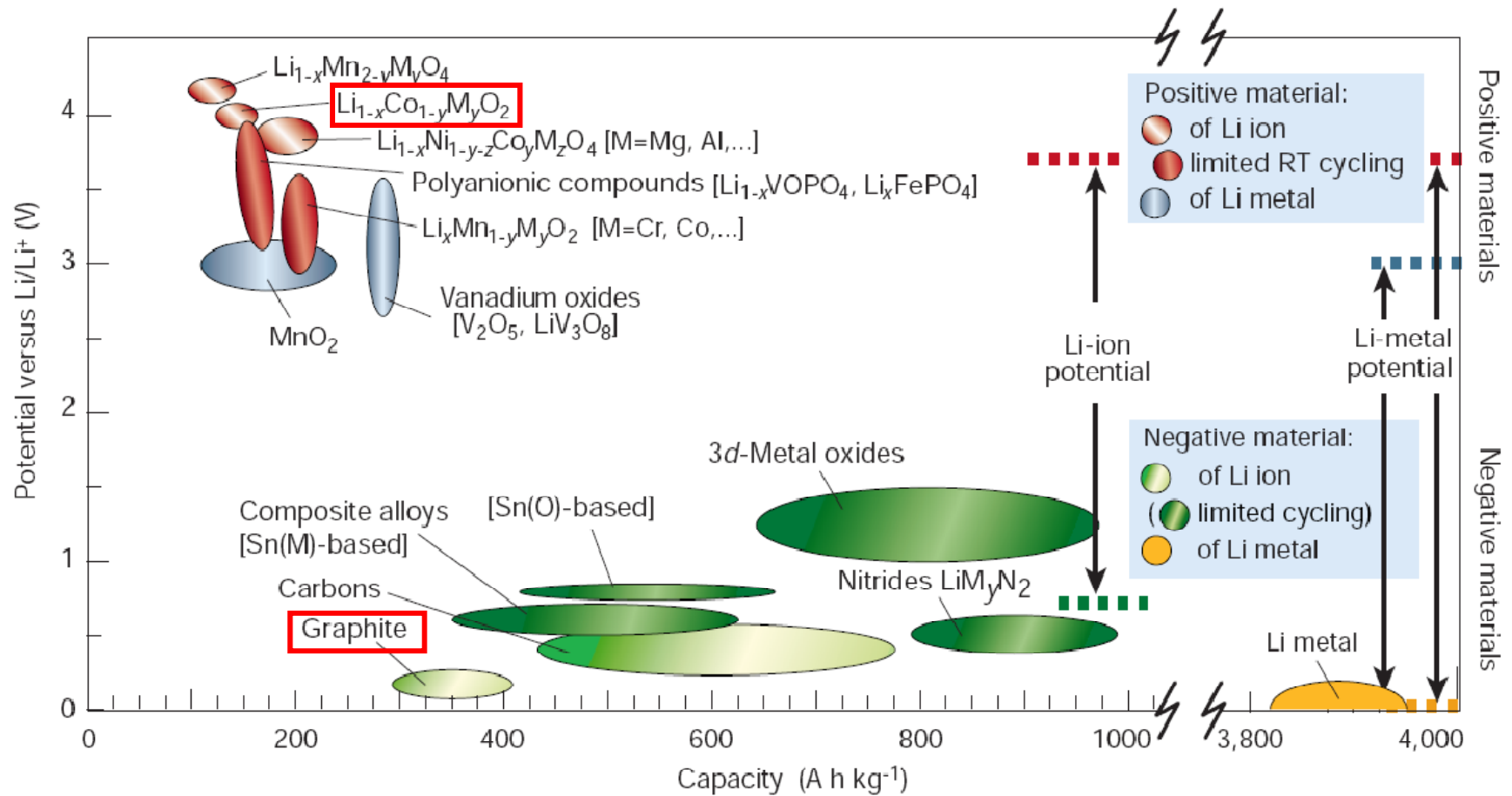
- Smart Card
- Portable Sensors
- ID Tags
- SRAM

Capsule-Type Endoscope



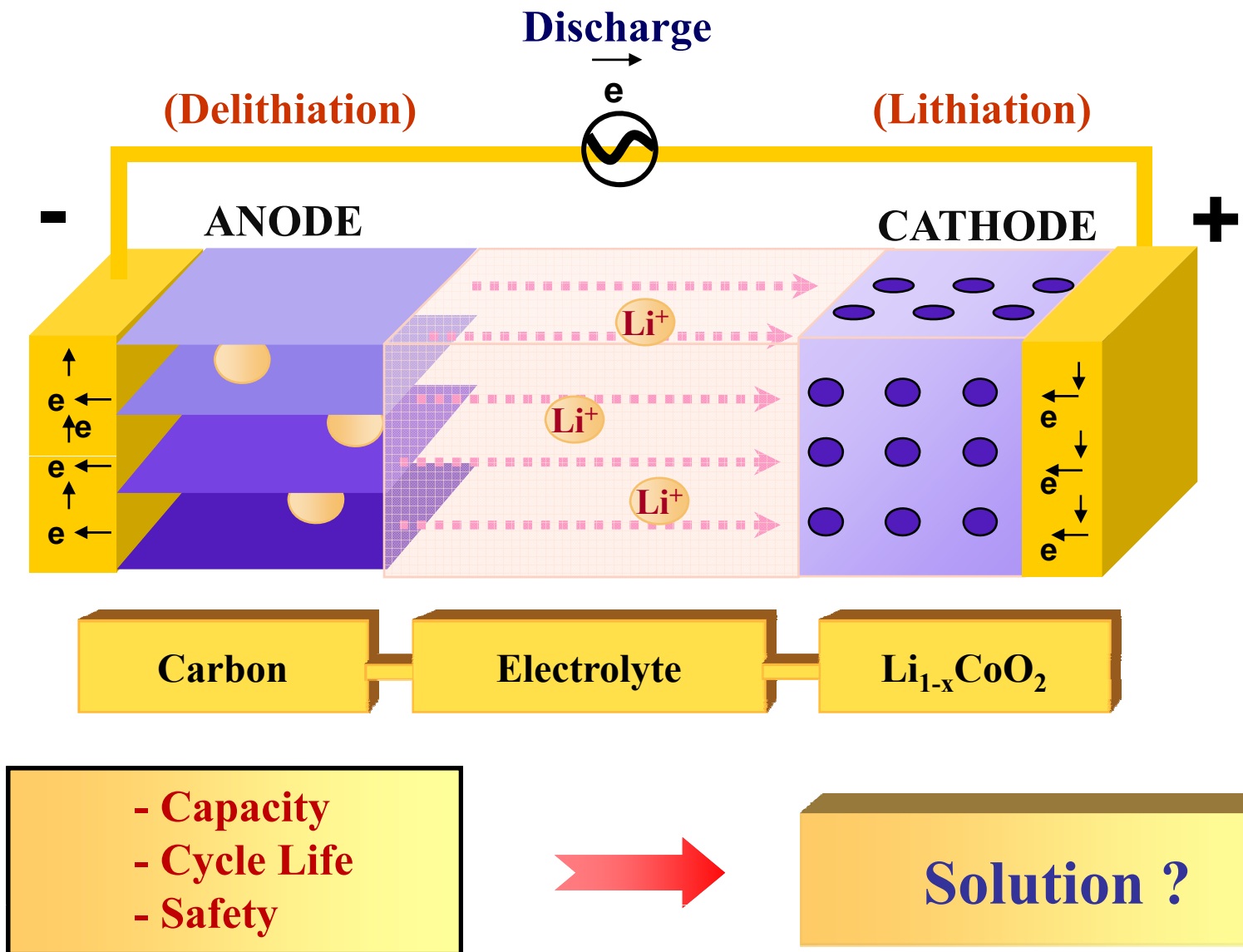
- Sensors
- RF Communication

Electrode Materials

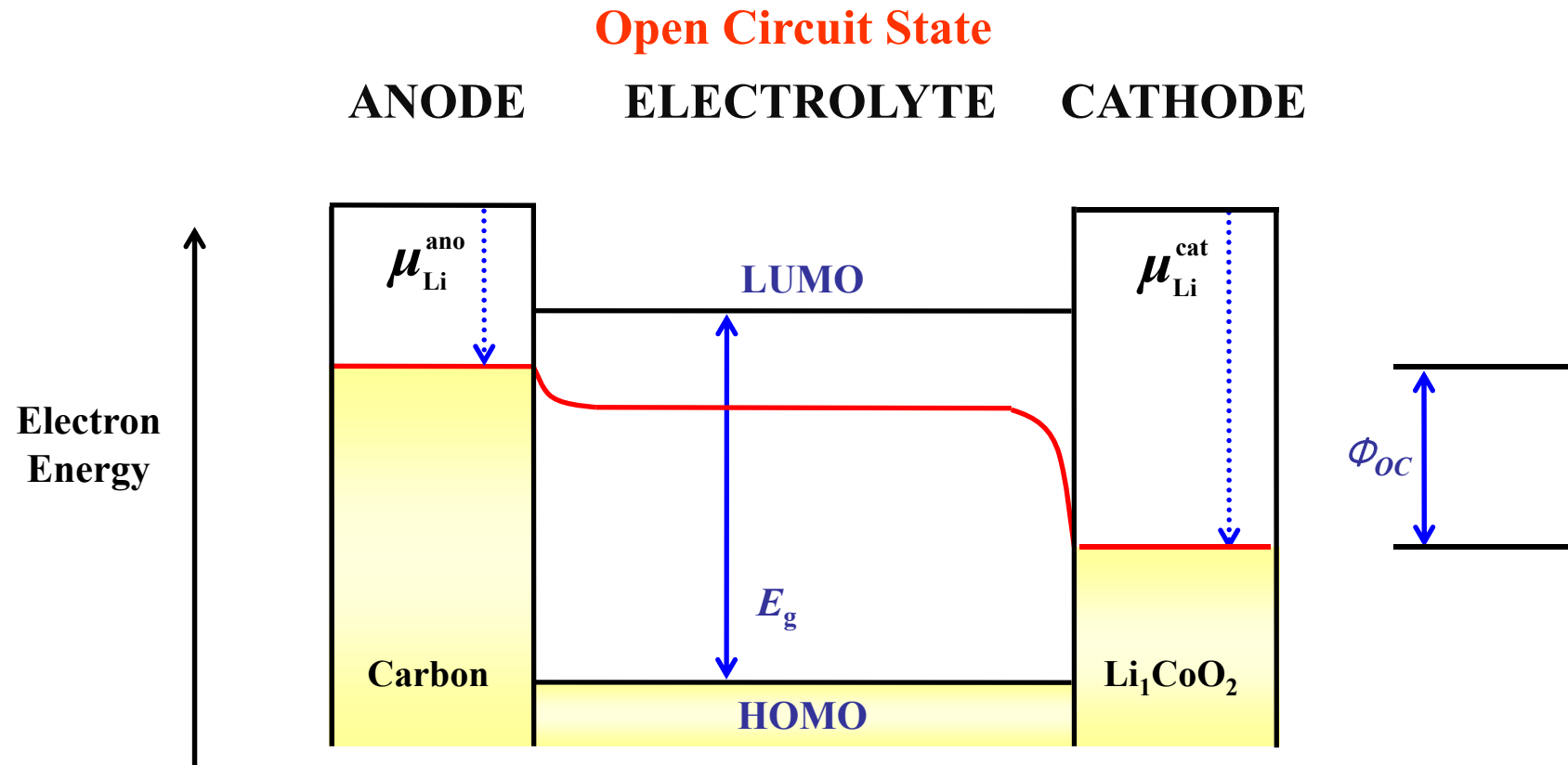


J.-M. Tarascon's group, *Nature* (2001)

Li-Ion Battery Mechanisms

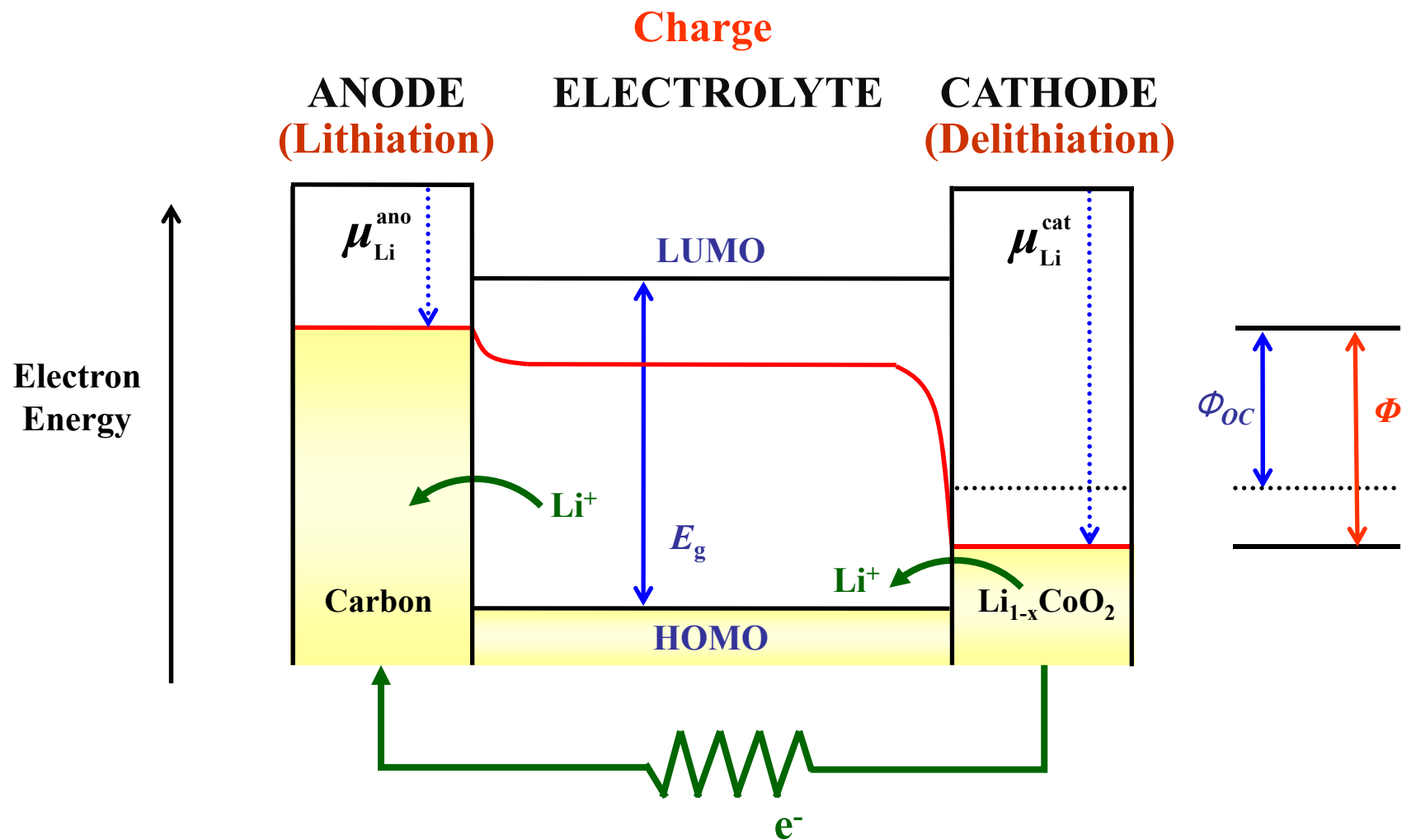


Energy Diagram of Li-Ion Battery (Open Circuit State)

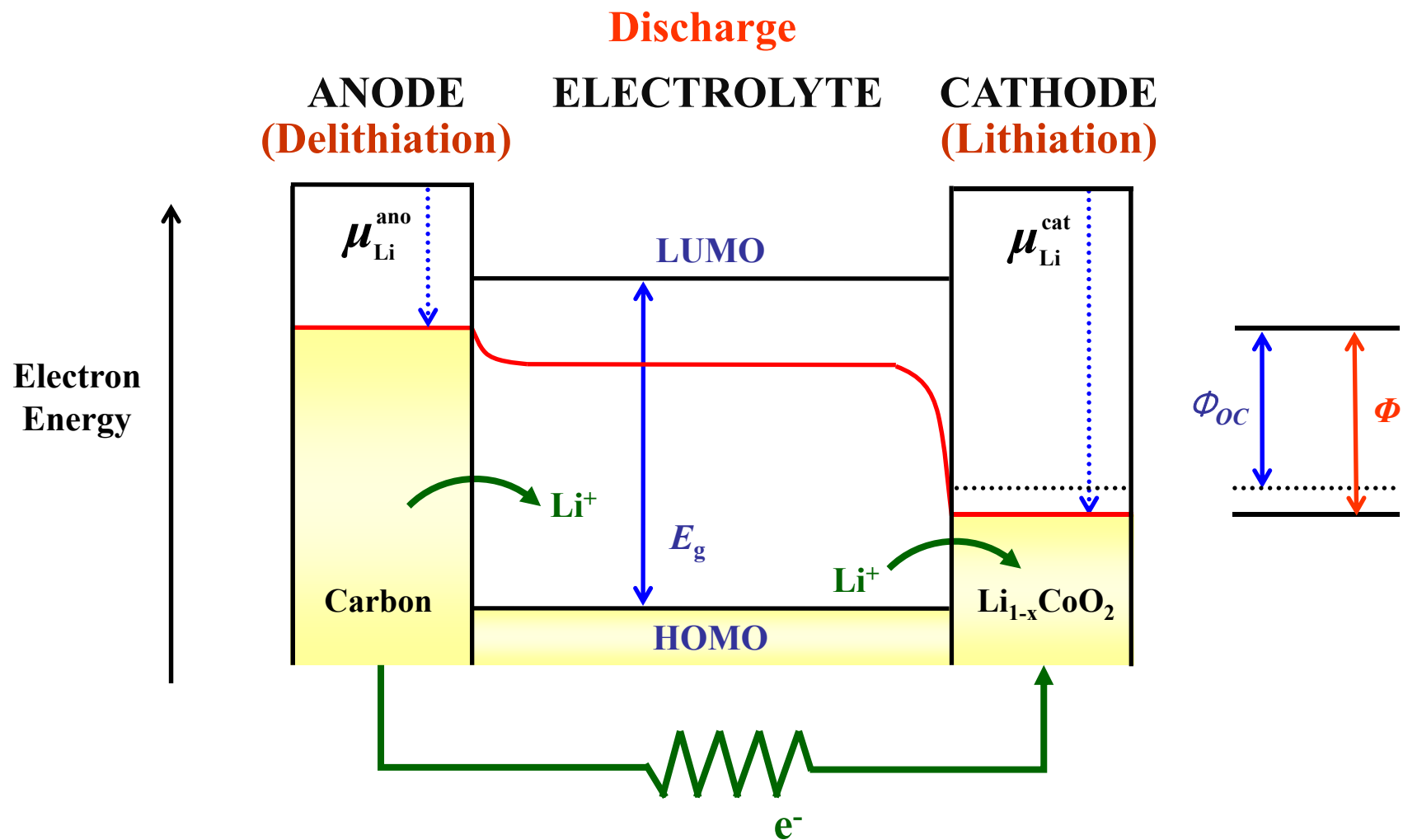


- **LUMO: Lowest Unoccupied Molecular Orbital**
- **HOMO: Highest Occupied Molecular Orbital**

Energy Diagram of Li-Ion Battery (Charge)



Energy Diagram of Li-Ion Battery (Discharge)

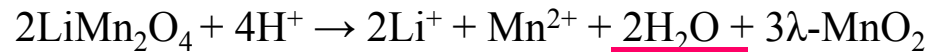


Degradation Mechanisms

1. H₂O 가 존재 시 acidic species 형성 가능성



2. Remained H⁺ can react with the spinel LiMn₂O₄, forming H₂O.



3. 다시 1번 reaction, HF 생성, H⁺ 반응 반복
Mn dissolution 가속

Degradation Mechanisms

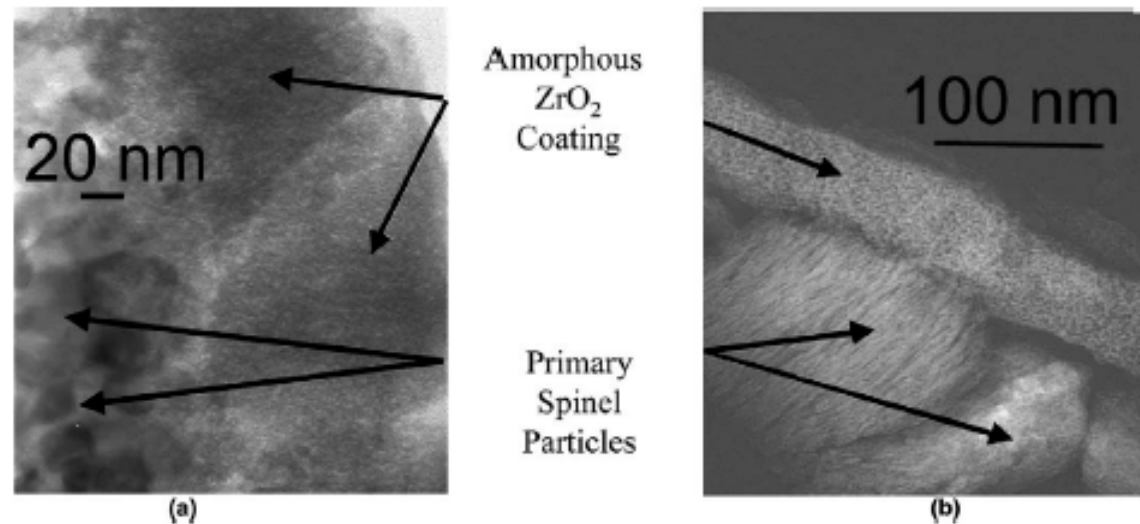


Fig. 1. TEM images of LiMn_2O_4 spinel particles with an amorphous ZrO_2 coating.

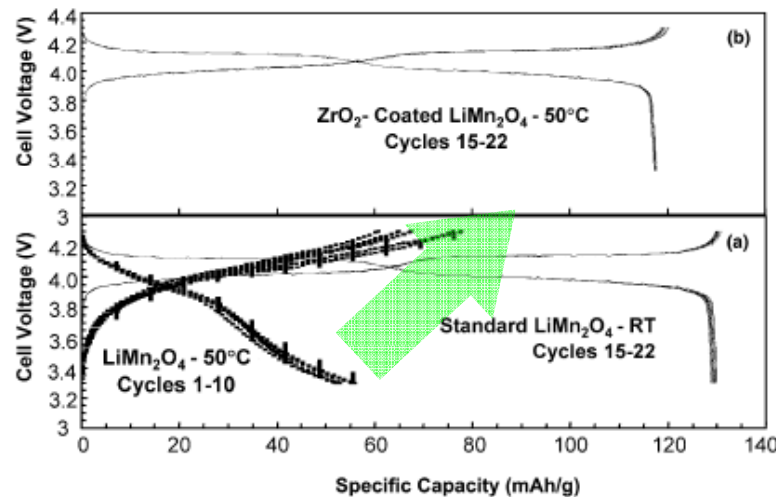


Fig. 2. Comparison of the electrochemical cycling stability of lithium cells with (a) uncoated LiMn_2O_4 electrodes at room temperature and 50°C , and (b) ZrO_2 -coated LiMn_2O_4 electrodes at 50°C .

ZrO_2 coated spinel LiMn_2O_4 에서 50°C 충방전시 성능향상 (50°C 에서 H^+ 와 반응 가속; uncoated LiMn_2O_4 는 열화가 심함)

ZrO_2 coating can scavenge HF attack.

Thackeray *et al.*, *Electrochem. Comm.* **5**, 752 (2003)

Argonne National Laboratory

Degradation Mechanisms

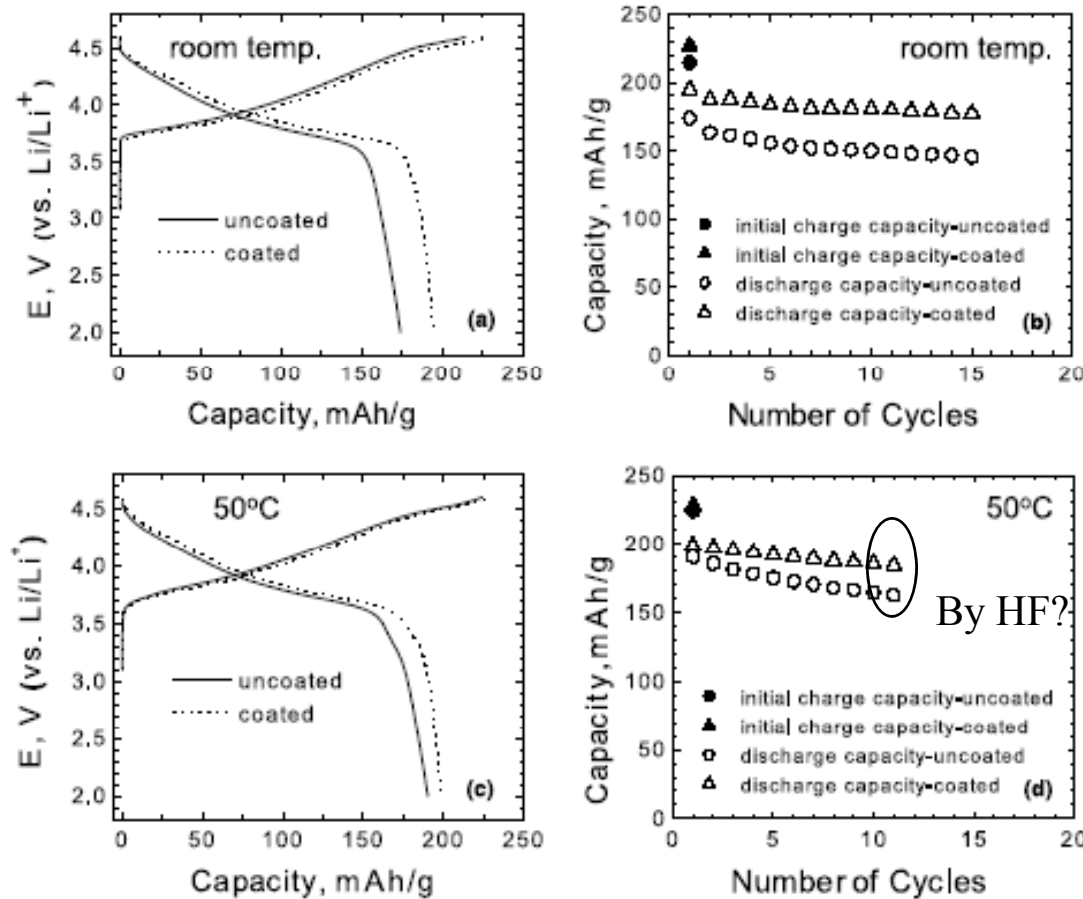


Fig. 3. Comparison of the electrochemical behavior of lithium cells with uncoated and ZrO₂-coated LiMn_{0.5}Ni_{0.5}O₂ electrodes (a, b) at room temperature, and (c, d) at 50 °C. Cells were charged and discharged at 0.1 mA/cm² between 4.6 and 2.0 V.

Thackeray *et al.*
Argonne National Laboratory
Electrochem. Comm. **5**, 752 (2003).

Layered structure 인 LiMn_{0.5}Ni_{0.5}O₂ 에서는 50°C 총방전시 성능이 비슷.
ZrO₂ 가 10% 의 성능향상을 보임.

ZrO₂- and Li₂ZrO₃-Stabilized Spinel and Layered Electrodes

Abstract

Strategies for countering the solubility of LiMn₂O₄ (spinel) electrodes at 50 °C and for suppressing the reactivity of layered LiMO₂ (M = Co, Ni, Mn, Li) electrodes at high potentials are discussed. Surface treatment of LiMn₂O₄ with colloidal zirconia (ZrO₂) dramatically improves the cycling stability of the spinel electrode at 50 °C in Li/LiMn₂O₄ cells. ZrO₂-coated LiMn_{0.5}Ni_{0.5}O₂ electrodes provide a superior capacity and cycling stability to uncoated electrodes when charged to a high potential (4.6 V vs Li⁰). The use of Li₂ZrO₃, which is structurally more compatible with spinel and layered electrodes than ZrO₂ and which can act as a Li⁺-ion conductor, has been evaluated in composite 0.03Li₂ZrO₃ · 0.97LiMn_{0.5}Ni_{0.5}O₂ electrodes; glassy Li_xZrO_{2+x/2} (0 < x ≤ 2) products can be produced from colloidal ZrO₂ for surface coatings.

© 2003 Elsevier B.V. All rights reserved.

Keywords: Lithium batteries; Stabilized electrode; Spinel; Layered; Zirconia; Coating

Thackeray *et al.*
Argonne National Laboratory
Electrochem. Comm. **5**, 752 (2003).

Anode for Li⁺ Battery

Anodes and Composite Anodes: An Overview

Table 4.1. Capacities and volume changes of different elements.

Starting material	C	Al	Si	Sn	Bi
Lithiated phase	LiC ₆	Li ₉ Al ₄	Li ₂₁ Si ₅	Li ₁₇ Sn ₄	Li ₃ Bi
Theoretical specific capacity (Ah/kg)	372	2235	4010	959	385
Theoretical volumetric capacity (Ah/l)	833	6035	9340	7000	3773
Volume changes (%)	12	238	297	257	115



Δa axis ~ 1%

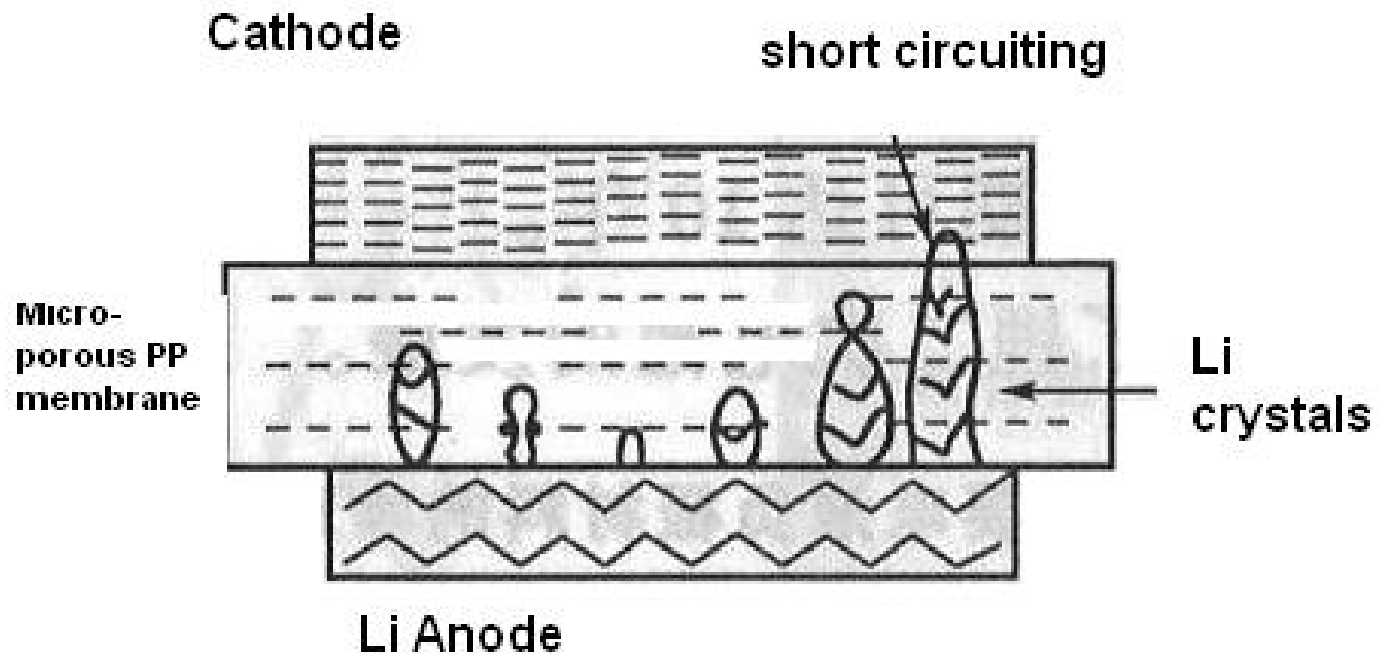
Δc axis ~ 10%

ΔV ~ 12%

Lithium Batteries – Science and Technology
edited by G.-A. Nazri and G. Pistoia

N. A. W. Holzwarth's group
(Exxon Research and Engineering Company)
Physical Review B **28**, 1013 (1983).

Short Circuiting due to Li Crystal Growth



Lithium Batteries – Science and Technology
edited by G.-A. Nazri and G. Pistoia

Lithium-Intercalated Graphite

Lithium-intercalated graphite: Self-consistent electronic structure for stages one, two, and three

N. A. W. Holzwarth*

*Corporate Research—Sciences Laboratory, Exxon Research and Engineering Company,
P. O. Box 45, Linden, New Jersey 07036*

Steven G. Louie

Department of Physics, University of California, Berkeley, California 94720

Sohrab Rabi

*Moore School of Electrical Engineering, University of Pennsylvania, Philadelphia, Pennsylvania 19104
(Received 23 February 1983)*

First-principles electronic structure calculations were carried out for LiC_6 , LiC_{12} , and LiC_{18} representing first-, second-, and third-stage model graphite intercalation compounds. By comparing the charge density of these compounds to that of reference graphite compounds, we could define a “total difference density” in order to quantify charge transfer and polarization in these materials. The total difference density is found to be highly concentrated near the intercalant ions. However, the conduction electrons (those in partially occupied bands) are found to have the distribution of virtually undistorted π wave functions and have a much more delocalized distribution than that of the total difference density. These two types of charge distributions account for many of the unusual electronic properties of graphite intercalation compounds.

N. A. W. Holzwarth's group
(Exxon Research and Engineering Company)
Physical Review B **28**, 1013 (1983).

Power Sources for HEV and LEV

The demand of battery materials: Hybrid electric vehicle Toyota “Prius” and its battery pack.



Hybrid Prius – 2008 Toyota Prius Hybrid Homepage

<http://www.toyota.com/prius-hybrid/>

Battery Pack – Panasonic EV Energy Homepage

<http://www.peve.jp/e/hevjyusi.html>



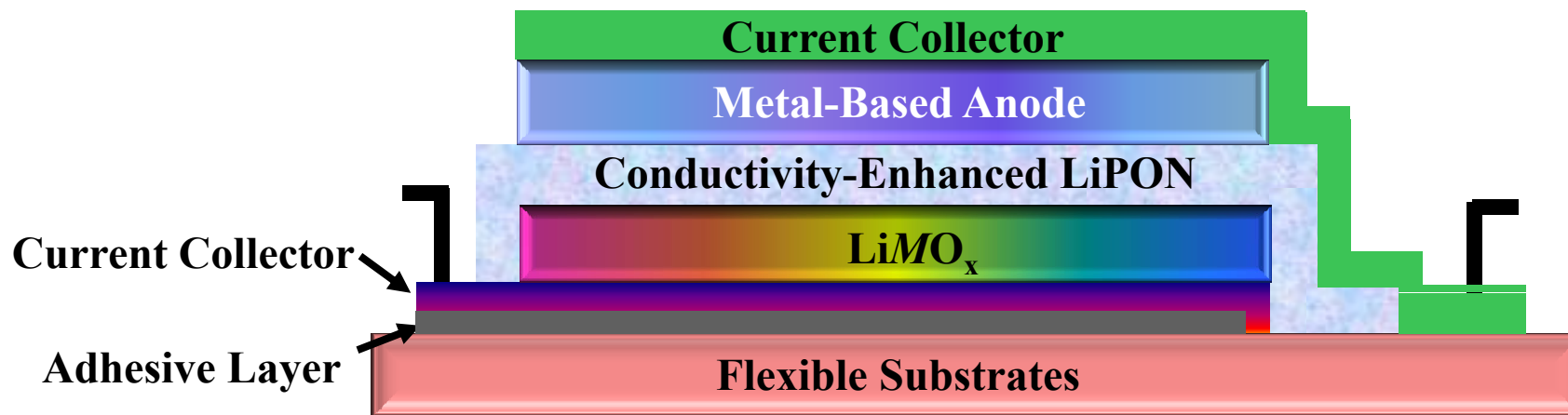
Remaining Challenges in Thin-Film Battery

Electrode: Novel Electrode with High Thermal/Electrochemical Stability
Electrolyte: Nanostructure-Controlled Solid Electrolyte

Current Collector: Metal or Metal Compounds

Substrate: Various Substrates such as Si Wafer, Flexible Polymer, etc.

Designs: Pile-Up Process for Capacity Control



Advance toward Next-Generation Flexible Battery

Technological improvements in rechargeable solid-state batteries are being driven by an ever-increasing demand for portable electronic devices. Lithium-ion batteries are the systems of choice, offering high energy density, flexible and lightweight design, and longer lifespan than comparable battery technologies. We present a brief historical review of the development of lithium-based rechargeable batteries, highlight ongoing research strategies, and discuss the challenges that remain regarding the synthesis, characterization, electrochemical performance and safety of these systems

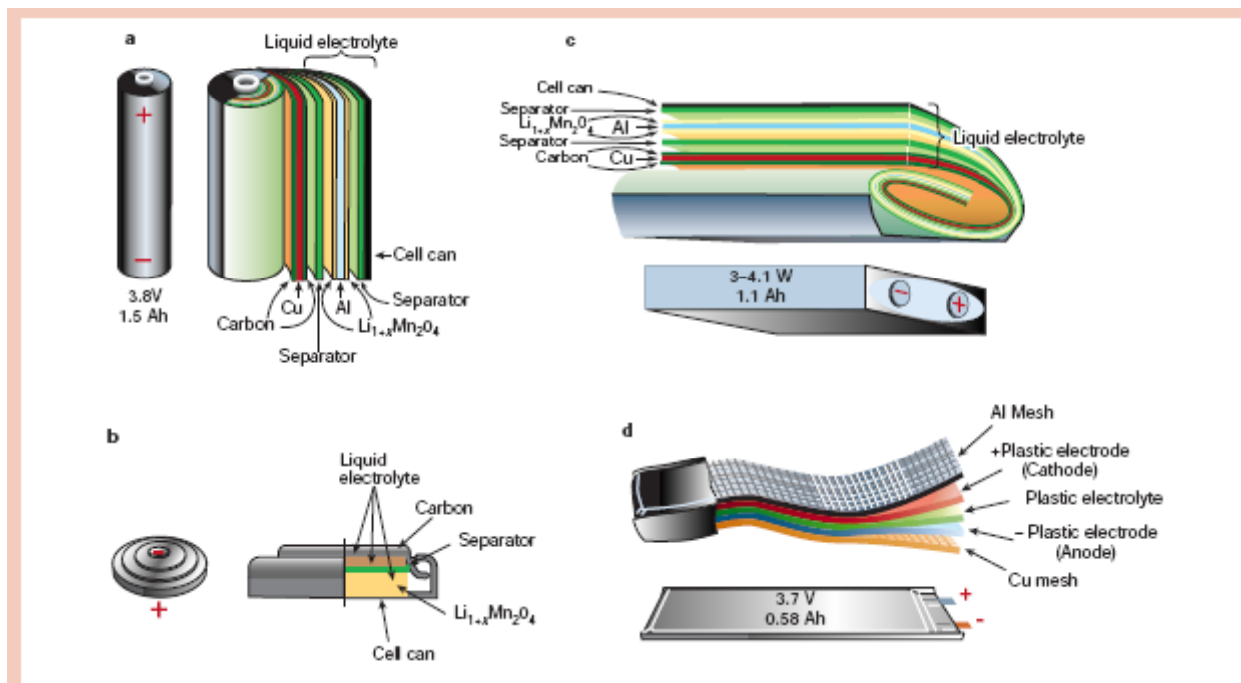


Figure 4 Schematic drawing showing the shape and components of various Li-ion battery configurations. a, Cylindrical; b, coin; c, prismatic; and d, thin and flat. Note the unique flexibility of the thin and flat plastic Li-ion configuration; in contrast to the other configurations, the PLi-ion technology does not contain free electrolyte.

Plastic Li-Ion Battery

J.-M. Tarascon *et al.*
Nature (2001)

Advance toward Next-Generation Flexible Battery

Batteries power a wide range of electronic devices including phones, laptop computers and medical devices such as cardiac pacemakers and defibrillators. In the near future, batteries may also help fight global warming by improving the performance of electric or hybrid vehicles with zero or reduced carbon emissions. With the ever-increasing demand for efficiency and design, there is a need for ultrathin, safe and flexible energy storage options.

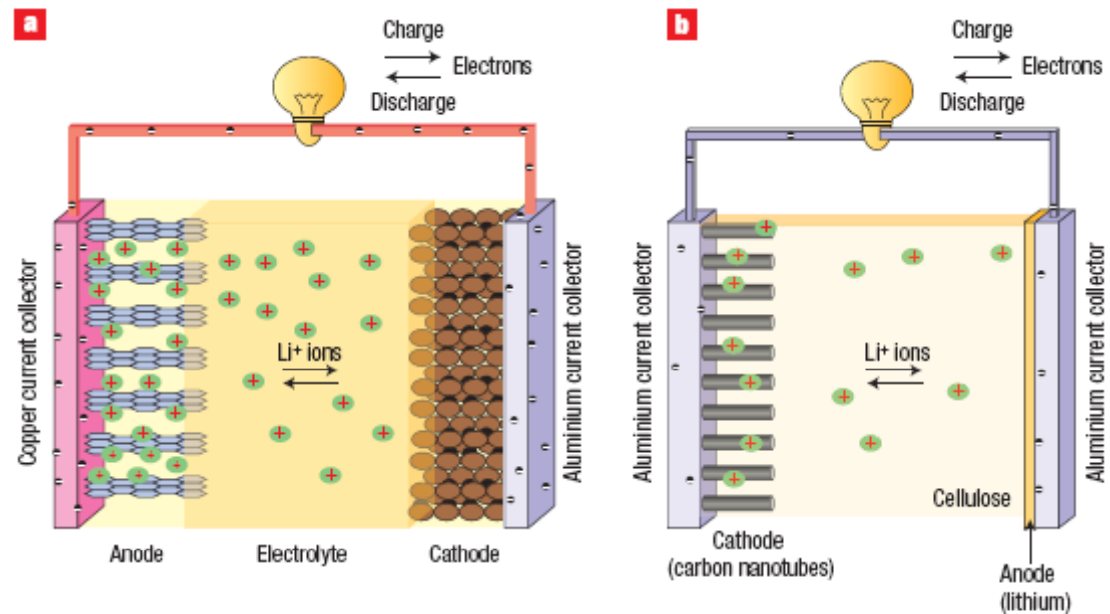


Figure 1 Schematic of different battery configurations. **a**, A conventional lithium-ion battery contains a graphite anode (grey hexagons), a lithium cathode (lithium cobalt oxide in this case; brown circles), and a liquid electrolyte containing lithium ions (green) in a fibre separator (orange). The removal of lithium ions by the simultaneous oxidation of cobalt in the cathode and insertion of lithium ions into the graphite anode charges the battery. Electricity is produced when ions move in the opposite direction and the cobalt is reduced. **b**, A lithium-ion battery made from nanocomposite paper is more compact and weighs less than a conventional lithium-ion battery. The paper, which is made by infiltrating cellulose into carbon nanotubes grown on a silicon substrate, is impregnated with the electrolyte, thus combining the cathode (the nanotubes) and the separator (the cellulose) in a single unit. Depositing a thin film of lithium on one side of the paper and adding aluminium current collectors completes the battery configuration. Electricity is produced when lithium is oxidized to form lithium ions, which are inserted into the nanotube cathode. Charging occurs when the ions move in the opposite direction and are deposited as lithium metal.

CNT and Cellulose-Based Paper-Type Battery

B. Scrosati

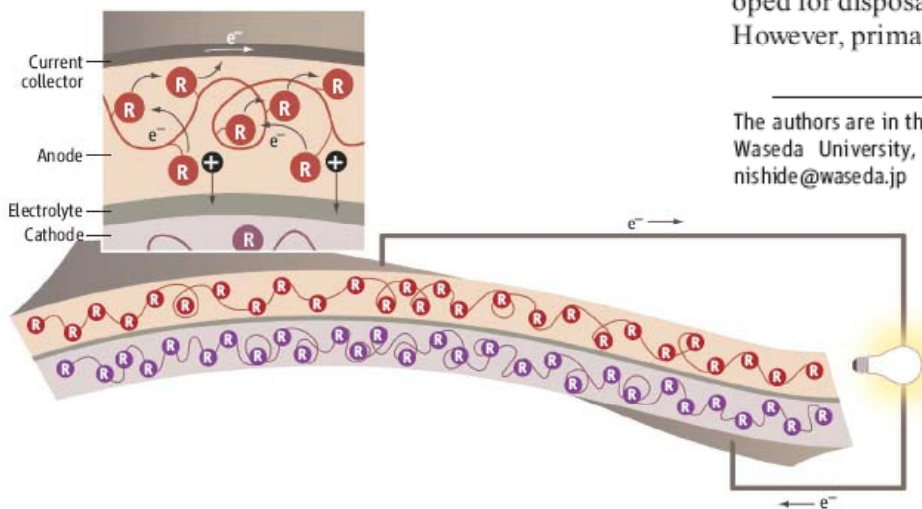
Nature Nanotechnology (2007)

Advance toward Next-Generation Flexible Battery

The design of soft portable electronic equipment, such as rollup displays and wearable devices, requires the development of batteries that are flexible. Active radio-frequency identification tags and integrated circuit smart cards also require bendable or flexible batteries for durability in daily use. Several routes toward the development of flexible batteries are being explored. Some involve batteries made mostly or entirely from plastic, with the added advantage of avoiding ignitable and toxic substances such as lithium and lead. An inorganic primary battery that can be bent like a piece of paper has been developed for disposable-card applications (1, 2). However, primary batteries produce current

by a one-way chemical reaction and are not rechargeable; their usefulness of in portable electronic equipment is therefore limited. Rechargeable secondary batteries are generally used to power portable equipment. There have been recent efforts to make secondary lithium-ion batteries into thin films while maintaining their high energy capacity (3).

Making a bendable lithium-ion battery requires the development of soft electrode-active materials, such as metal oxide nanoparticles or nanocoatings for cathodes and lithium foil or nanocarbon materials for anodes (4, 5). Virus-templated Co_3O_4 nanowires have been shown to improve the capacity of thin, bendable lithium-ion batteries (6). The charging/discharging process of batteries is generally dominated by the electron and counterion transport at the surface of the electrodes. By using nanostruc-



The authors are in the Department of Applied Chemistry, Waseda University, Tokyo 169-8555, Japan. E-mail: nishide@waseda.jp

Example of a flexible plastic battery. The R groups in the cathode and in the anode have different redox potentials. During the charging process, charge is stored by oxidizing R groups at the cathode and reducing R groups at the anode. The output voltage of the battery corresponds to the gap between the redox potentials. The curves connecting the R groups are polymer chains, which give flexibility. Many R groups are attached to the polymer chain, so that electrons can hop between neighboring R groups to produce the output current.

Flexible Plastic Battery Using Organic Polymers

H. Nishide's group
Science (2008)

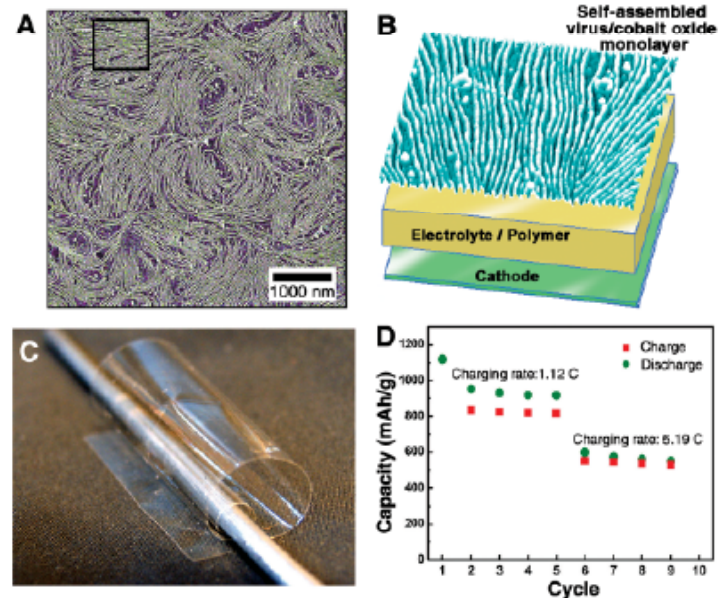
Advance toward Next-Generation Flexible Battery

Virus-Enabled Synthesis and Assembly of Nanowires for Lithium Ion Battery Electrodes

Ki Tae Nam,^{1,4} Dong-Wan Kim,^{1*} Pil J. Yoo,^{2,4} Chung-Yi Chiang,^{1,5} Nonglak Meethong,¹ Paula T. Hammond,^{2,4} Yet-Ming Chiang,¹ Angela M. Belcher^{1,3,4,5†}

The selection and assembly of materials are central issues in the development of smaller, more flexible batteries. Cobalt oxide has shown excellent electrochemical cycling properties and is thus under consideration as an electrode for advanced lithium batteries. We used viruses to synthesize and assemble nanowires of cobalt oxide at room temperature. By incorporating gold-binding peptides into the filament coat, we formed hybrid gold-cobalt oxide wires that improved battery capacity. Combining virus-templated synthesis at the peptide level and methods for controlling two-dimensional assembly of viruses on polyelectrolyte multilayers provides a systematic platform for integrating these nanomaterials to form thin, flexible lithium ion batteries.

Fig. 4. Two-dimensional assembly of Co_3O_4 nanowires driven by liquid crystalline ordering of the engineered M13 bacteriophage viruses. (A and B) Phase-mode atomic force microscope image of macroscopically ordered monolayer of Co_3O_4 -coated viruses. The Z range is 30° (C) Digital camera image of a flexible and transparent free-standing film of $(\text{LPEI/PAA})_{100.5}$ on which Co_3O_4 viral nanowires are assembled into nanostructured monolayer with dimensions of 10 cm by 4 cm. (D) Capacity for the assembled monolayer of Co_3O_4 nanowires/Li cell at two different charging rates.



2-Dimensional Assembly of Metal Oxide Nanowires

A. M. Belcher's group
Science (2006)

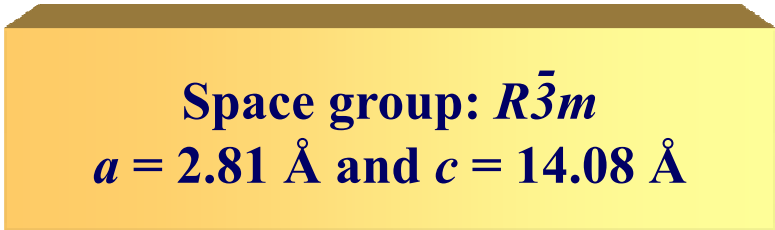
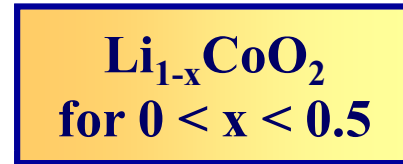
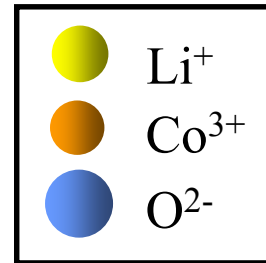
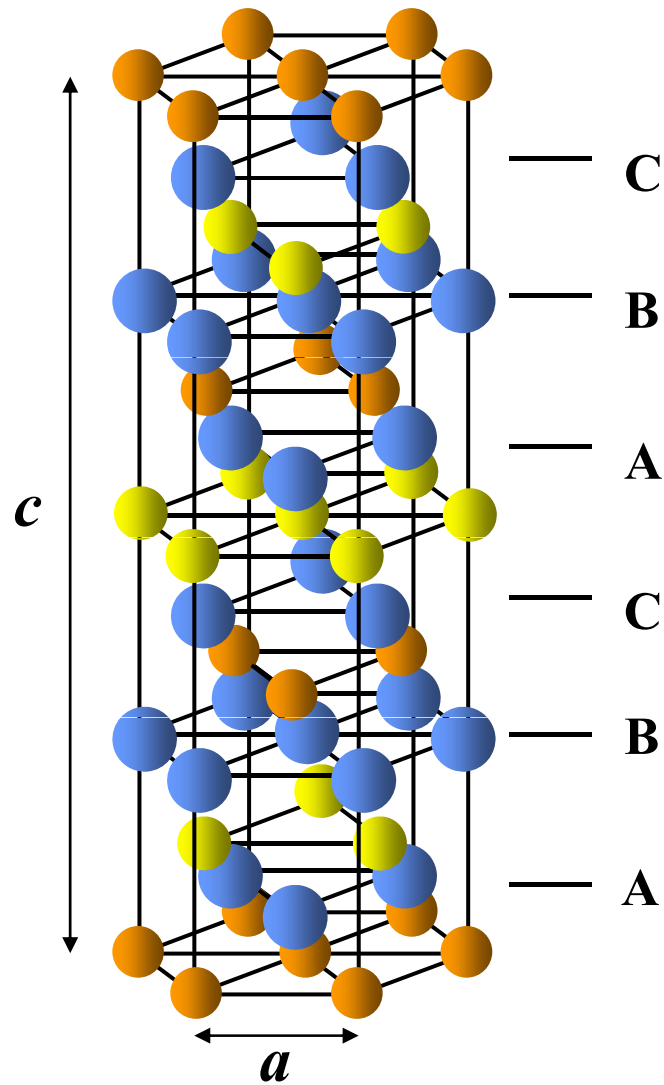
The Effect of Metal-Oxide Coating in LiCoO_2 Cathodes

Y. J. Kim, H. Kim, B. Kim, D. Ahn, J.-G. Lee, T.-J. Kim, D. Son, J. Cho,
Y.-W. Kim, and B. Park
Chem. Mater. **15**, 1505 (2003).

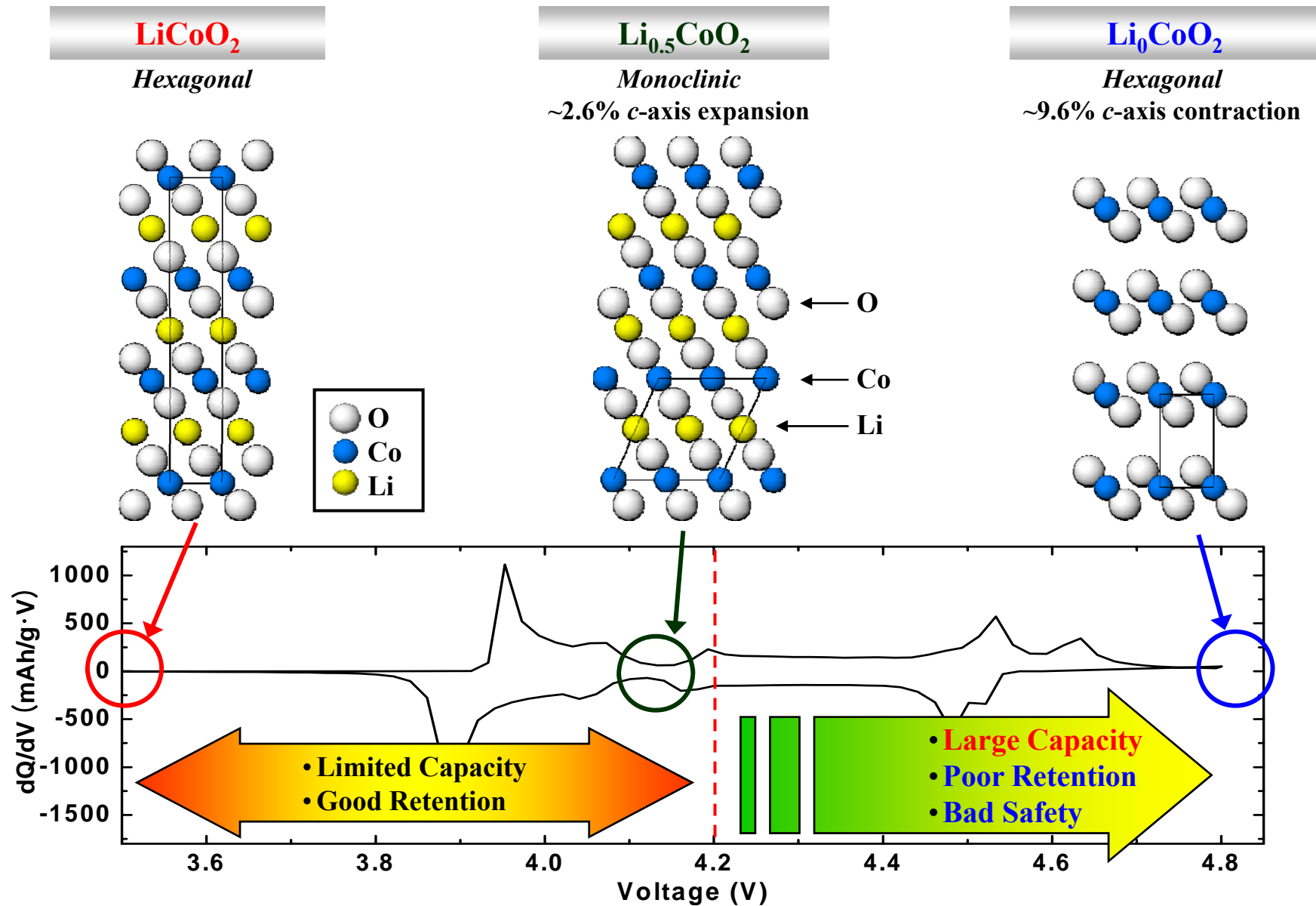
Y. J. Kim, E.-K. Lee, H. Kim, J. Cho, Y. W. Cho, B. Park, S. M. Oh, and
J. K. Yoon
J. Electrochem. Soc. **151**, A1063 (2004).

J. Cho, Y. J. Kim, T.-J. Kim, and B. Park
Angew. Chem. Int. Ed. **40**, 3367 (2001).

Structure of LiCoO_2

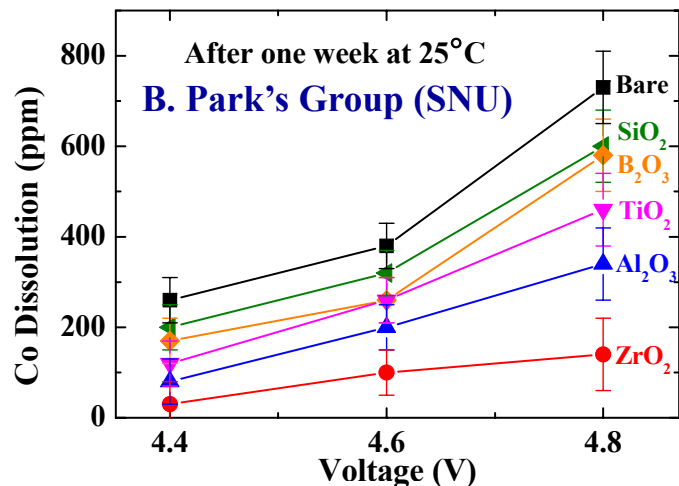


Structure of LiCoO_2

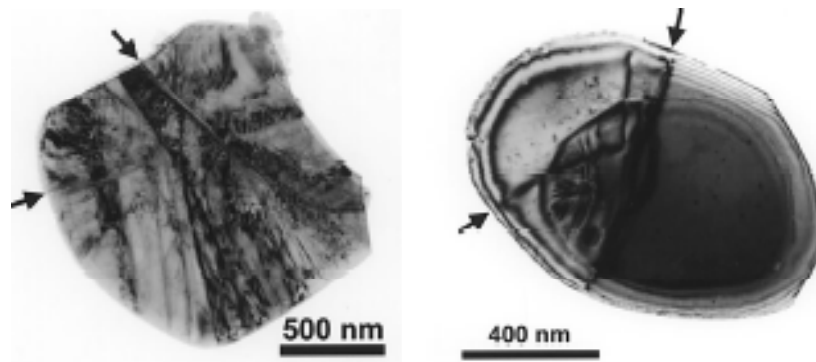


Mechanisms of Capacity Fading and Safety

❖ Cobalt Loss from $\text{Li}_{1-x}\text{CoO}_2$

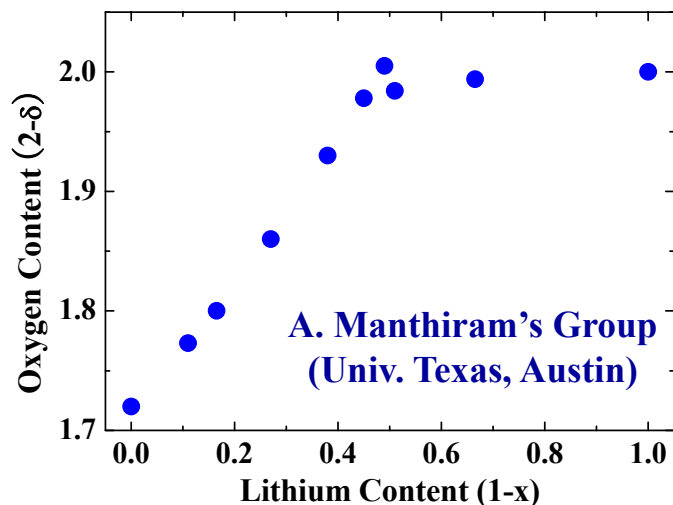


❖ Structural Instability



Y.-M. Chiang's Group (MIT)

❖ Oxygen Loss from $\text{Li}_{1-x}\text{CoO}_{2-\delta}$

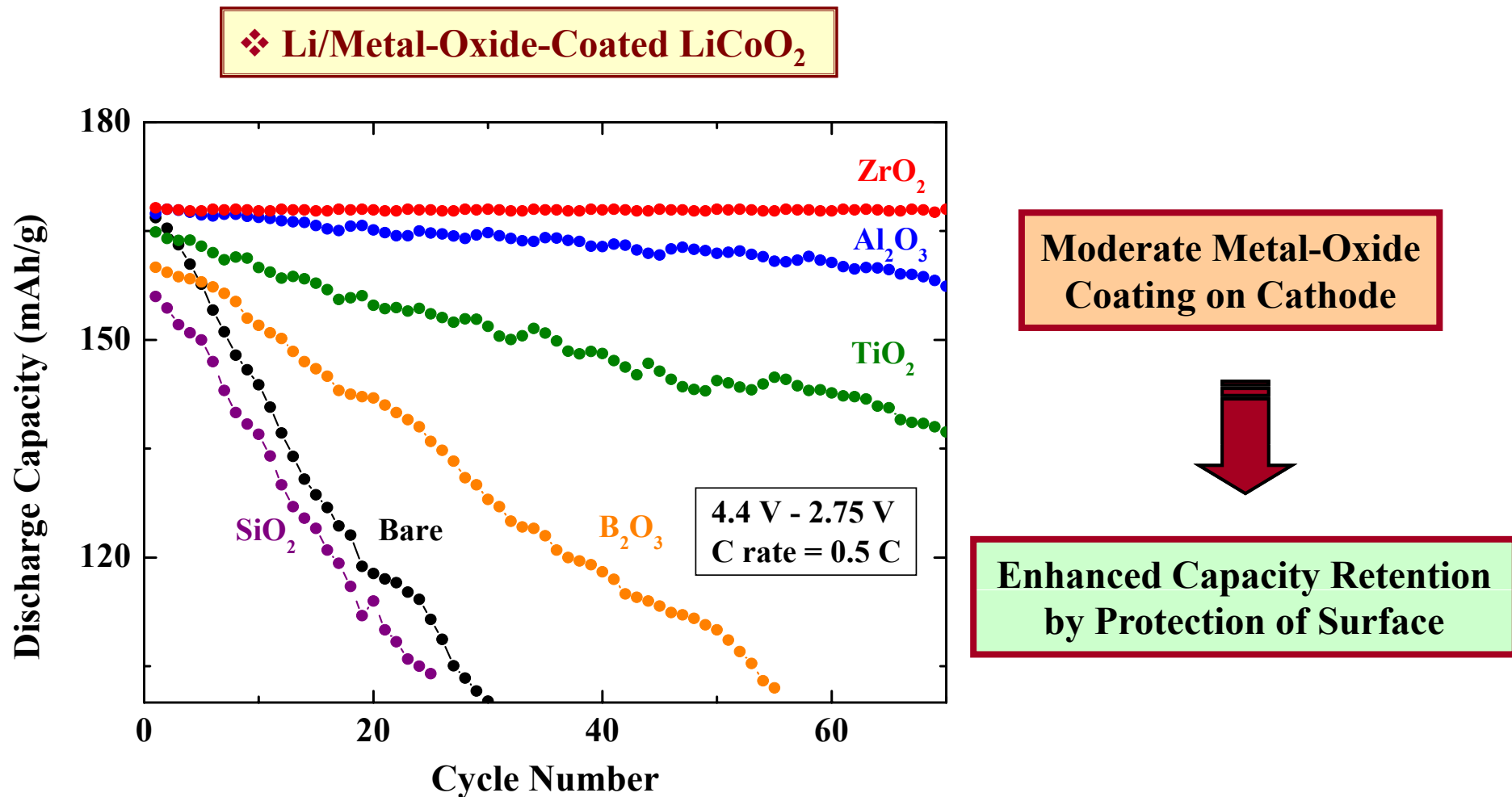


❖ Exothermic Reaction with Electrolyte



<http://www.citynews.ca>

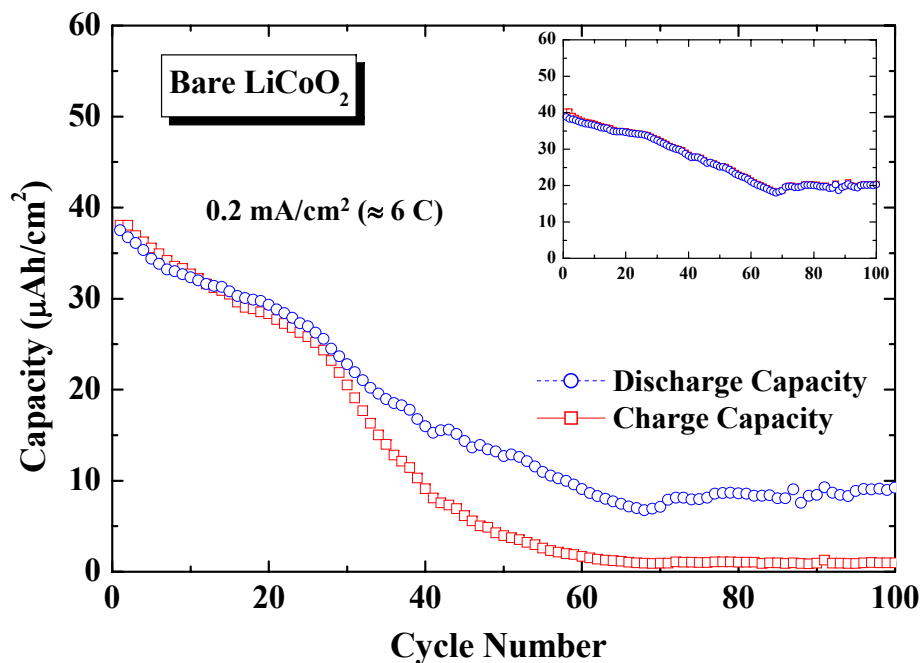
Capacity Retention of Metal-Oxide-Coated LiCoO_2



➤ J. Cho, Y. J. Kim, T.-J. Kim, and B. Park
Angew. Chem. Int. Ed. **40**, 3367 (2001).

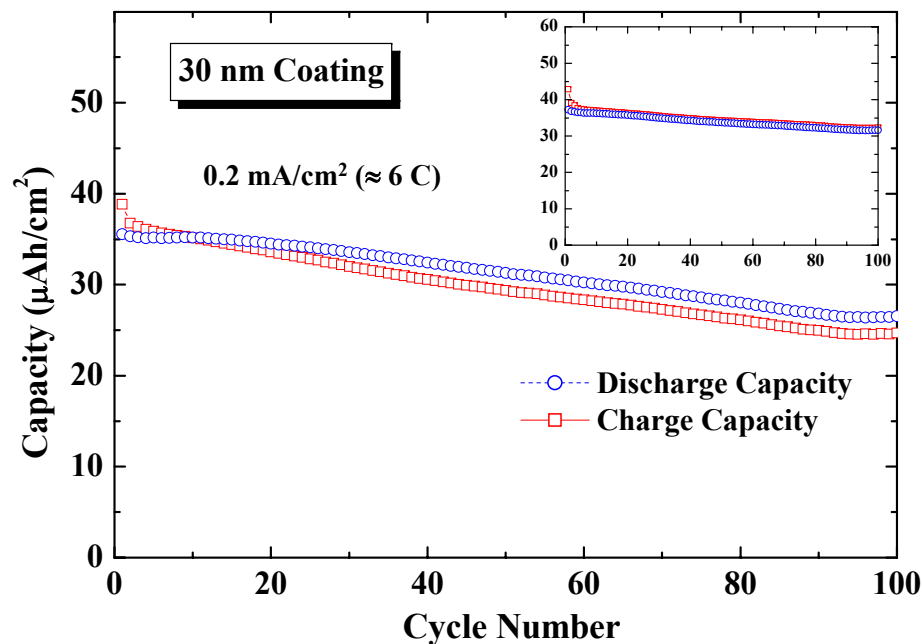
Charge-Discharge Experiments in Thin Films

Uncoated LiCoO₂ Thin Film



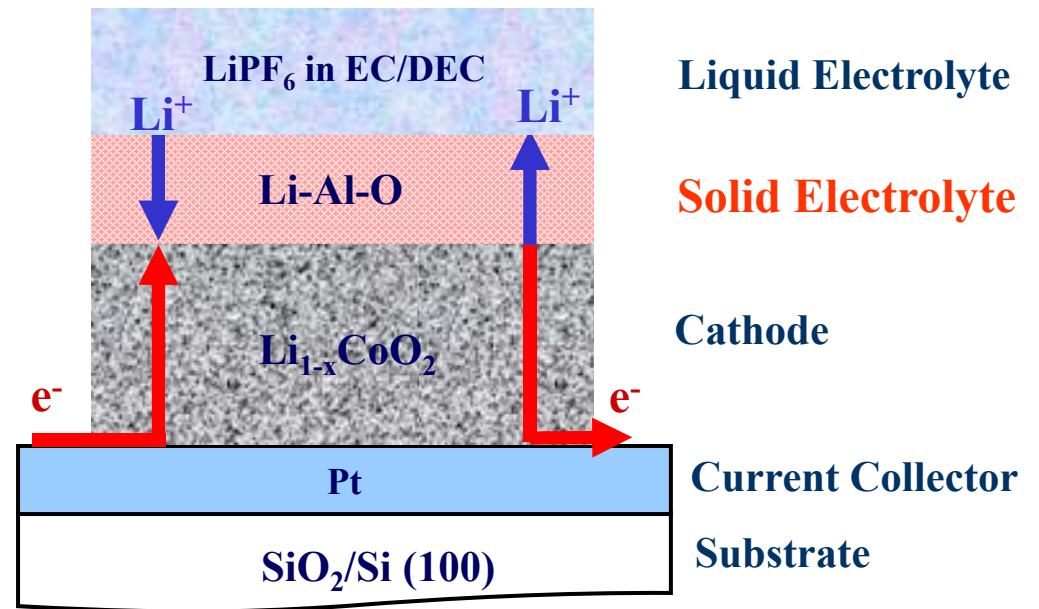
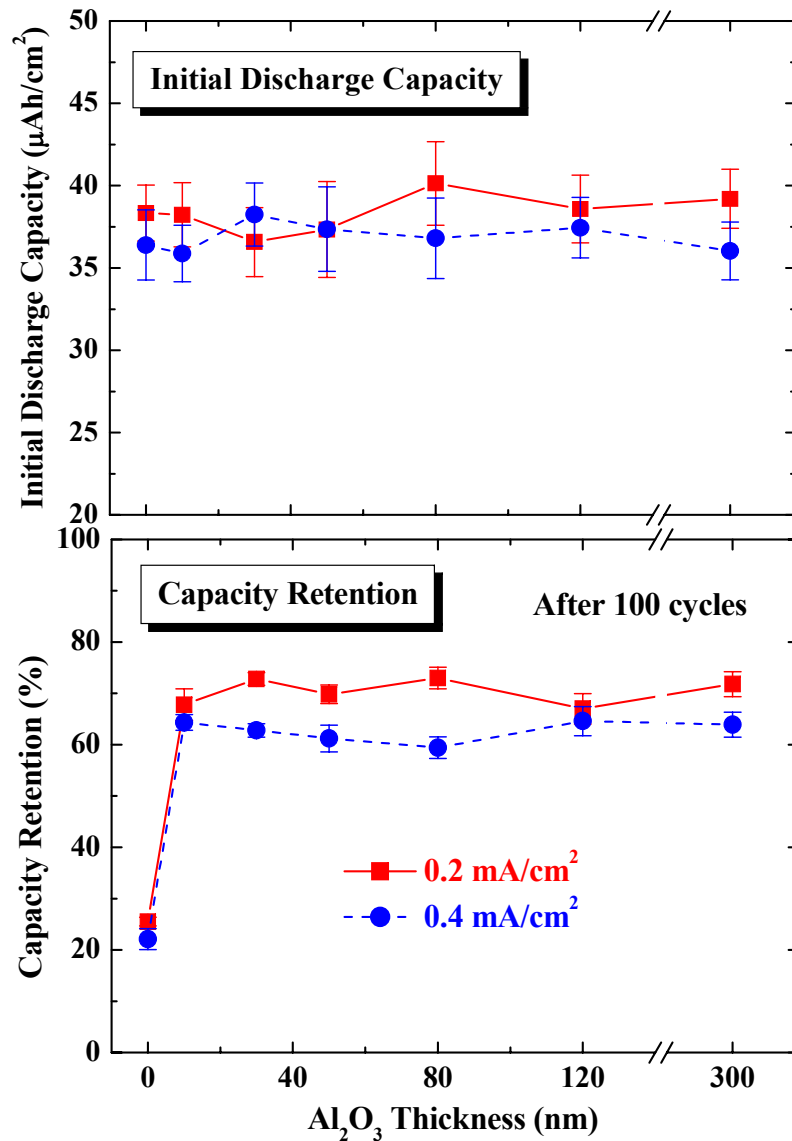
The charge capacity (for Li deintercalation) shows faster deterioration than the discharge capacity (for Li intercalation).

Al₂O₃-Coated LiCoO₂ Thin Film



- Cell voltage : 4.4 V - 2.75 V
- Current rates : 0.1 - 0.8 mA/cm²
- Half-cells (Li/LiCoO₂), 1 M LiPF₆ in EC/DEC
- At each cutoff step, the voltage was potentiostated until the current decreased to 10%.

Al_2O_3 Coating Layer as a Solid Electrolyte



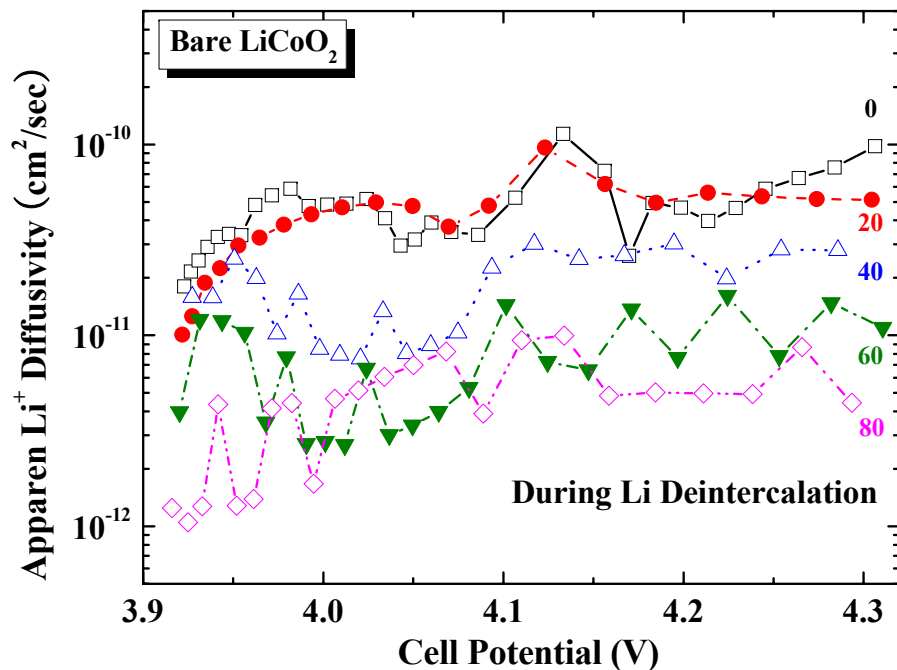
Oxidation/reduction reaction occurs at the Li-Al-O / LiCoO₂ interface.

Composition of Li-Al-O needs to be determined.

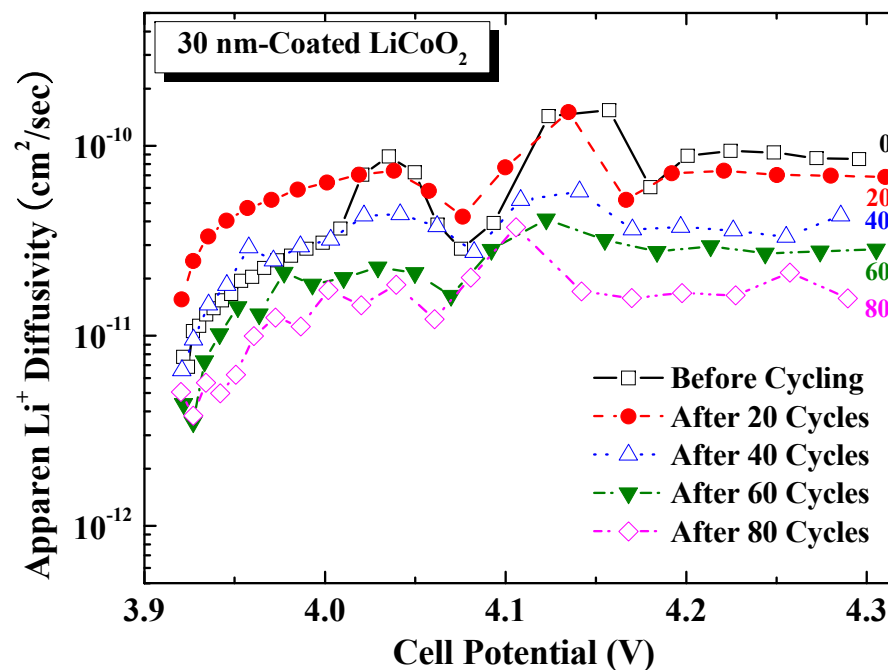
Ex) 0.7Li₂O-0.3Al₂O₃: $\sim 10^{-7}$ S/cm at 23°C
 A. M. Glass *et al.*, *J. Appl. Phys.* (1980).

Apparent Li^+ Diffusivity during Li Deintercalation (Charging)

Uncoated LiCoO_2 Thin Film

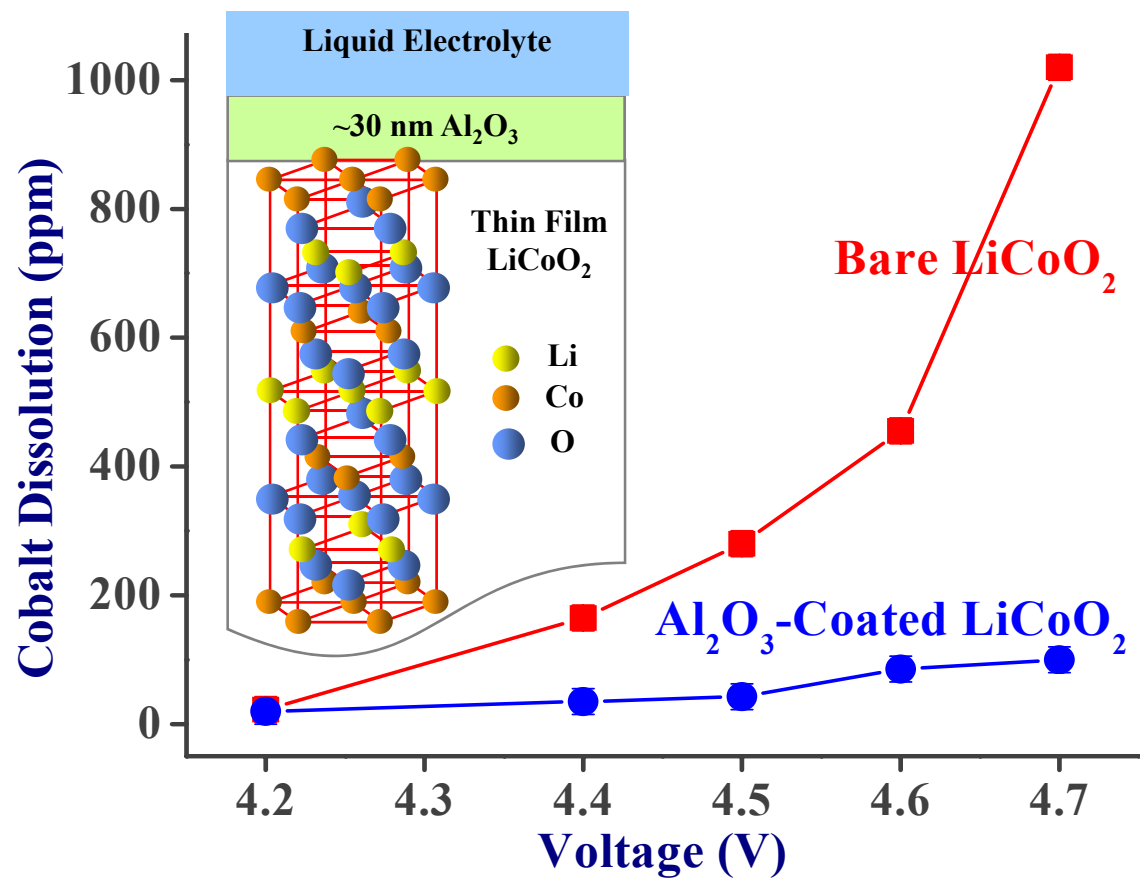


Al_2O_3 -Coated LiCoO_2 Thin Film



- Clearly enhanced by 30 nm-thick Al_2O_3 coating.
- Maxima at ~ 4.13 V, corresponding to the monoclinic phase.
- Two minima at the cell potential, corresponding to the phase transition between a hexagonal and monoclinic phase.

Cobalt Dissolution from Thin-Film LiCoO_2 Cathodes



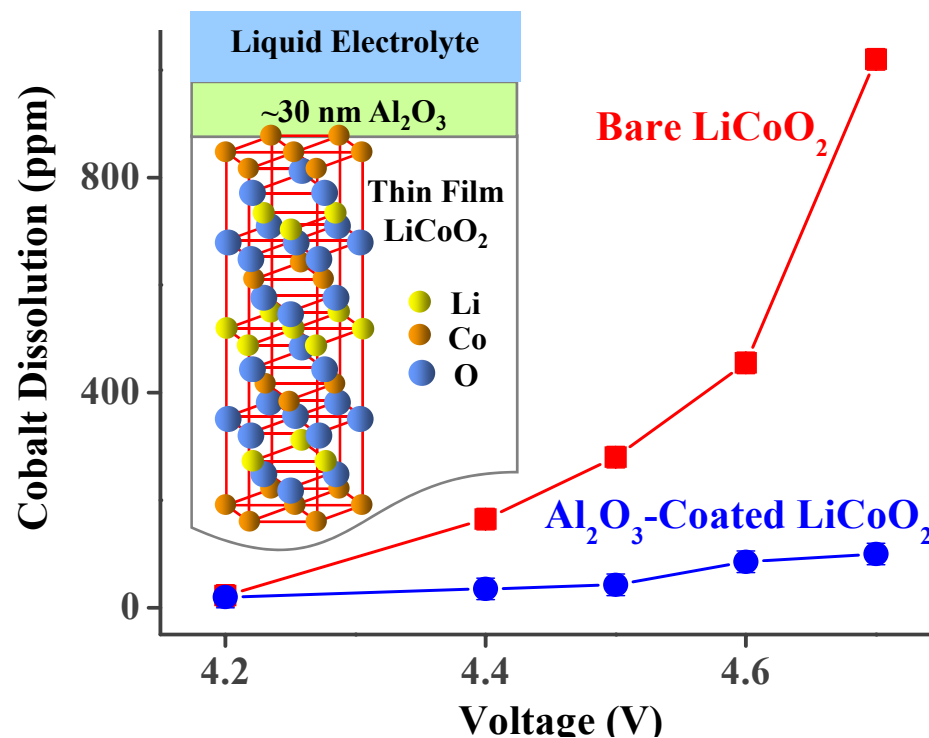
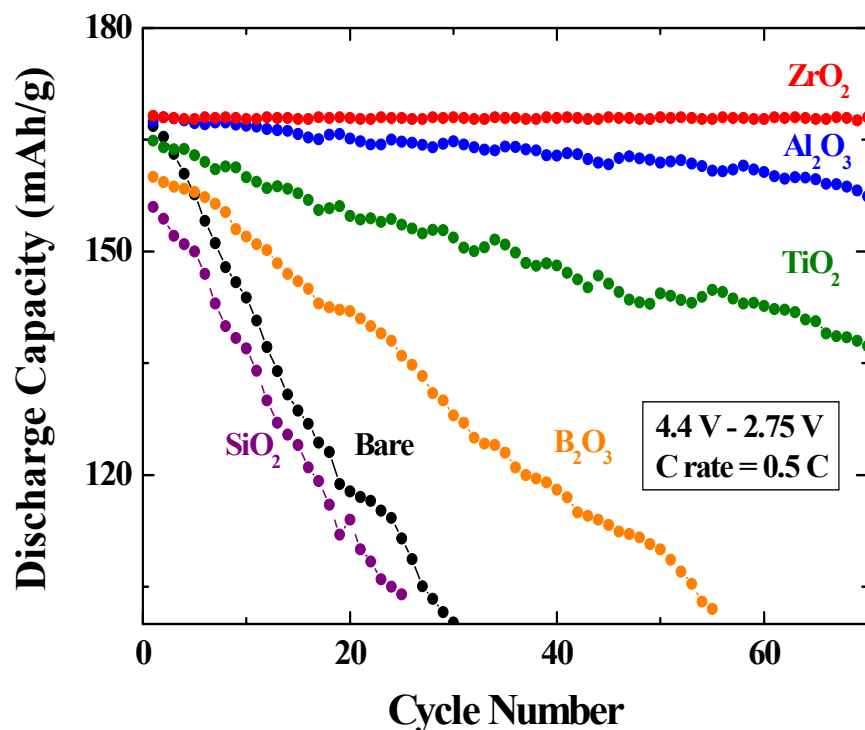
ICP-MS after floating for 12 days



Al_2O_3 coating can effectively suppress the Co dissolution

➤ Y. J. Kim, H. Kim, B. Kim, D. Ahn, J.-G. Lee, T.-J. Kim, D. Son, J. Cho, Y.-W. Kim, and B. Park, *Chem. Mater.* **15**, 1505 (2003).

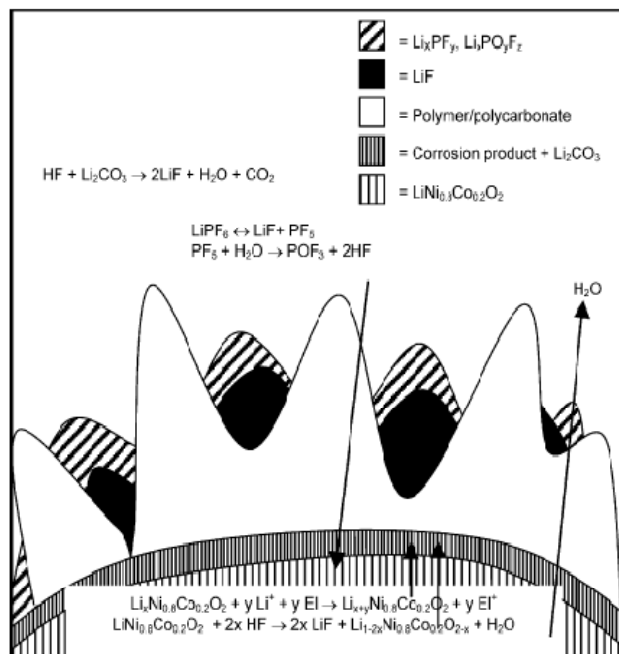
The Effect of Metal-Oxide Coating in LiCoO_2



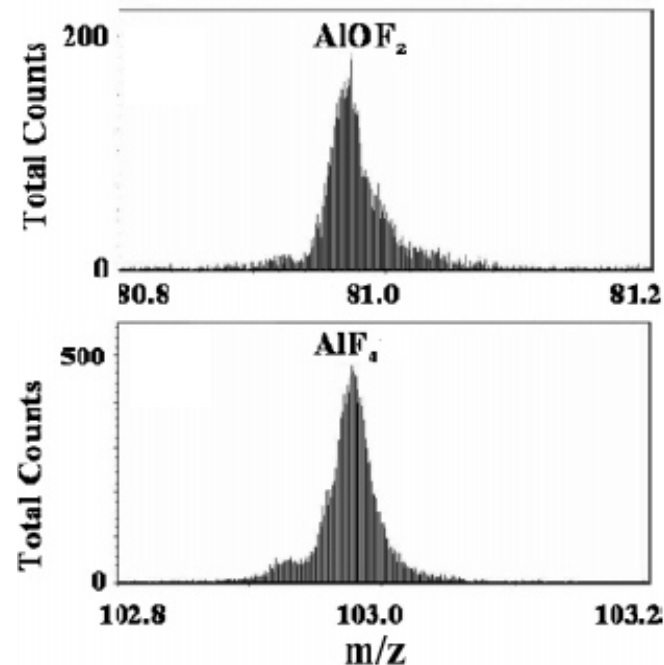
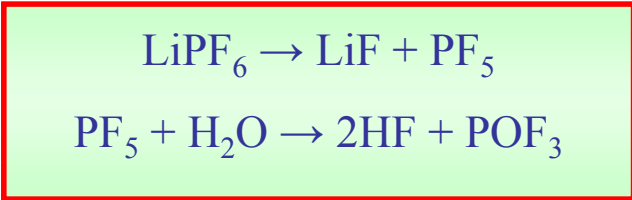
Enhanced Stability by Nanoscale Coating

- J. Cho, Y. J. Kim, T.-J. Kim, and B. Park, *Angew. Chem. Int. Ed.* **40**, 3367 (2001).
- J. Cho, Y. J. Kim, and B. Park, *Chem. Mater.* **12**, 3788 (2000).

HF Scavenging Effect



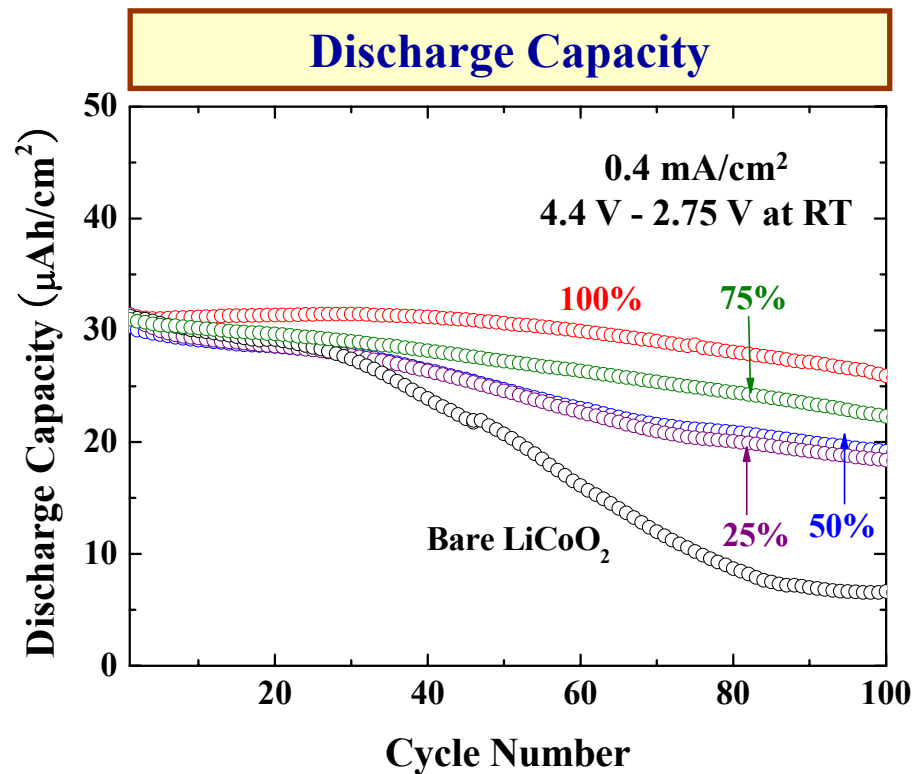
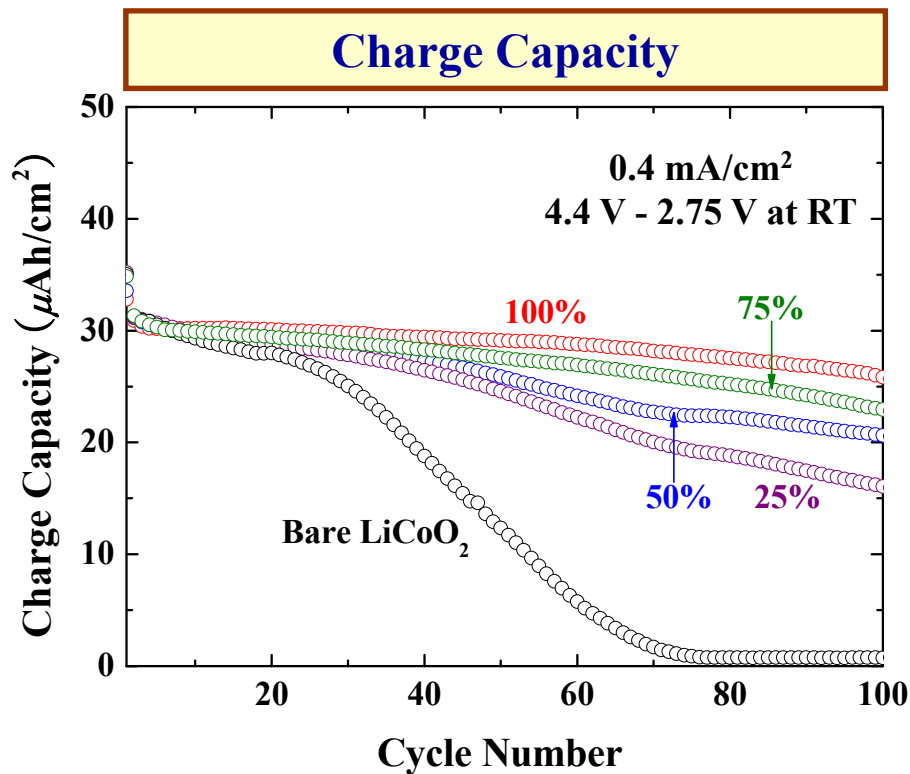
Aurbach's group, *J. Electrochem. Soc.* (1989).
Edstrom's group, *Electrochim. Acta* (2004).



Y.-K. Sun's group, *Chem. Mater.* (2005).



Al₂O₃-Coating Coverage Effect on Cycling Performance

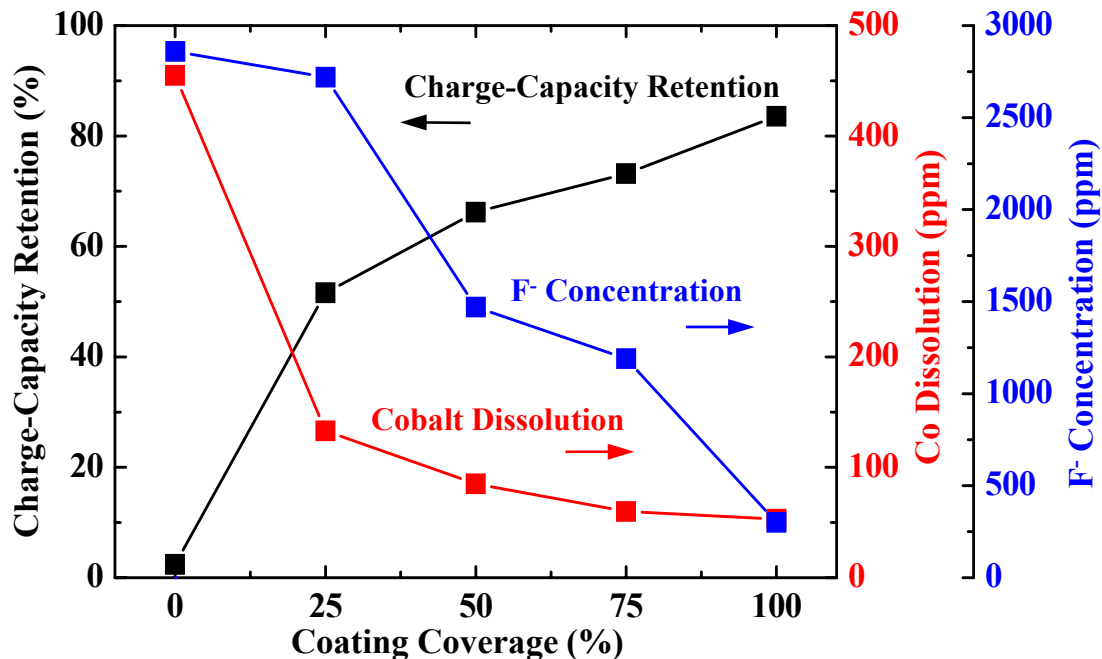


**Enhanced cycle-life performances
by Al₂O₃ coating**



**Suppression of HF attack by
Al₂O₃ partial coating**

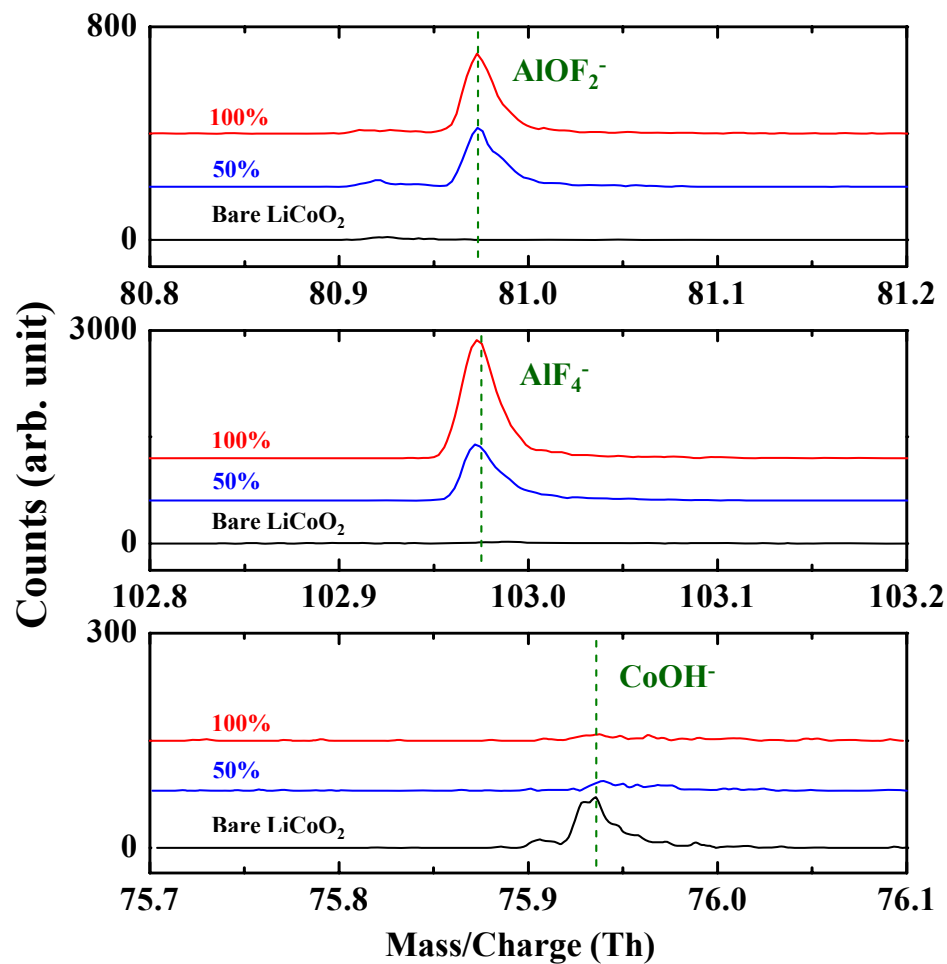
Co Dissolution and F⁻ Concentration as Coating Coverage



Protection from HF attack
↓
Lowered amount of HF
↓
Decreased Co dissolution

As coating coverage increases,
Co dissolution and F⁻ concentration decrease.

Secondary Ion Mass Spectroscopy (SIMS)

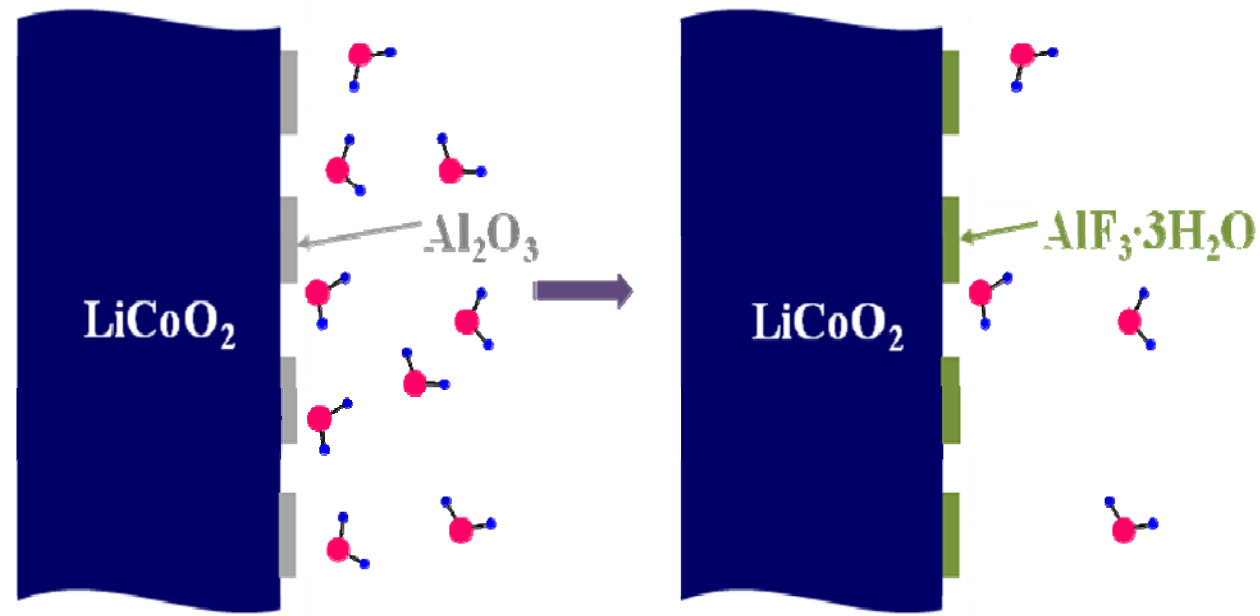


Mass/Charge (Th)

- AlF₄⁻: 102.98 Th
- AlOF₂⁻: 80.97 Th
- CoOH⁻: 75.94 Th

AlF₄⁻ and AlOF₂⁻ from AlF₃·3H₂O generated by the reaction among Al₂O₃, HF and H₂O.

Schematic Figure



- Al_2O_3 coating layer: Transformed into $\text{AlF}_3 \cdot 3\text{H}_2\text{O}$ layer
- H_2O decreased in the electrolyte.

Metal-Phosphate-Coated LiCoO_2 Cathode Materials

J. Cho, Y.-W. Kim, B. Kim, J.-G. Lee, and B. Park
Angew. Chem. Int. Ed. **42**, 1618 (2003).

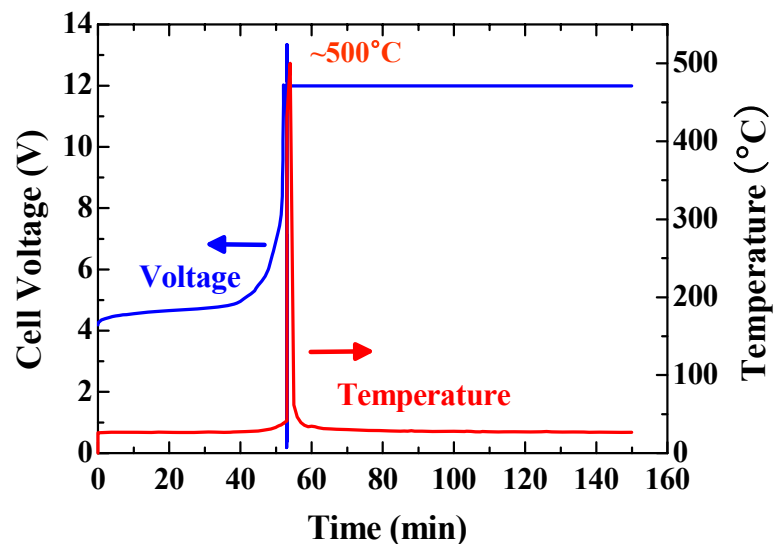
J.-G. Lee, B. Kim, J. Cho, Y.-W. Kim, and B. Park
J. Electrochem. Soc. **151**, A801 (2004).

B. Kim, C. Kim, D. Ahn, T. Moon, J. Ahn, Y. Park, and B. Park
Electrochem. Solid-State Lett. **10**, A32 (2007).

D. Ahn, C. Kim, J.-G. Lee, B. Kim, Y. Park, and B. Park
J. Mater. Res. **22**, 688 (2007).

12 V Overcharge Test at 1 C Rate

Bare LiCoO₂

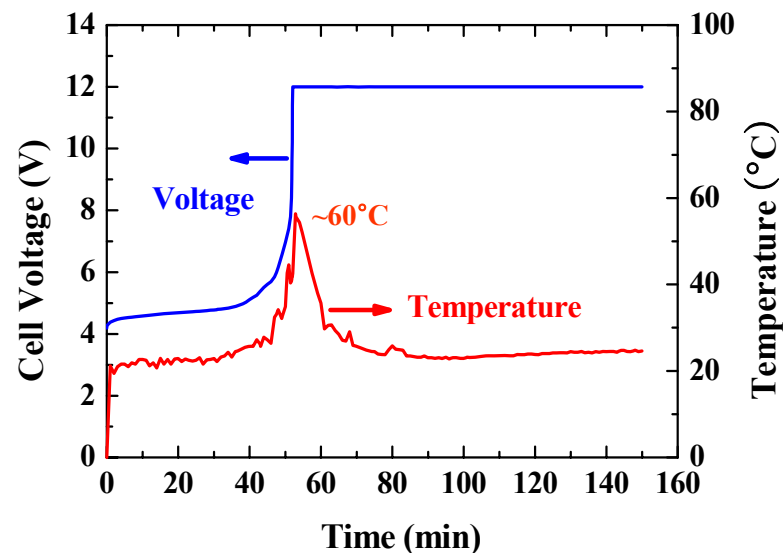


Short Circuit & Temperature Uprise



Cell Fired and Exploded

AlPO₄-Coated LiCoO₂



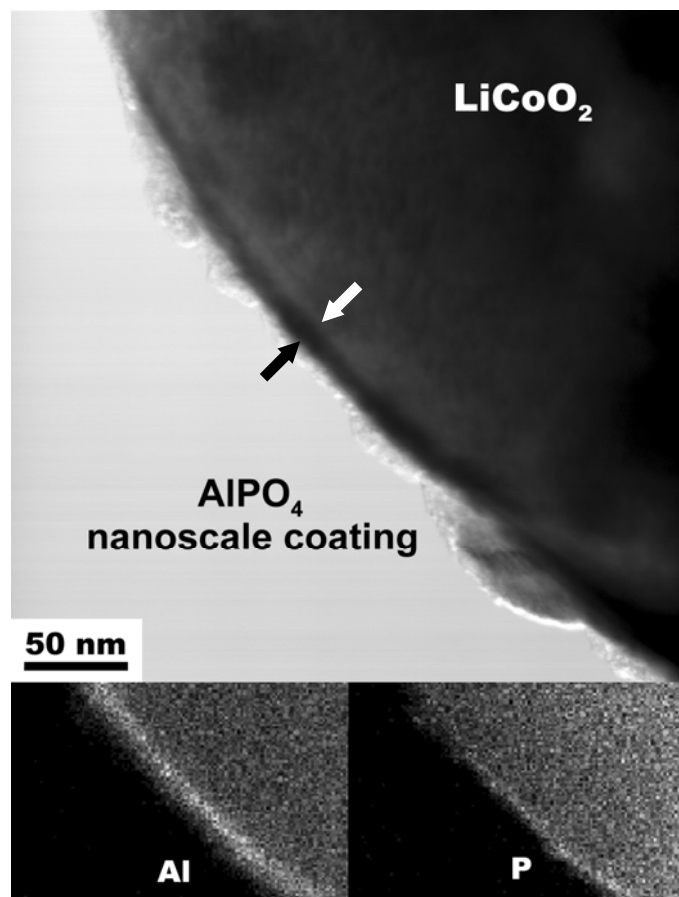
Temperature only ~60°C



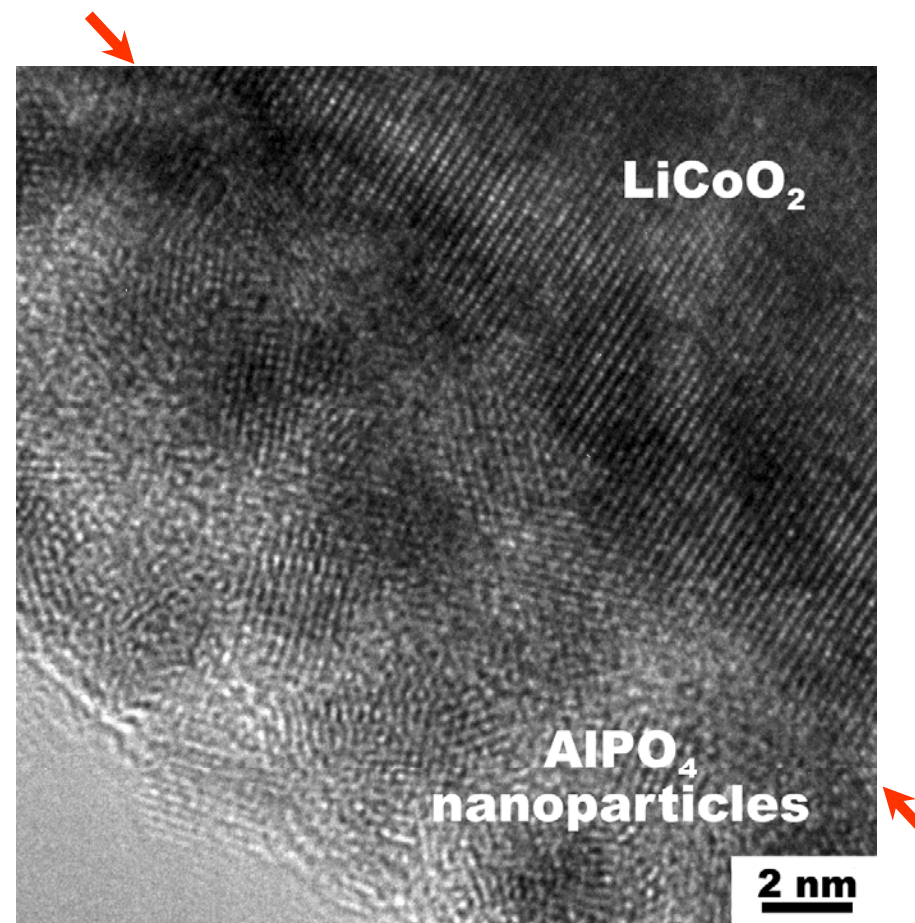
Excellent Thermal Stability

➤ B. Park's group, *Angew. Chem. Int. Ed.* (2001).

TEM Image of AlPO_4 Nanoparticle-Coated LiCoO_2

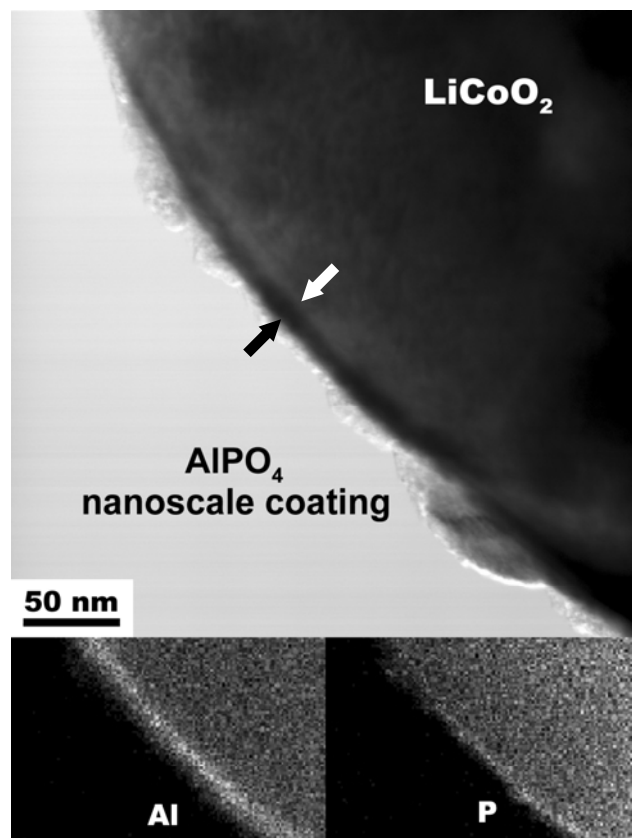


EDS confirms the Al and P components in the nanoscale-coating layer.



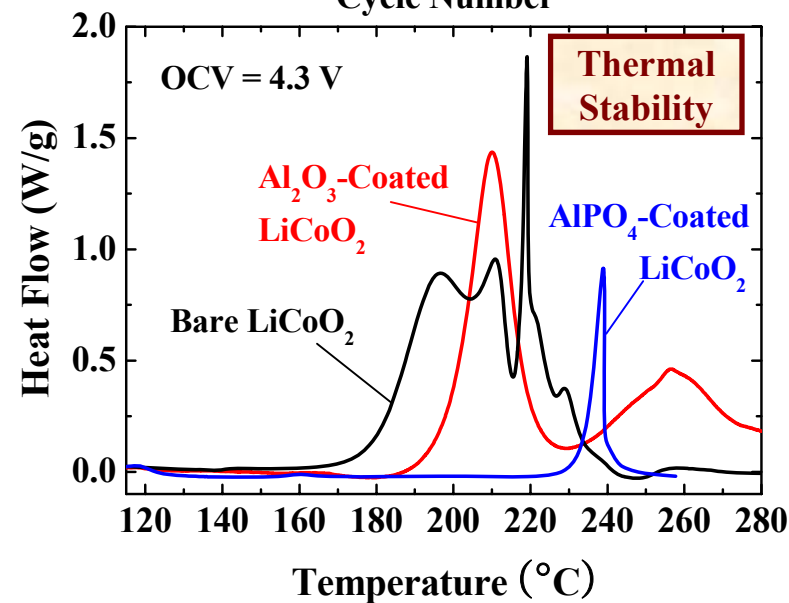
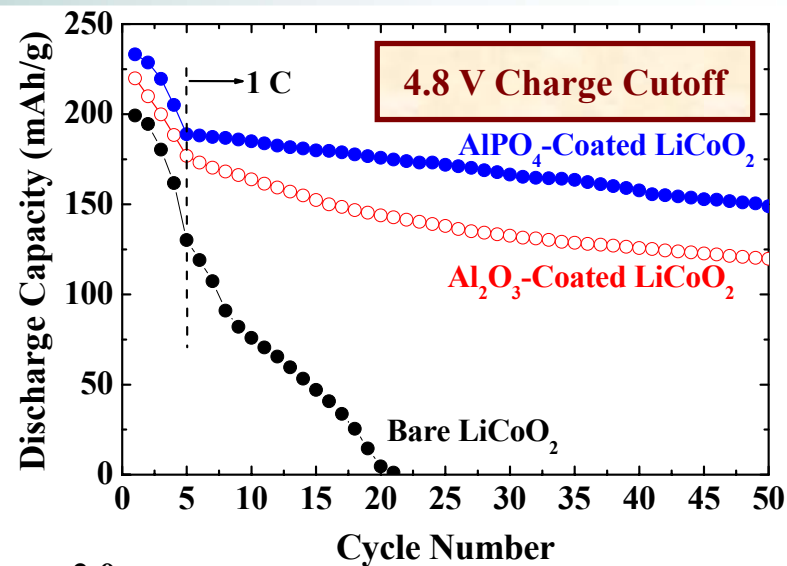
AlPO_4 nanoparticles (~3 nm) embedded in the coating layer (~15 nm).

AlPO_4 -Nanoparticle-Coated LiCoO_2



TEM bright-field image of the AlPO_4 nanoparticle-coated LiCoO_2 ; EDS confirms the Al and P components in the coating layer.

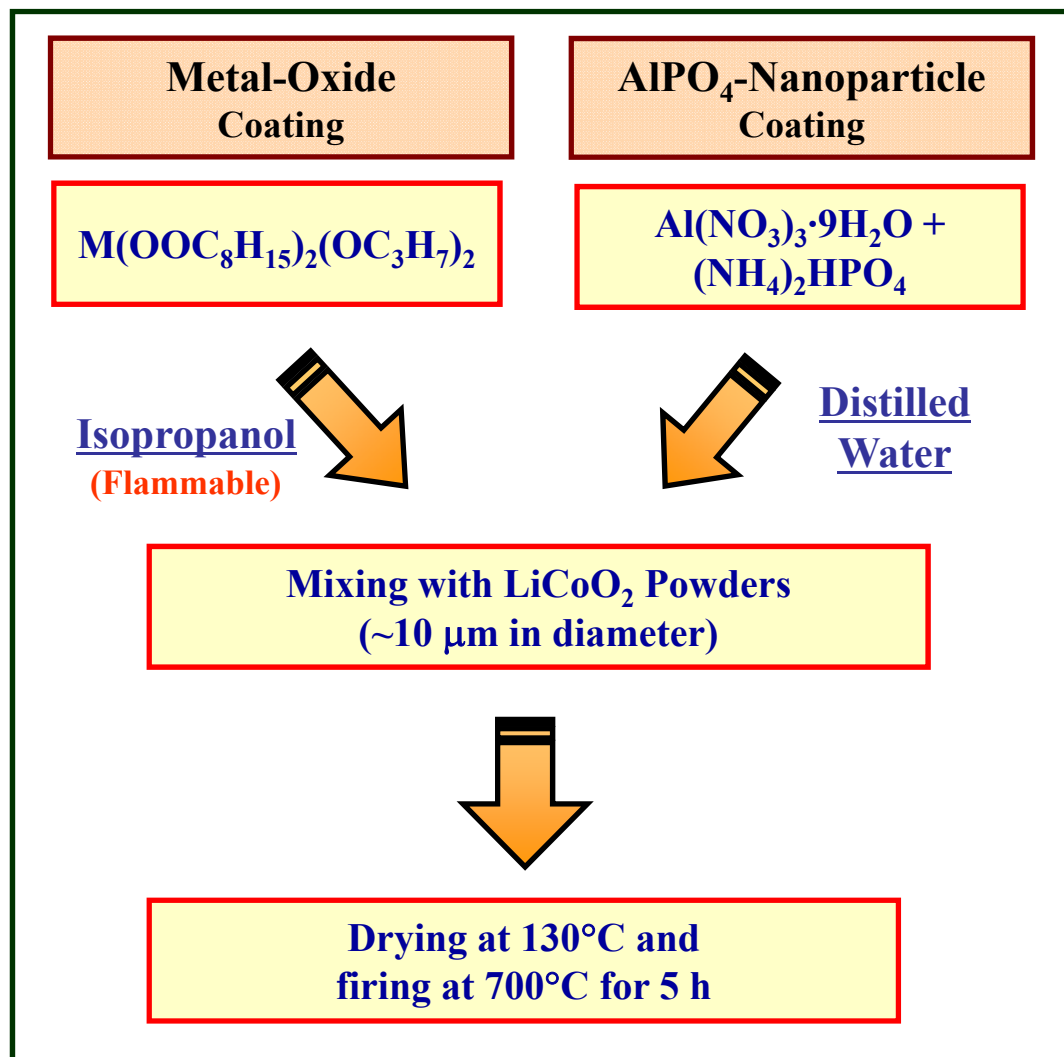
EDS confirms the Al and P components in the nanoscale-coating layer.



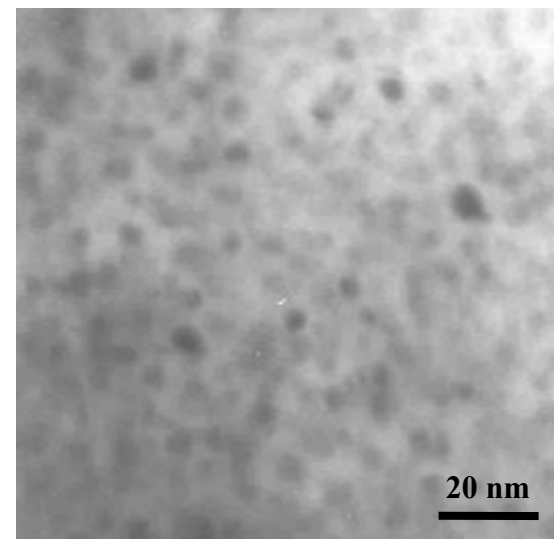
➤ B. Park's group, *Angew. Chem. Int. Ed.* (2003).

➤ B. Park's group, *J. Power Sources* (2005).

Sample Preparation

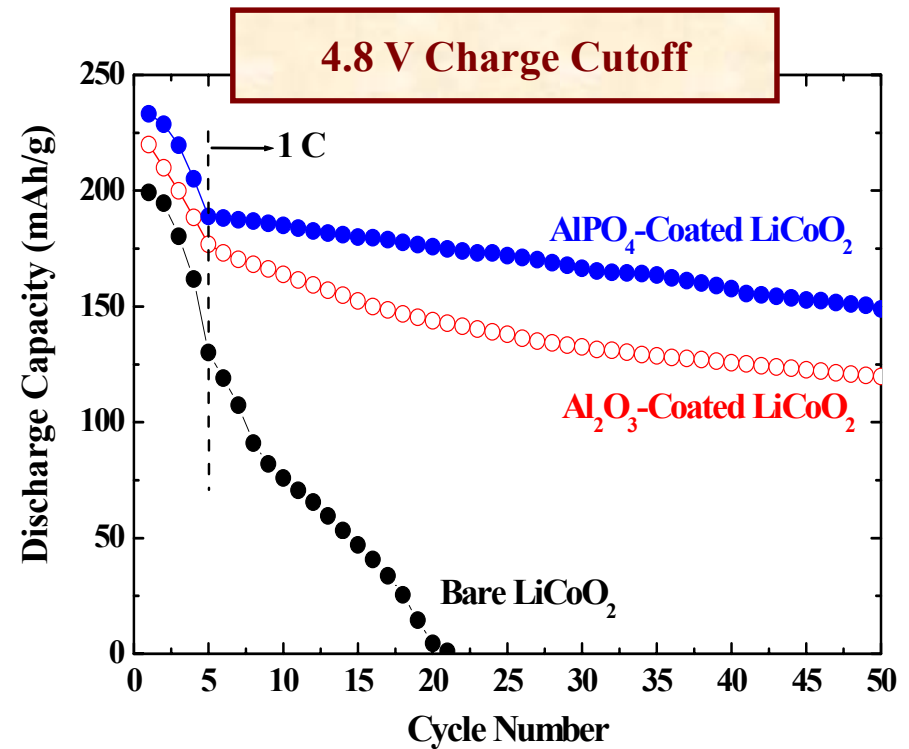
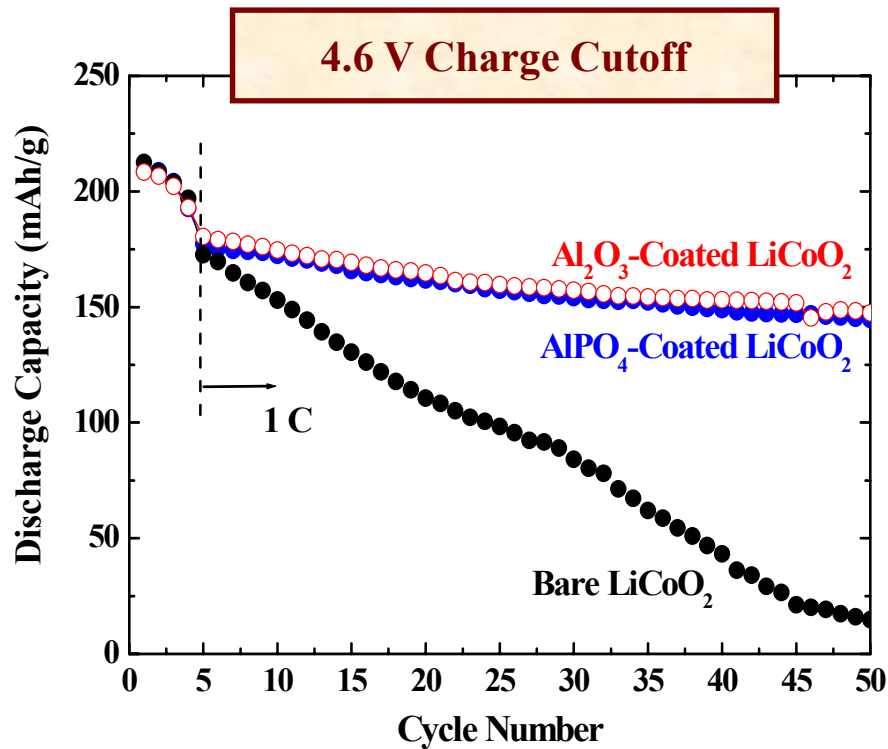


AlPO₄-Nanoparticle Solution



- **AlPO₄-Nanoparticle Coating**
 - Continuous Coating Layer
 - Easy Control (shape, size, coating thickness)

Charge-Discharge Tests

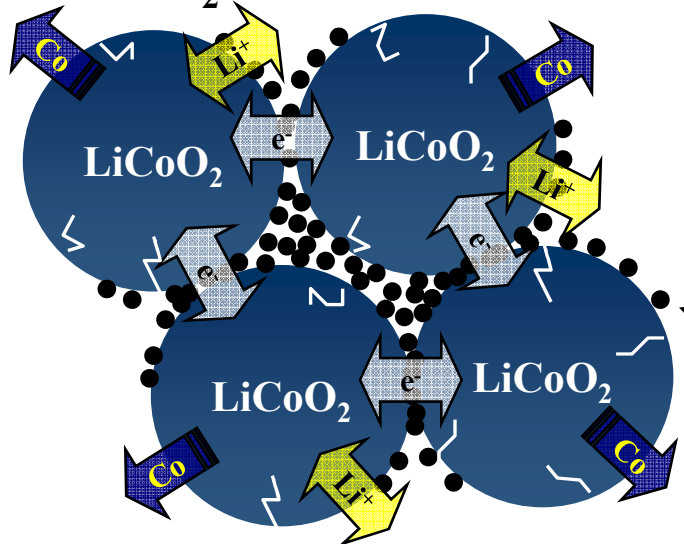


AlPO₄-coated LiCoO₂ is very stable at the high-charged state.

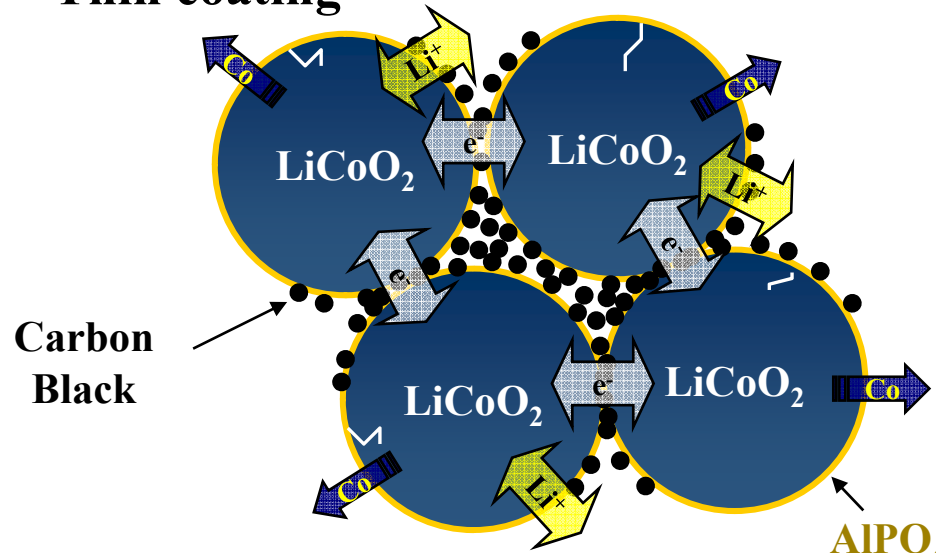
➤ J. Cho, T.-G. Kim, C. Kim, J.-G. Lee, Y.-W. Kim, and B. Park
J. Power Sources **146**, 58 (2005).

Coating-Thickness Effect

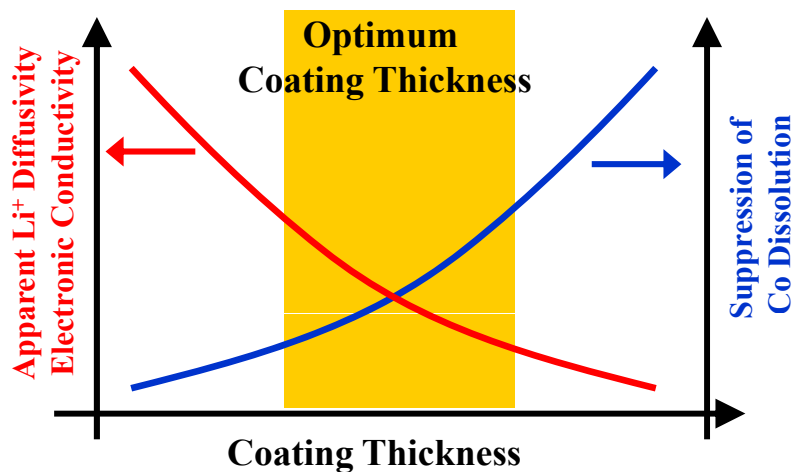
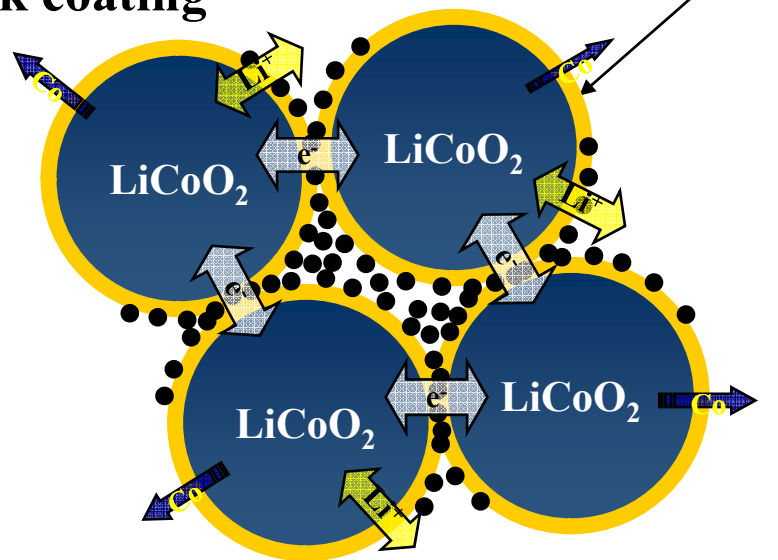
Bare LiCoO_2



Thin coating

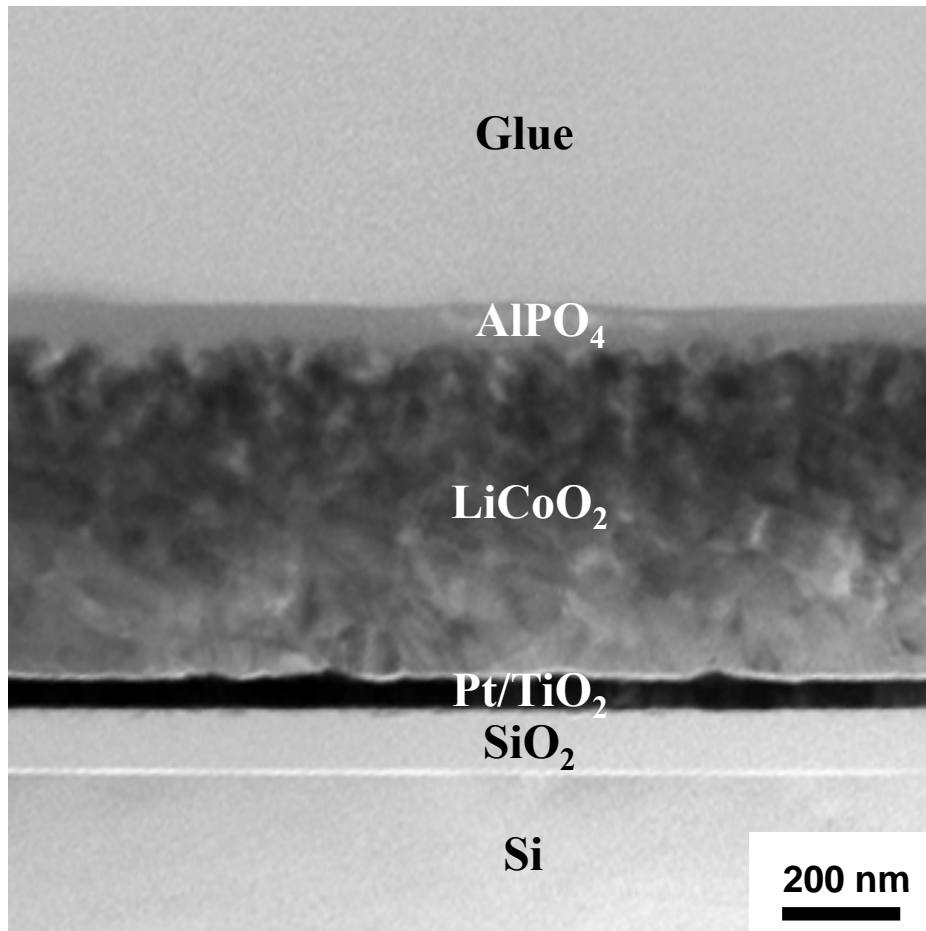


Thick coating

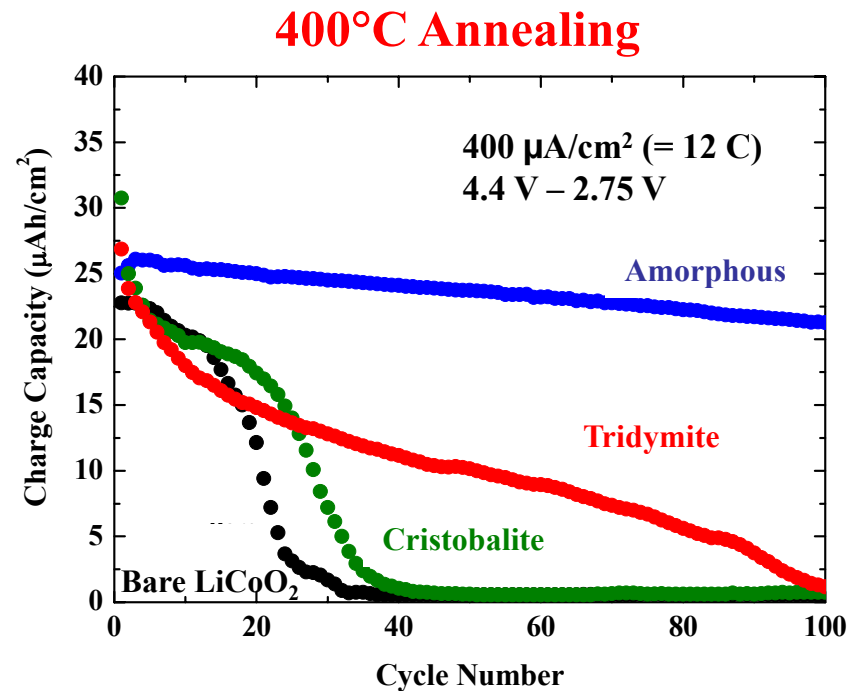


Below 1.0 wt. %-coated LiCoO_2 ?

Spin Coating of AlPO_4 Nanoparticles with Various Nanostructures



TEM confirms the uniform coating layer on LiCoO_2 thin film.



Optimum Nanostructures?

- B. Kim, C. Kim, D. Ahn, T. Moon, J. Ahn, Y. Park, and B. Park, *Electrochem. Solid-State Lett.* **10**, A32 (2007).

SnO₂ Nanoparticles

C. Kim, M. Noh, M. Choi, J. Cho, and B. Park
Chem. Mater. **17**, 3297 (2005).

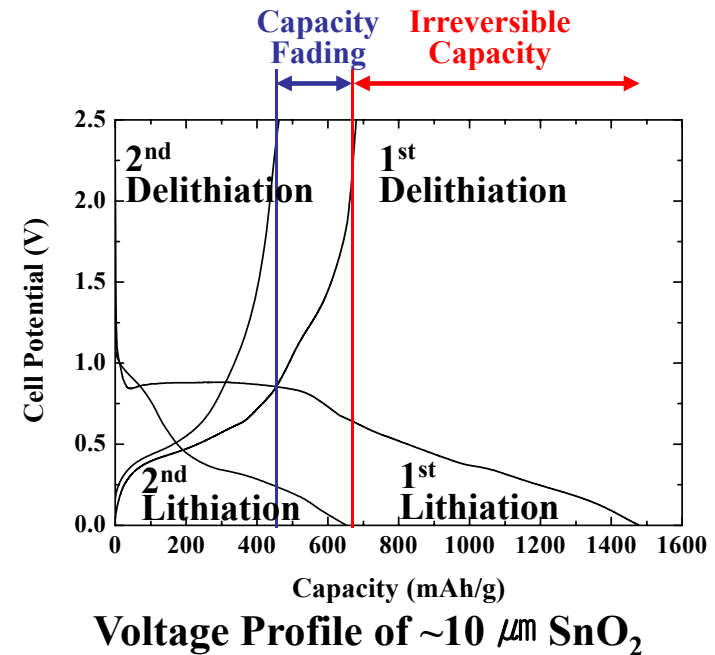
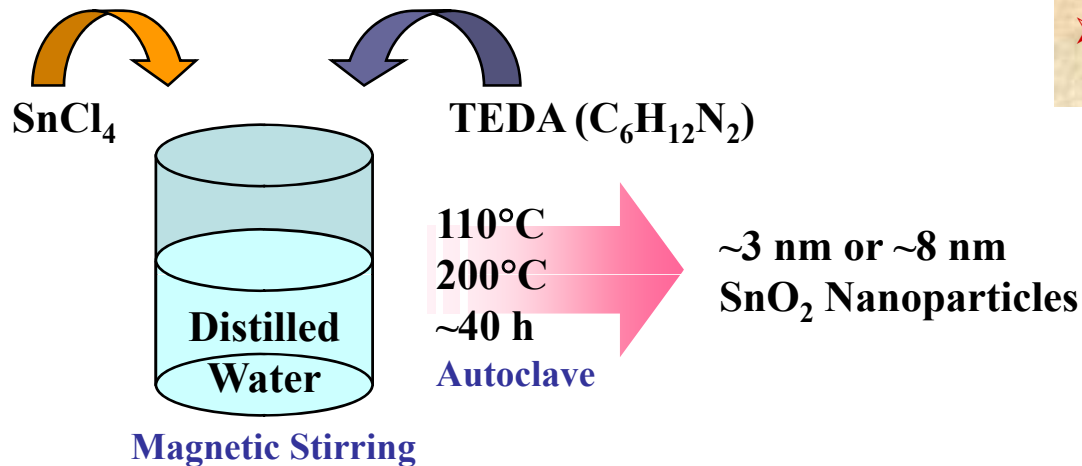
T. Moon, C. Kim, S.-T. Hwang, and B. Park
Electrochem. Solid-State Lett. **9**, A408 (2006).

SnO₂ Nanoparticles: Mechanisms and Synthesis

Problems of SnO₂ Electrode

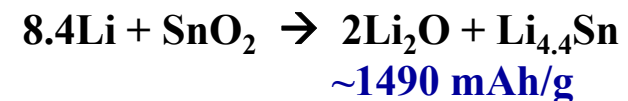
- Severe capacity loss by volume change between Li_xSn and Sn phases (~300%).
- Particles become detached and electrically inactive.

SnO₂ Nanoparticles: Effective Solution

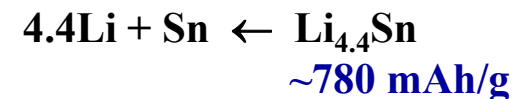


➤ T.-J. Kim, D. Son, J. Cho, B. Park, and H. Yang *Electrochim. Acta* **49**, 4405 (2004).

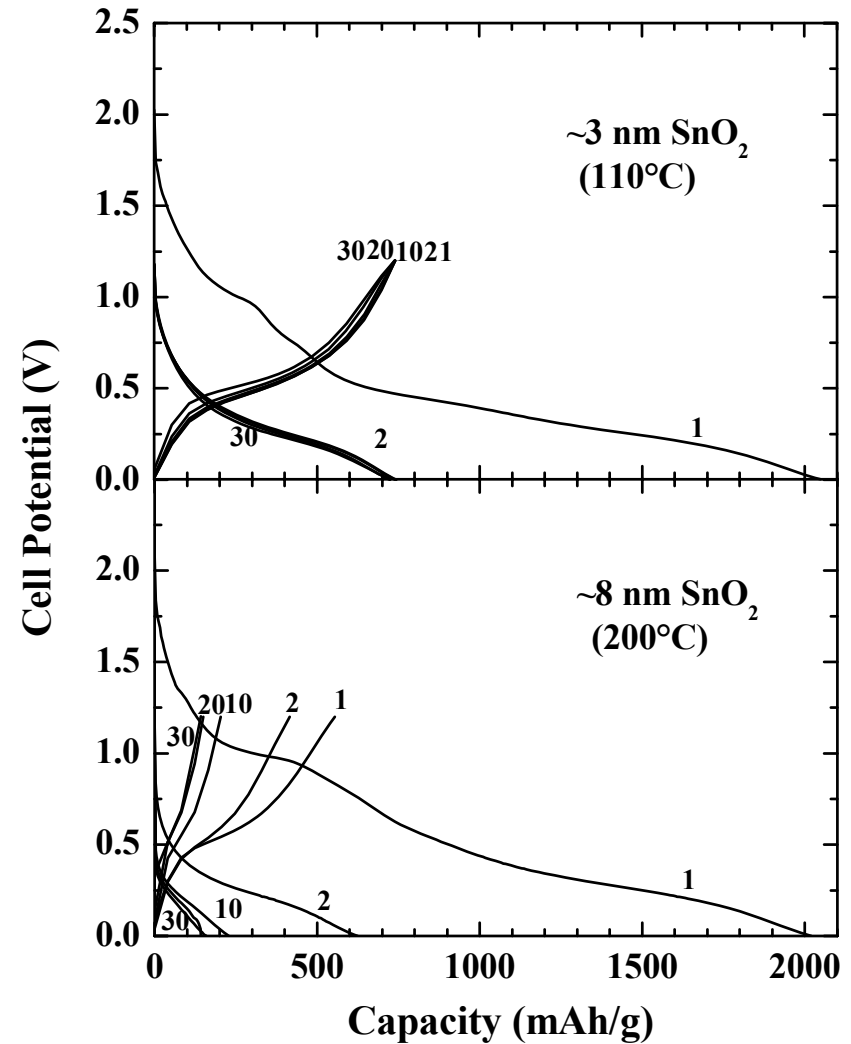
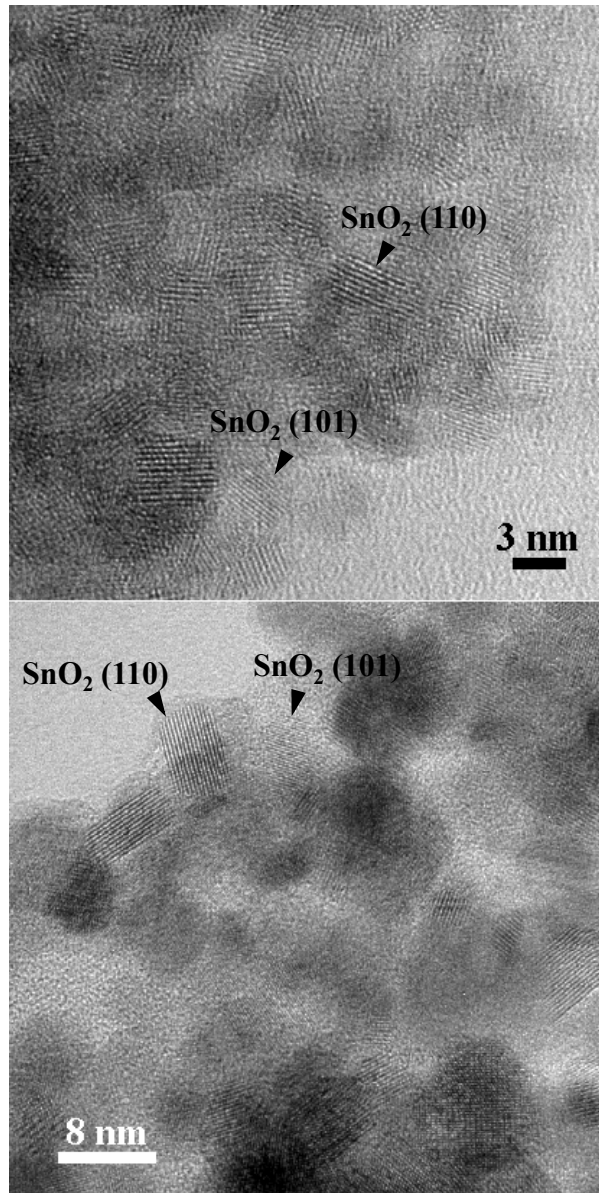
1st Lithiation:



1st Delithiation:

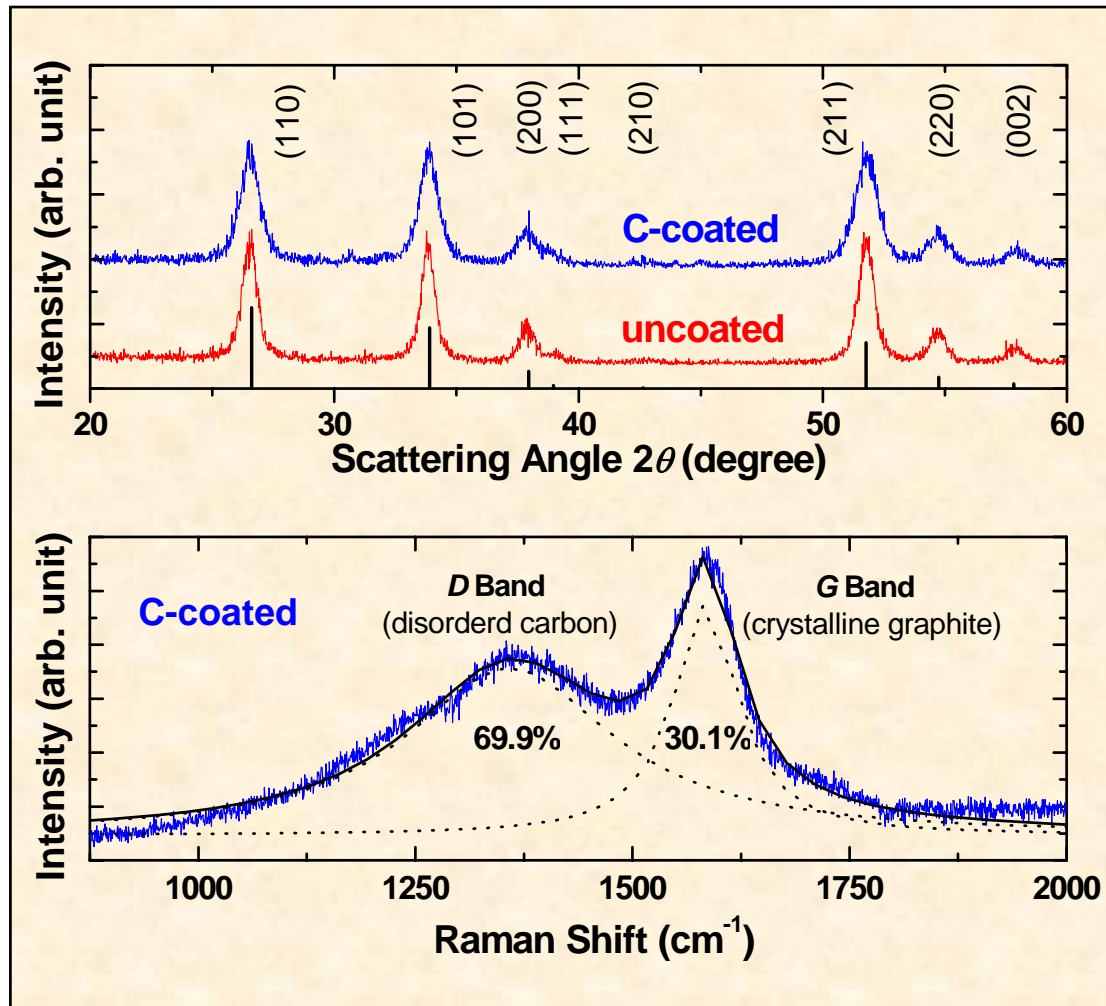


SnO₂-Nanoparticle Anode with Different Particle Sizes

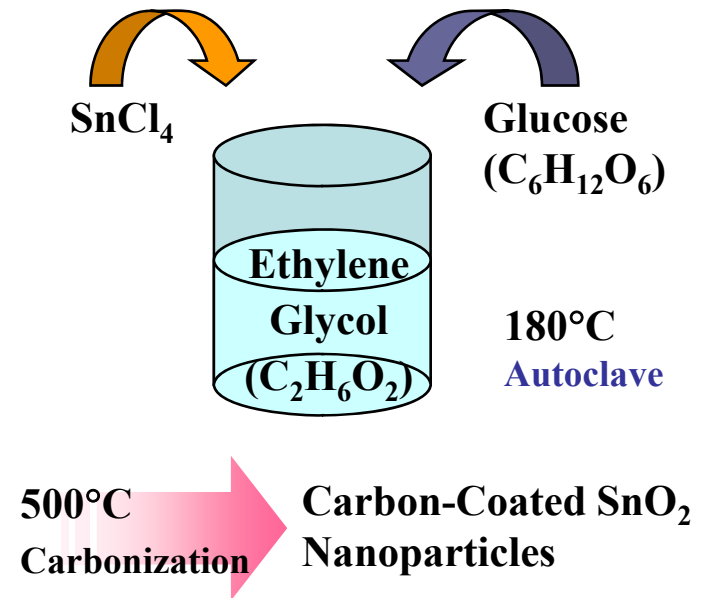


➤ C. Kim, M. Noh, M. Choi, J. Cho, and B. Park *Chem. Mater.* **17**, 3297 (2005).

Carbon-Coated SnO₂ Nanoparticles: Synthesis



Disordered-carbon-coated SnO₂ nanoparticles

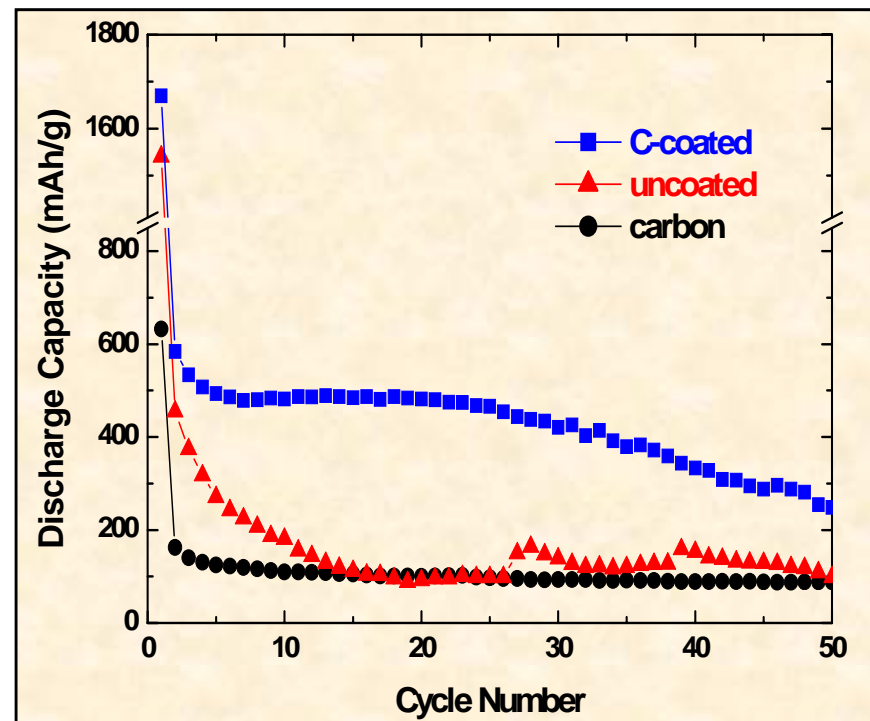
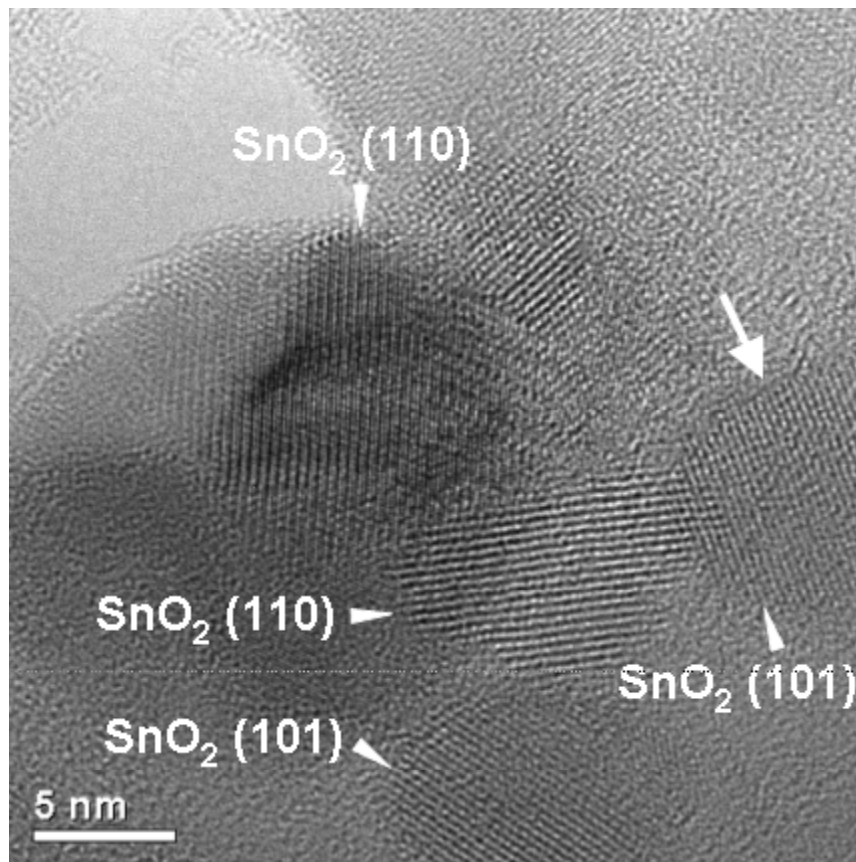


	Size	Local Strain
C-coated	8.8 ± 0.9 nm	0.59 ± 0.13%
uncoated	13.2 ± 1.1 nm	0.13 ± 0.08%

	SnO ₂ (wt. %)	C (wt. %)	H (wt. %)
C-coated	90	4.9	0.35
uncoated	97	0.061	0.074

by ICP

Carbon-Coated SnO₂ Nanoparticles



➤ T. Moon, C. Kim, S.-T. Hwang, and B. Park
Electrochem. Solid-State Lett. **9**, A408 (2006).

- Most of the nanoparticles are well dispersed.
- SnO₂ nanoparticles are surrounded by disordered carbon.
(graphite-interlayer spacing \cong 0.35 nm)
- Capacity contribution of disordered carbon is \sim 10 mAh/g.

Mesoporous Tin Phosphate

E. Kim, D. Son, T.-G. Kim, J. Cho, B. Park, K.-S. Ryu, and S.-H. Chang
Angew. Chem. Int. Ed. **43**, 5987 (2004).

J.-G. Lee, D. Son, C. Kim, and B. Park
J. Power Sources **172**, 908 (2007).

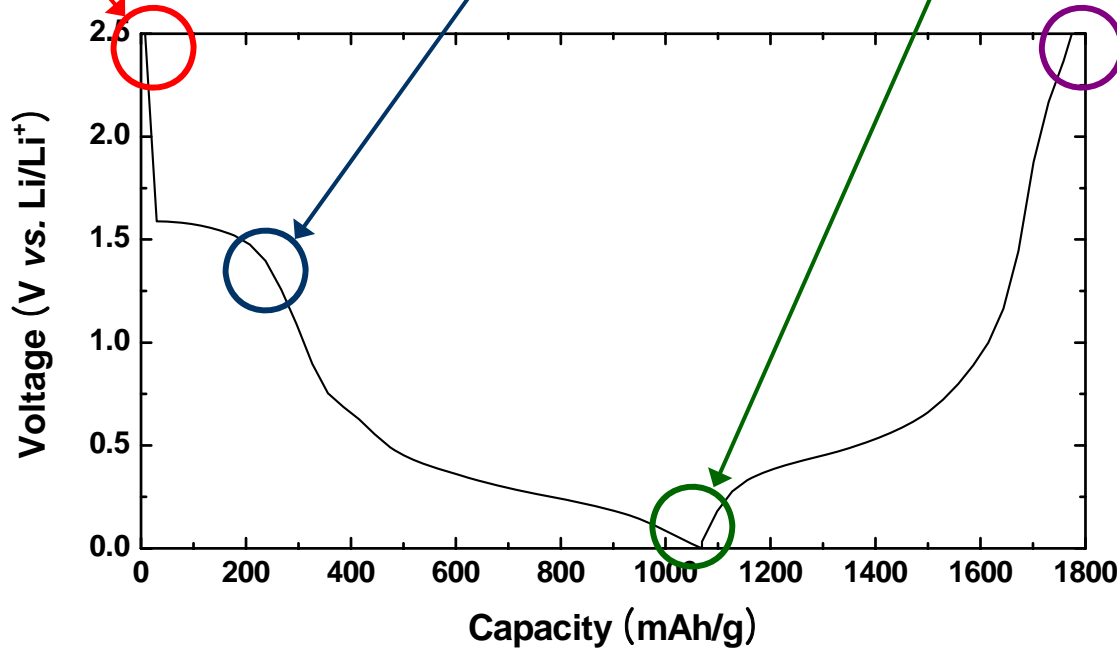
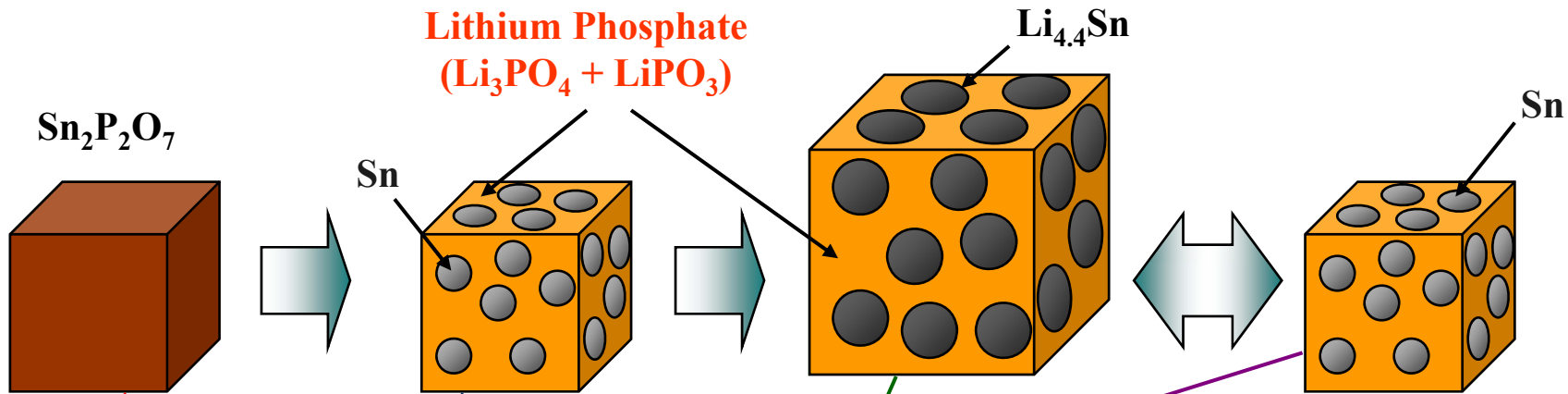
Tin-Phosphate Anodes

Open Circuit

Reduction of Sn

Fully Lithiated

Fully Delithiated



Volume expansion problem

Nanostructural approach
Mesoporous structure

Mesoporous Materials

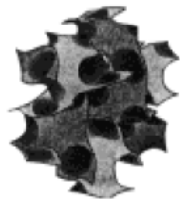
Mesoporous material:

- Inorganic solids with pore diameters of 2 – 50 nm
- Long-range ordering of pores

Hexagonal

Cubic

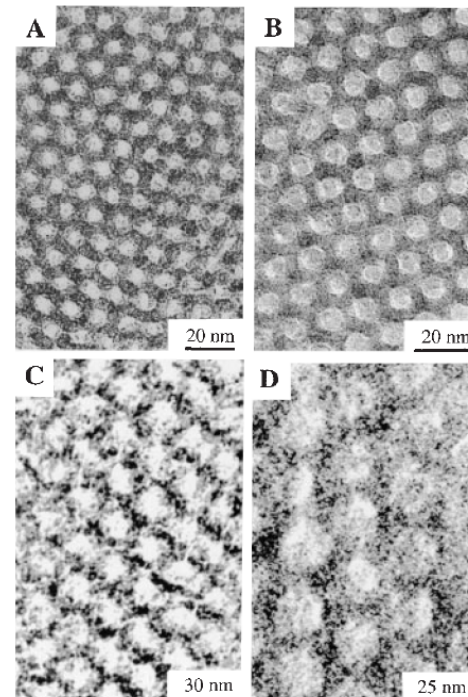
Layered



d_{100} spacing

➤ J. Y. Ying's group (MIT),
Angew. Chem. Int. Ed. (1999).

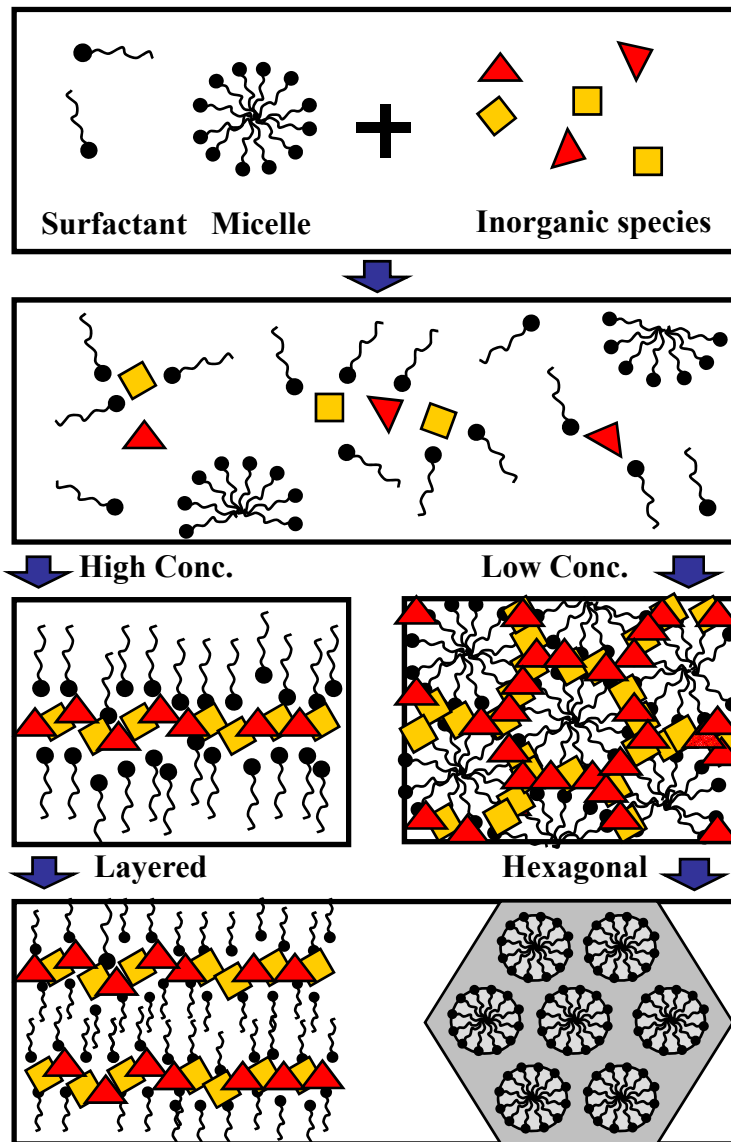
TEM Images of Hexagonal Mesoporous Silica



TEM images of calcined hexagonal SBA-15 mesoporous silica with different average pore sizes, from BET and XRD results (24): (A) 60 Å, (B) 89 Å, (C) 200 Å, and (D) 260 Å. The thicknesses of the silica walls are estimated to be (A) 53 Å, (B) 31 Å, (C) 40 Å, and (D) 40 Å. The micrographs were recorded digitally with a Gatan slow-scan charge-coupled device (CCD) camera on a JEOL 2010 electron microscope operating at 200 kV. The samples were prepared by dispersing the powder products as a slurry in acetone, which was then deposited and dried on a holey carbon film on a Cu grid. A low-exposure technique was used to reduce the effect of beam damage and sample drift. Focus-series measurements show that the bright areas correspond to the pores and dark areas to the silica walls.

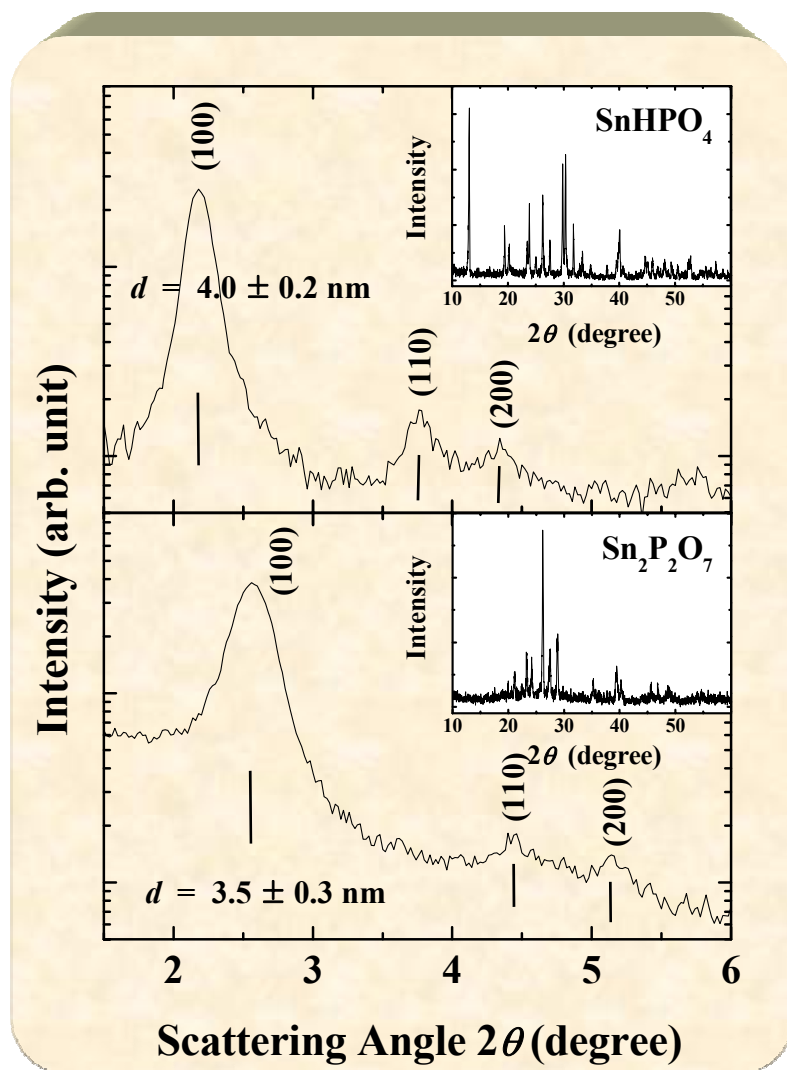
➤ G. D. Stucky's group (UC Santa Barbara),
Science (1998).

Mesoporous Materials



➤ G. D. Stucky's group (UC Santa Barbara),
Chem. Mater. (1994).

Synthesis of Mesoporous Tin Phosphates



Hexagonal mesostructure

SnF₂ and H₃PO₄ dissolved in distilled water
+
CTAB (CH₃(CH₂)₁₅N(CH₃)₃Br)
90°C Aging

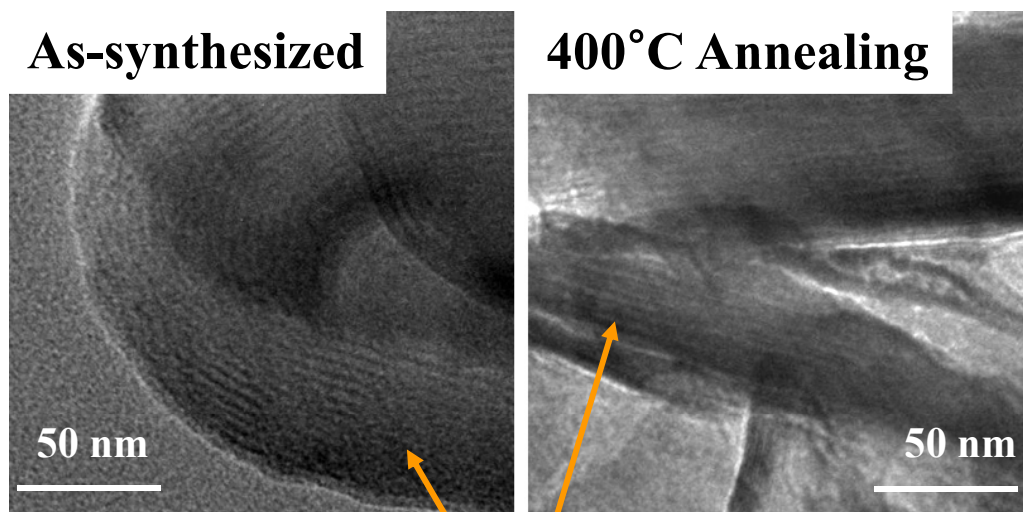
As Synthesized
Mesoporous Tin Phosphate / SnHPO₄

400°C Calcination
Mesoporous Tin Phosphate / Sn₂P₂O₇

➤ B. Park's group, *Angew. Chem. Int. Ed.* (2004).

Mesoporous Tin Phosphates

TEM Images



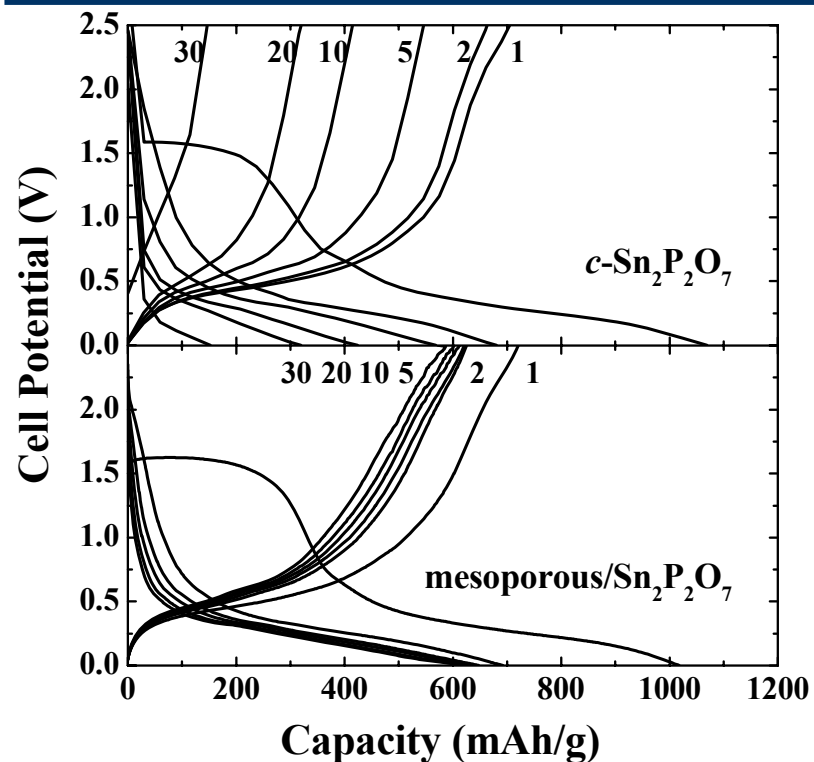
d spacing: ~ 3.8 nm

d spacing: ~ 3.3 nm

Mesopore channel (bright stripes)
Tin phosphate wall (dark stripes)

➤ B. Park's group, *Angew. Chem. Int. Ed.* (2004).

Electrochemical Properties

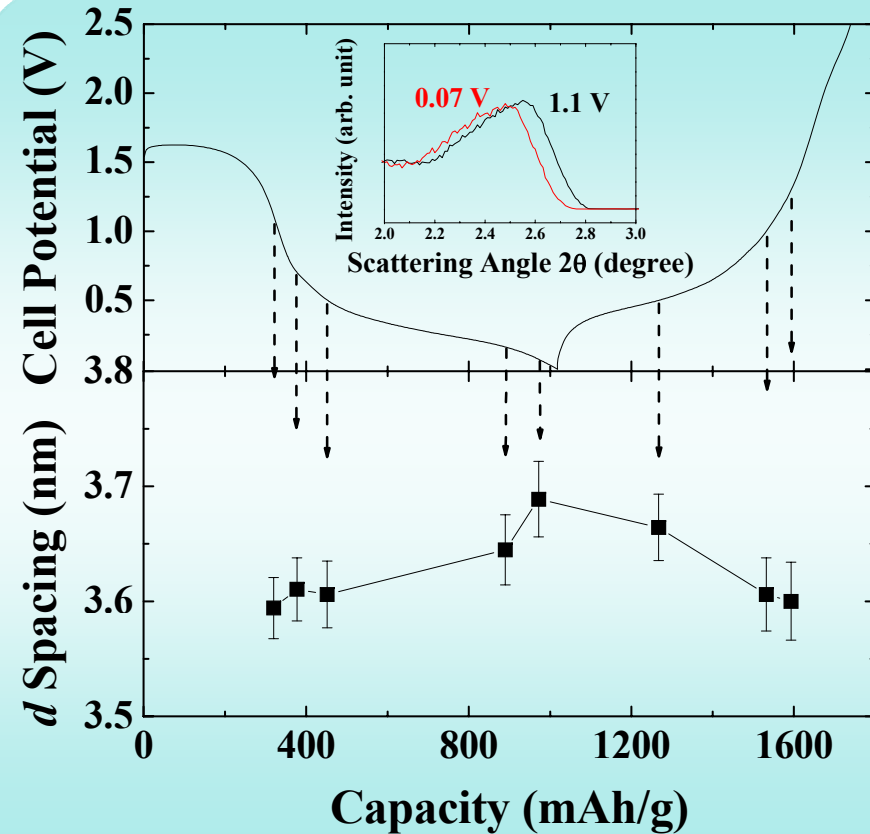


Novel Mesoporous/Crystalline Composite:

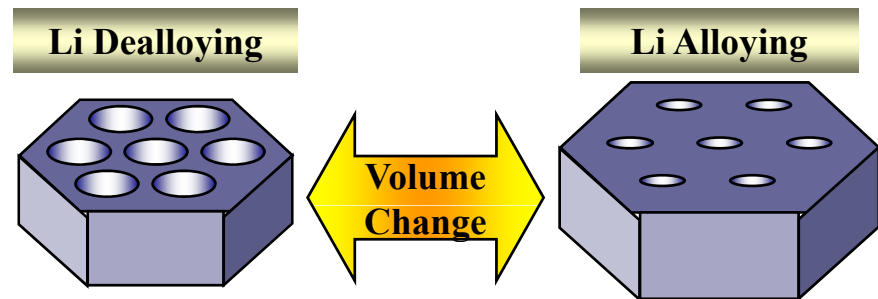
- High initial charge capacity (721 mAh/g)
- Excellent cycling stability (among the tin-based anodes)

Change of Mesoporous Structure during Charge/Discharge

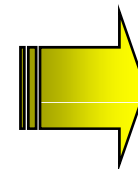
The Corresponding d Spacing



- ▶ The d spacing expands and shrinks with Li alloying/dealloying.
- ▶ The mesopores do not collapse during the 1st discharge and charge.

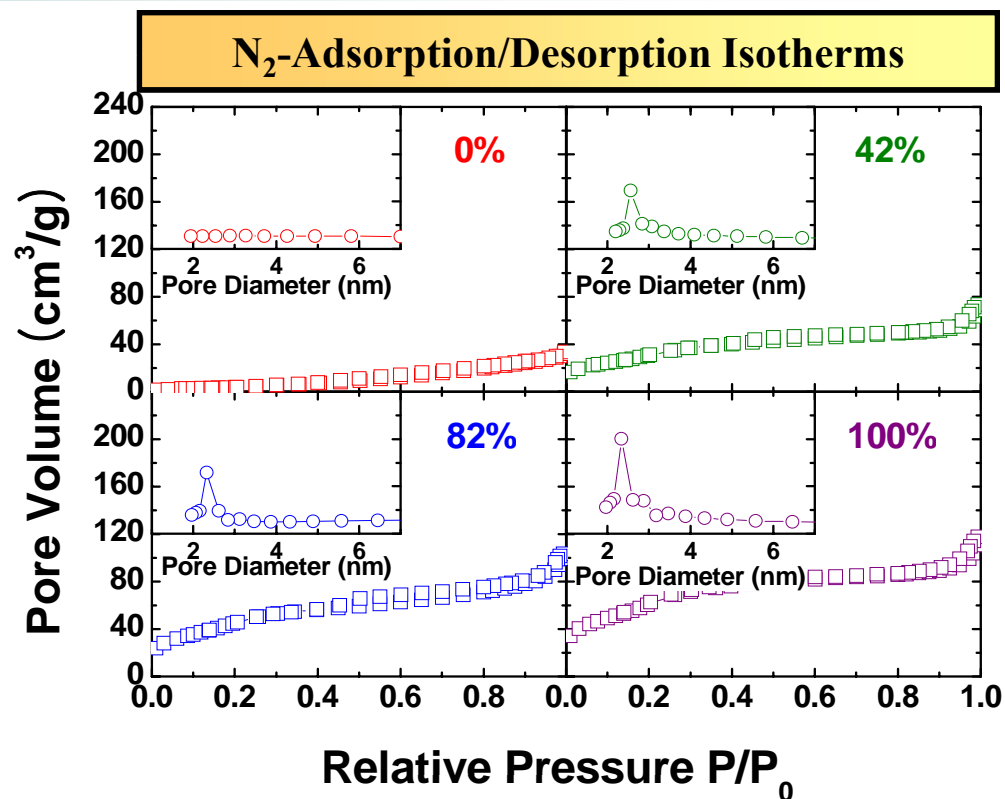
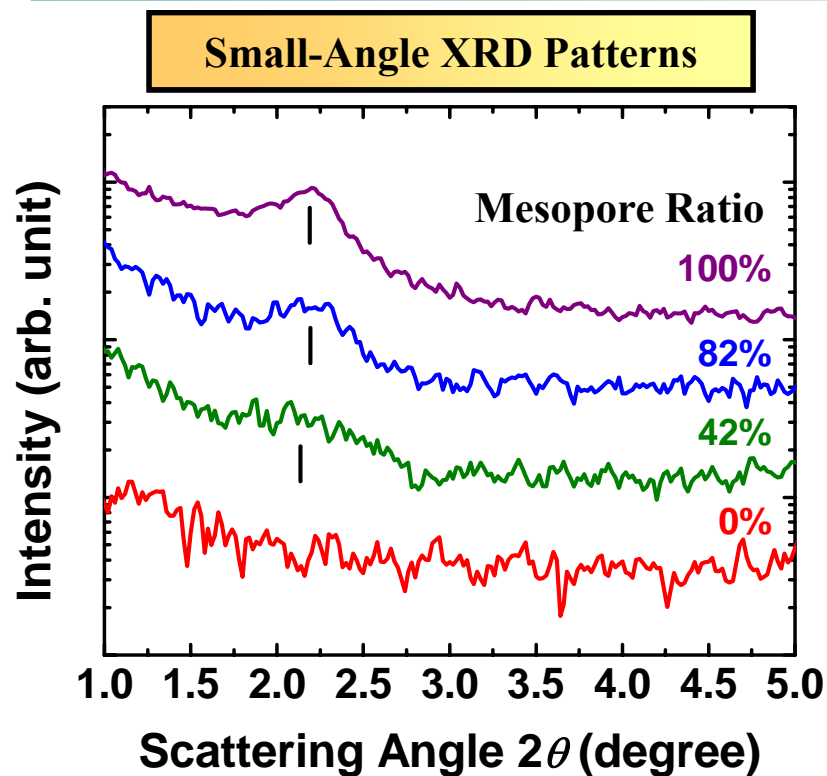


Mesopore ratio (mesoporous:
non-mesoporous tin phosphate) $\approx 1 : 3$



Control of Mesopore Ratio
(Surfactant/Precursor Ratio)

Characterization of Mesoporous Structures



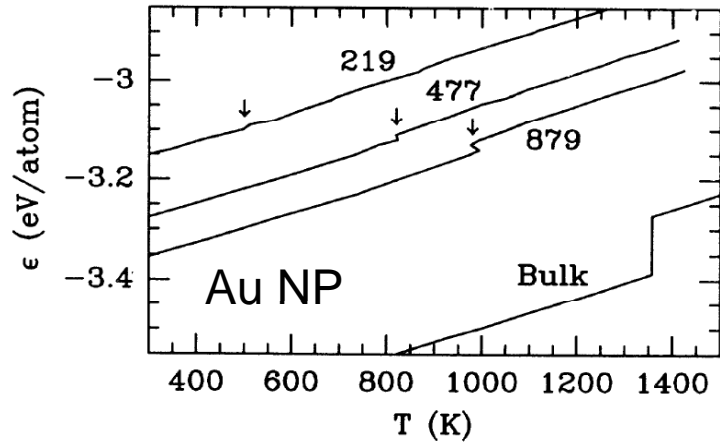
Precursor Molar Ratio	Mesopore d Spacing (nm)	Average Pore Size (nm)	BET Surface Area (m ² /g)	Relative Mesopore Ratio	Composition of Synthesized
0.11	—	—	15	0%	Sn _{1.94} P ₂ O _{7.3}
0.22	4.29 ± 1.21	2.56	114	42%	Sn _{2.30} P ₂ O _{7.5}
0.54	4.34 ± 0.68	2.32	167	82%	Sn _{2.61} P ₂ O _{7.8}
1.10	4.20 ± 0.63	2.33	221	100%	Sn _{2.77} P ₂ O _{8.1}

Tridymite FePO₄ in the Low Voltage Range

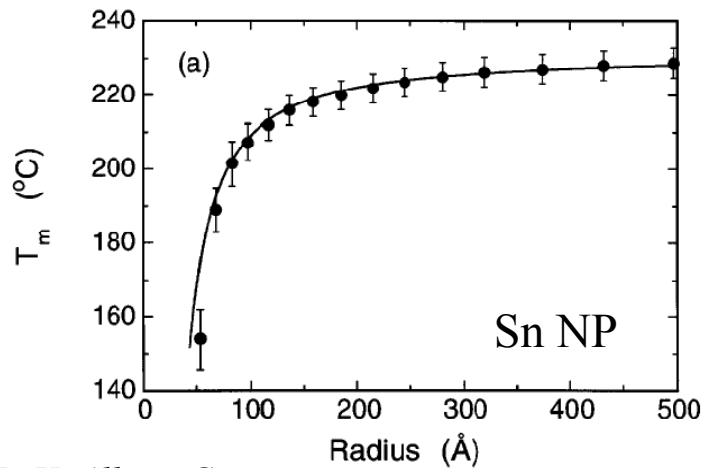
D. Son, E. Kim, T.-G. Kim, M. G. Kim, J. Cho, and B. Park
Appl. Phys. Lett. **85**, 5875 (2004).

T.-G. Kim, J.-G. Lee, D. Son, S. Jin, M. G. Kim, and B. Park
Electrochim. Acta **53**, 1843 (2007).

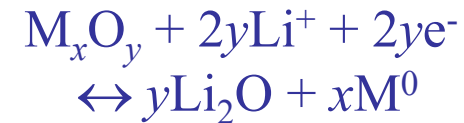
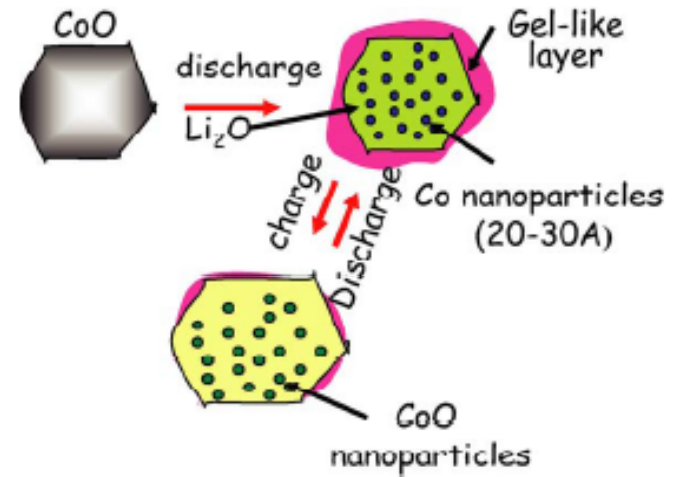
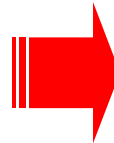
High Reactivity of Metallic Nanoparticles



F. Ercolessi et al.
IBM Zurich, Phys. Rev. Lett. (1991)



L. H. Allen's Group
UIUC, Phys. Rev. Lett. (1996)

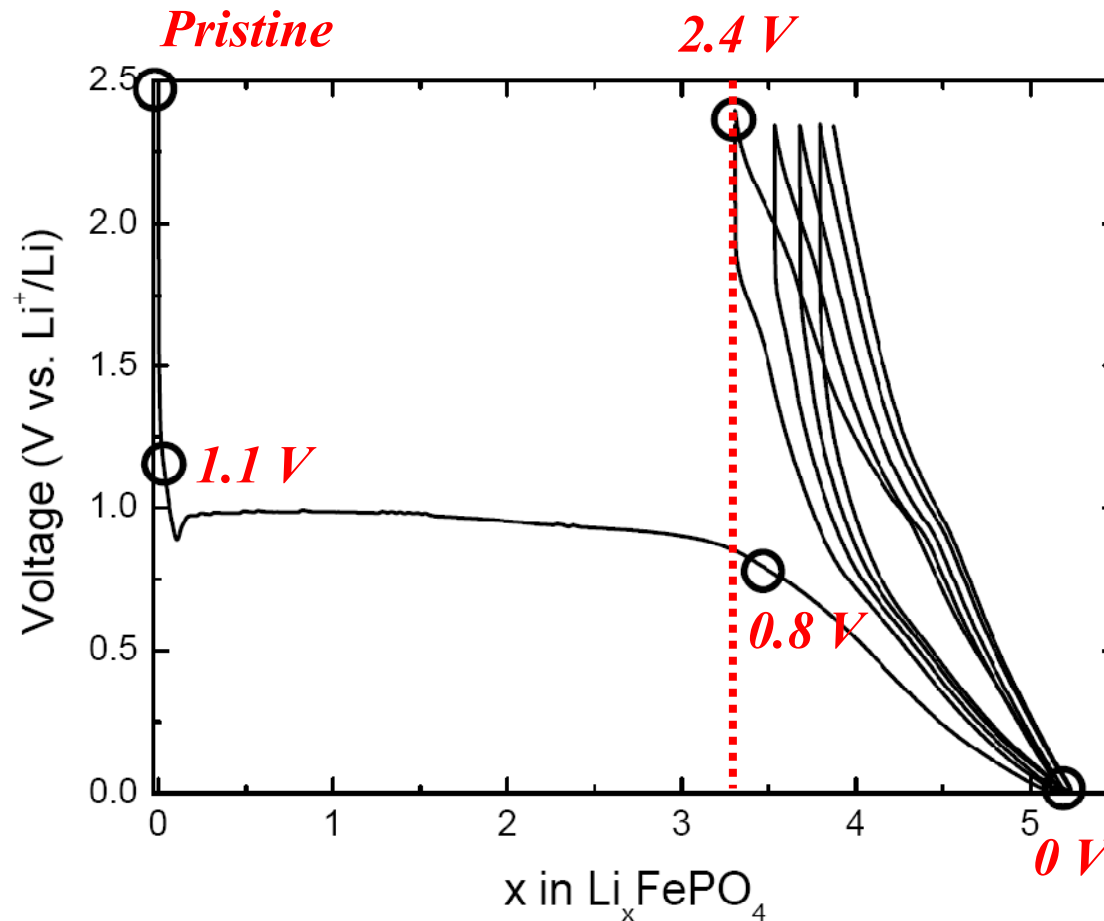


ex.) CoO, Cu_2O , FeO, NiO

J.-M. Tarascon's Group
U. Picardie Jules Verne, Nature (2000)

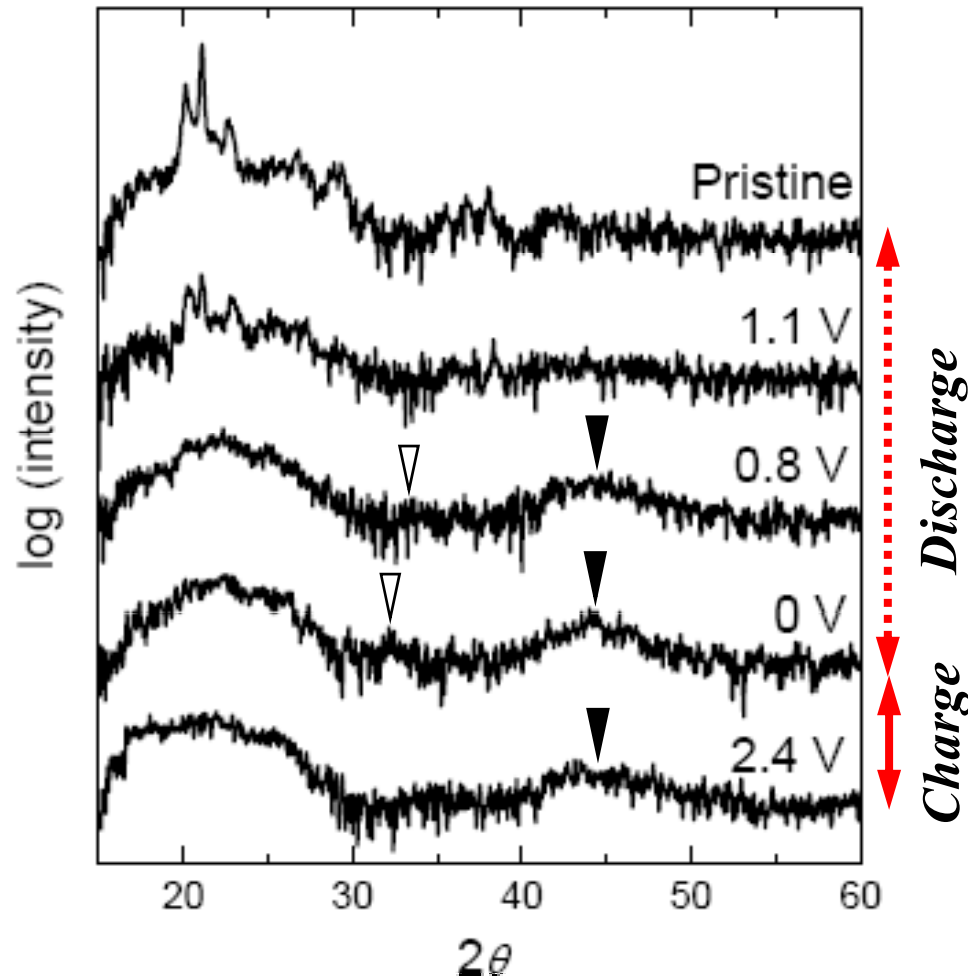
Nanoscale metallic nanoparticles show higher electrochemical reactivity than bulk

Electrochemical Reactivity of FePO_4 with Lithium



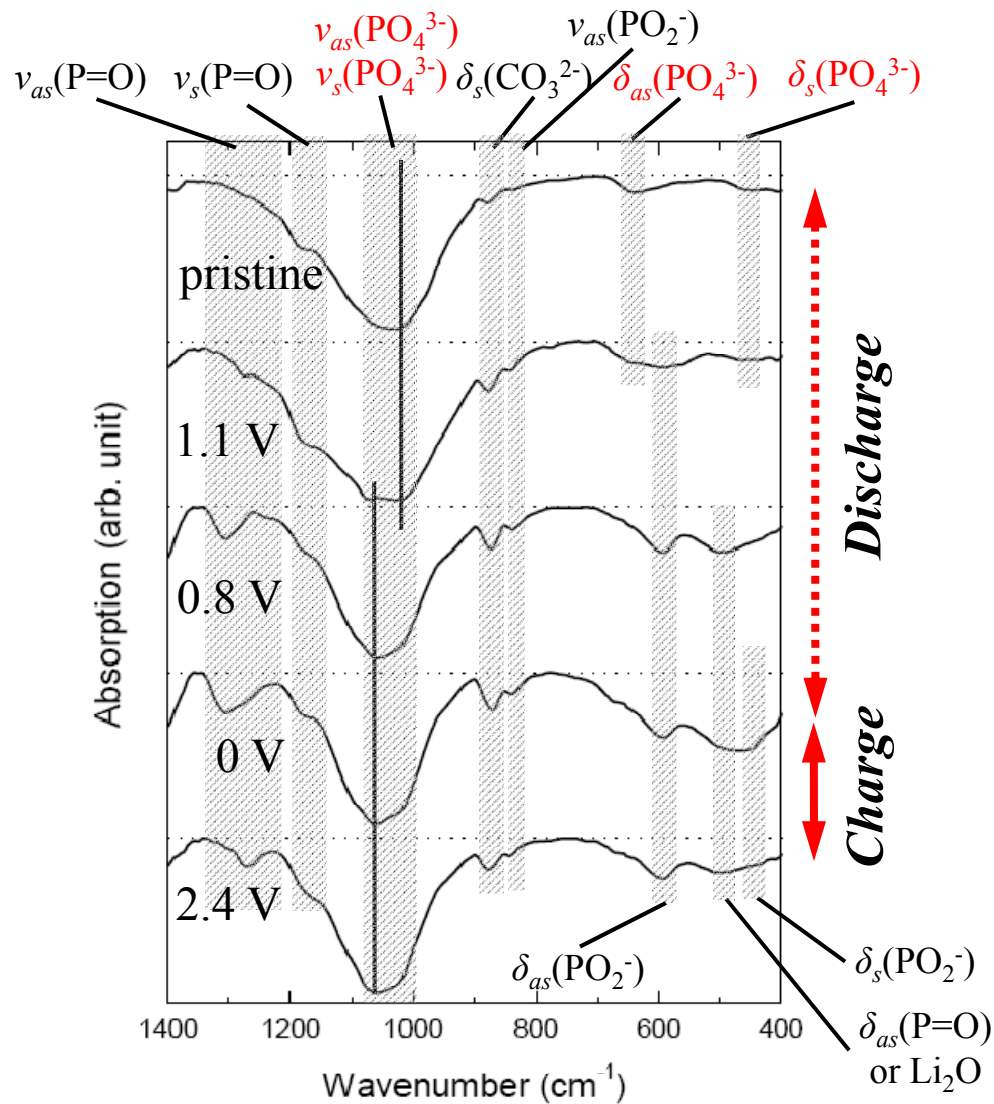
Investigation of Nanostructures with XAS, XRD, FT-IR, TEM, NMR, etc.
→ Revealing the reaction mechanisms of FePO_4 with Li

Phase Variation during Discharge and Charge



1. Amorphization during discharge
- not recovered during charge
2. ▼ : Fe metal (110) peak
- ~ 1 – 1.5 nm (*Scherrer eq.*)
- slight decrease
of intensity during charge
→ *Fe redox reaction*
3. ▽ : Li₂O (111) peak
- lower shift during discharge
- disappear after charge
→ *Li₂O redox reaction*

Structural Variation during Discharge and Charge

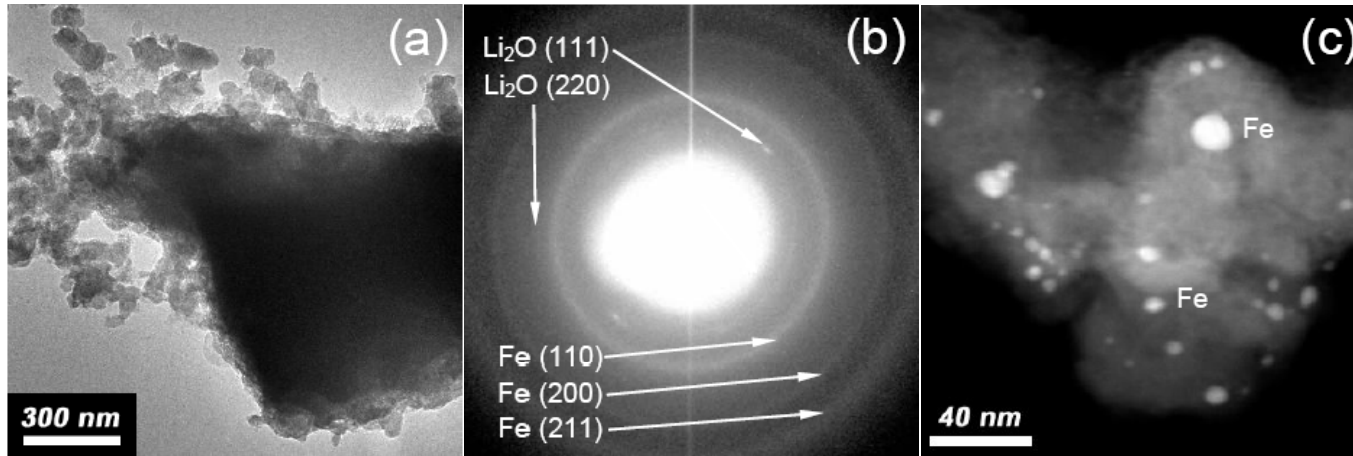


During discharge/charge process

- PO_4 structure is sustained
- Fe-O-P changes to Li-O-P (Li_3PO_4 is formed)
- P=O and PO_2^- (defective bonds) structures are formed
- Li_2O seems to be formed

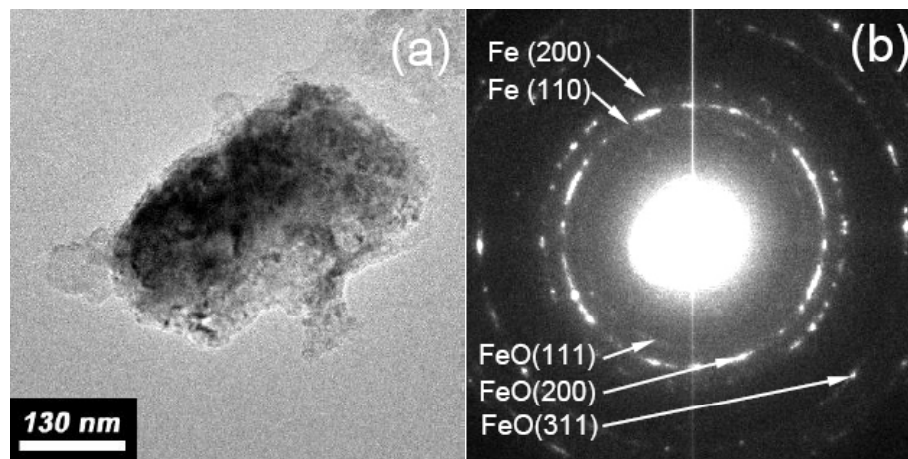
TEM Investigation (Fully Discharged/Charged Sample)

Fully Discharged Sample (0 V)



Fe nanoparticles
in Li_2O matrix

Fully Charged Sample (2.4 V)

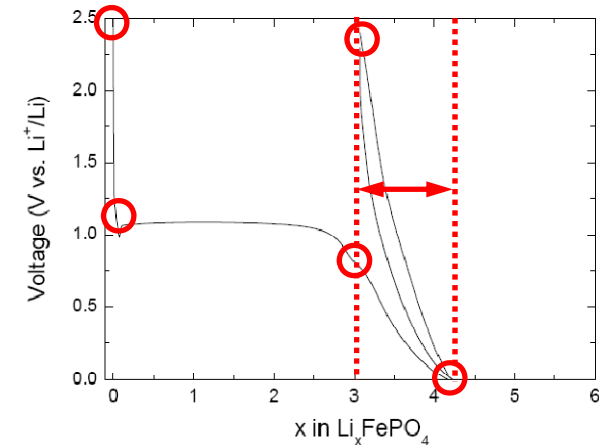
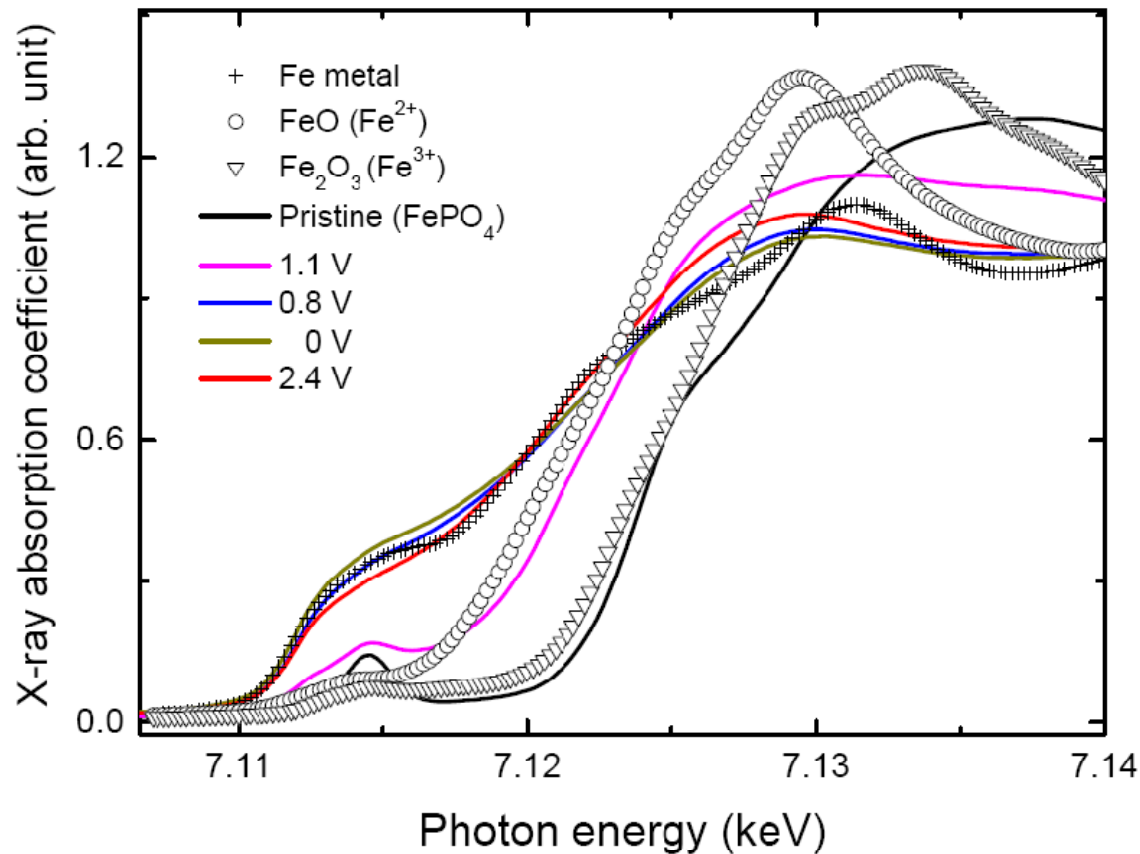


Coexistence of Fe and FeO

residual Fe:
Origin of small recovery

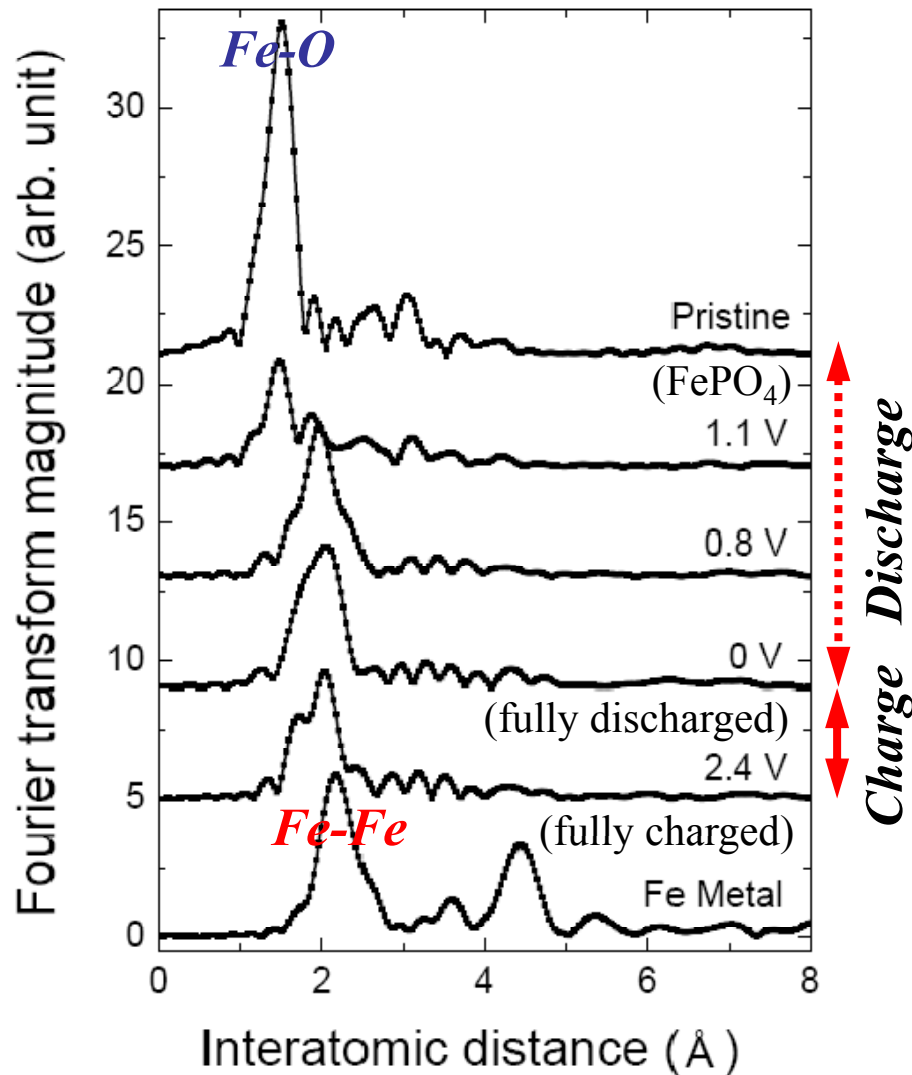
Valence Electron of Fe (XANES)

※ From the sample with very small reversible capacity



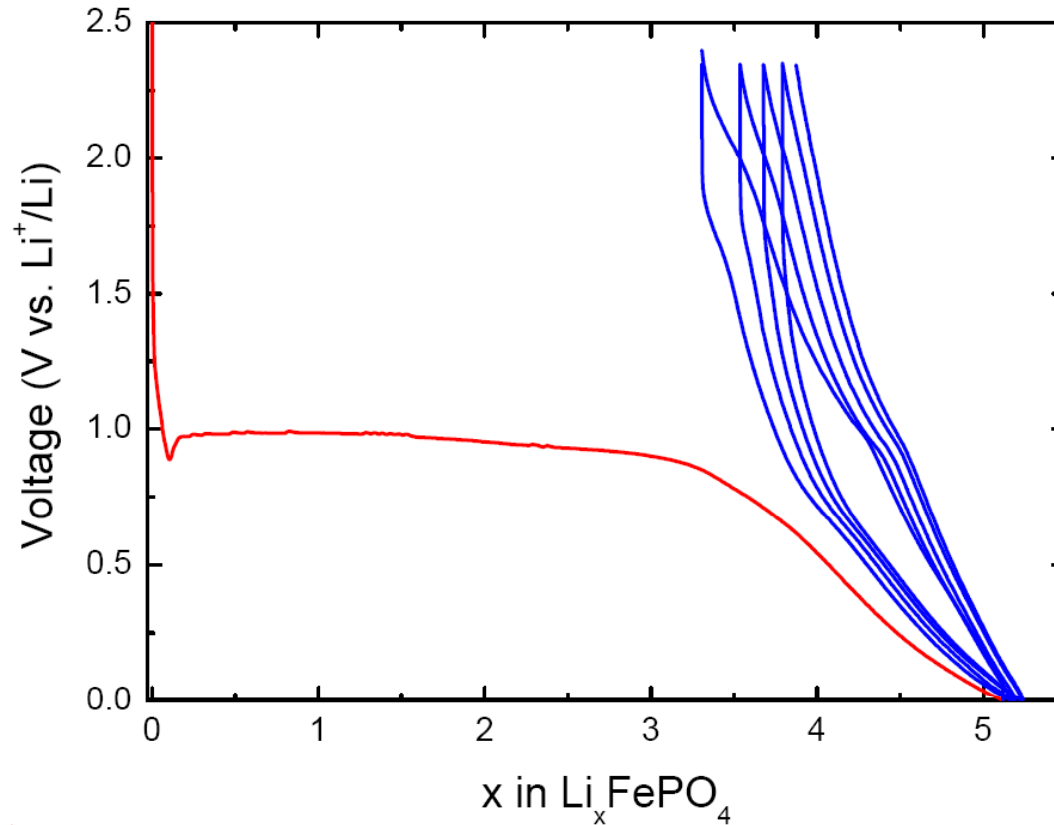
- Change of valence # of Fe
- FePO₄ is almost discharged at 0.8 V
- Small recovery of valence # of Fe

Radial Distribution Function for Fe (EXAFS)

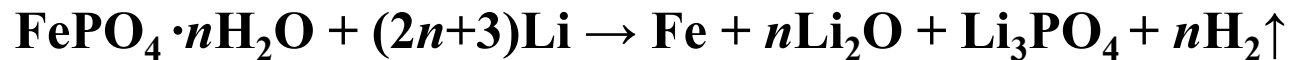


- **Pristine**: well defined Fe-O
($\text{FeO}_4\text{-PO}_4$ structure)
- **1.1 V** : poorly defined Fe-O
(LiFePO_4 structure)
- **0.8 V** : Fe-Fe (reduced Fe metal NP)
- **0 V** : Fe-Fe (reduced Fe metal NP)
- **2.4 V** : Fe-Fe and Fe-O mixed phase
(residual Fe metal NP and FeO or Fe_2O_3)

Suggested Mechanisms



❖ **1st discharge:**



❖ **Subsequent reversible reaction:**

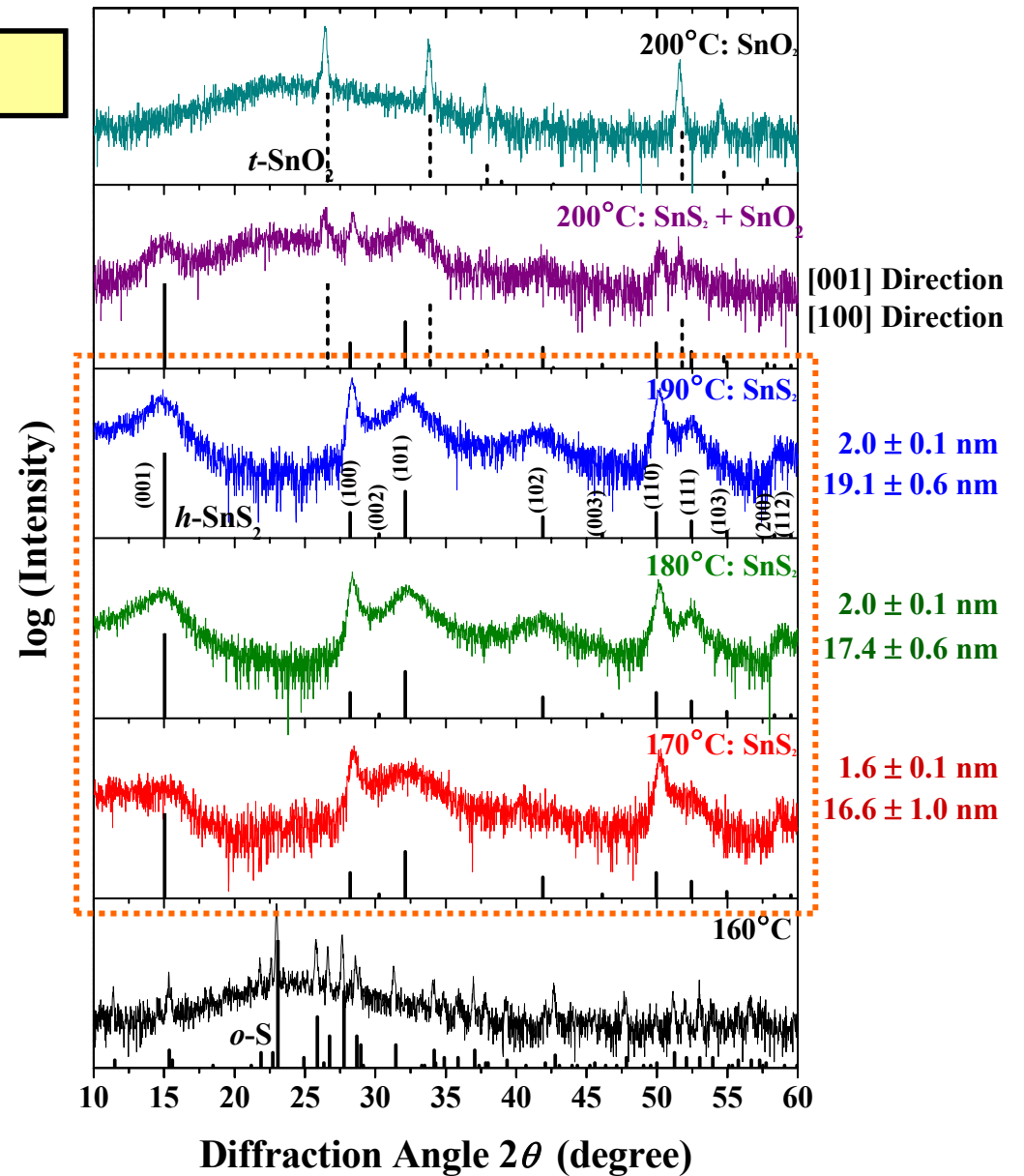
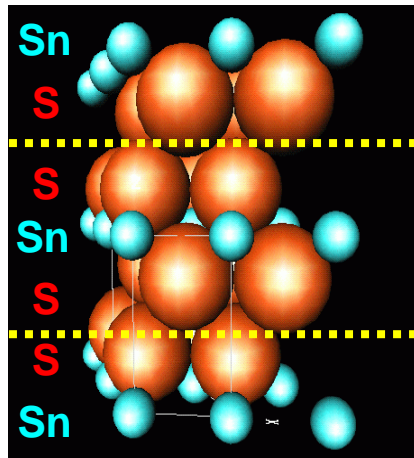
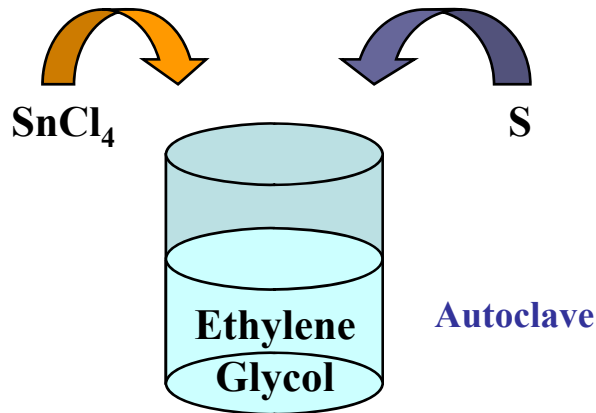


SnS₂ Nanosheet Anode Materials

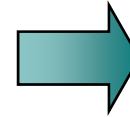
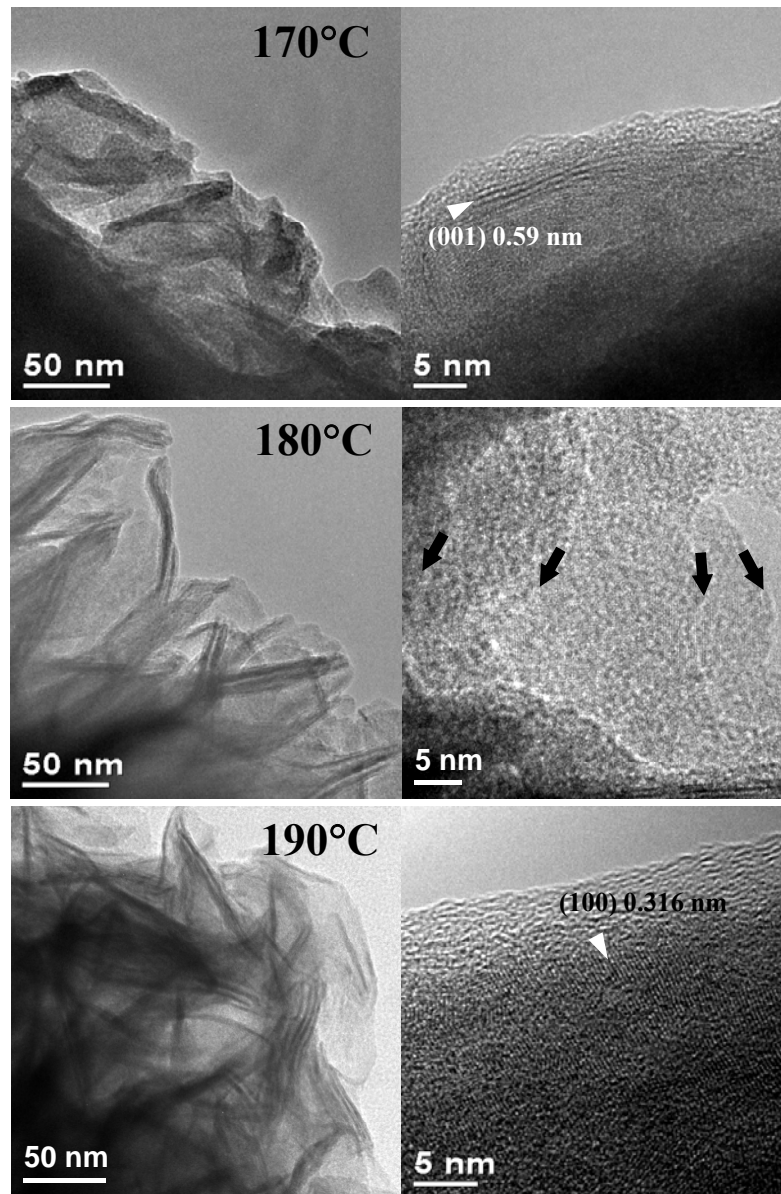
T.-J. Kim, C. Kim, D. Son, M. Choi, and B. Park
J. Power Sources **167**, 529 (2007).

Synthesis of SnS₂ Nanosheets

Synthesis of SnS₂ Nanosheets



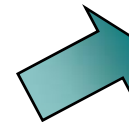
TEM Images of SnS₂ Nanosheets



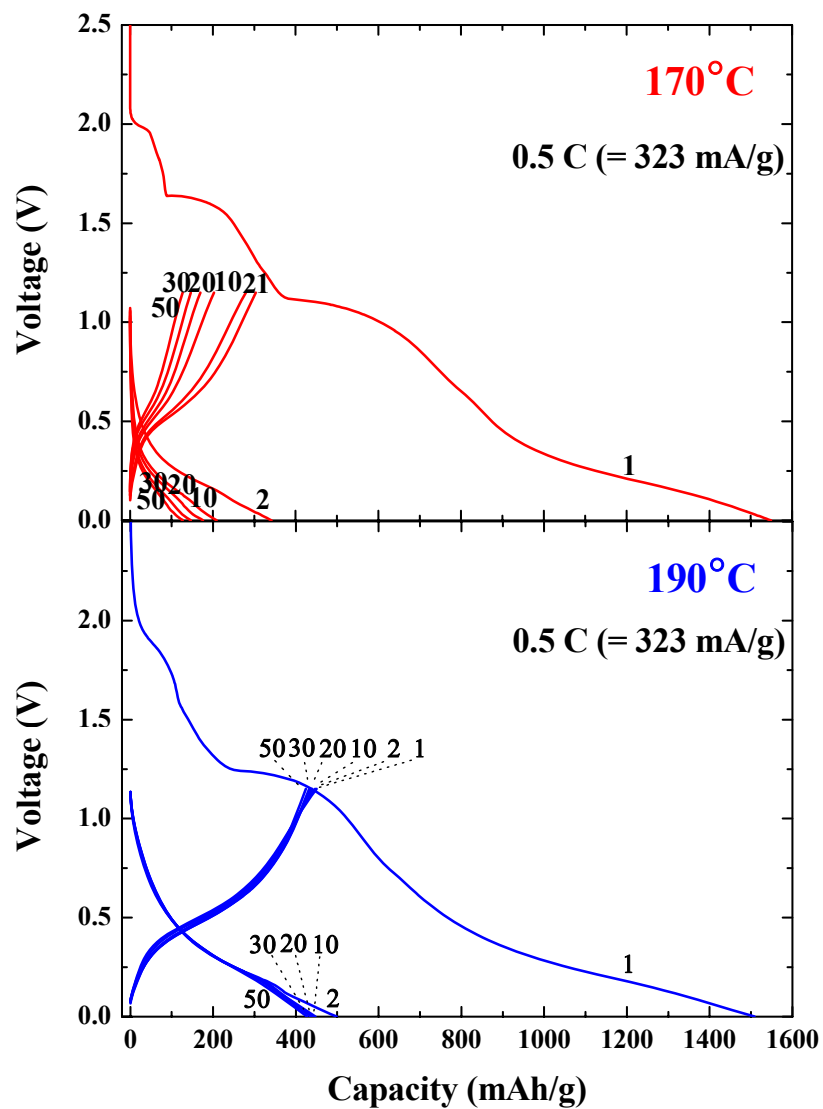
Short Stumpy Flakes



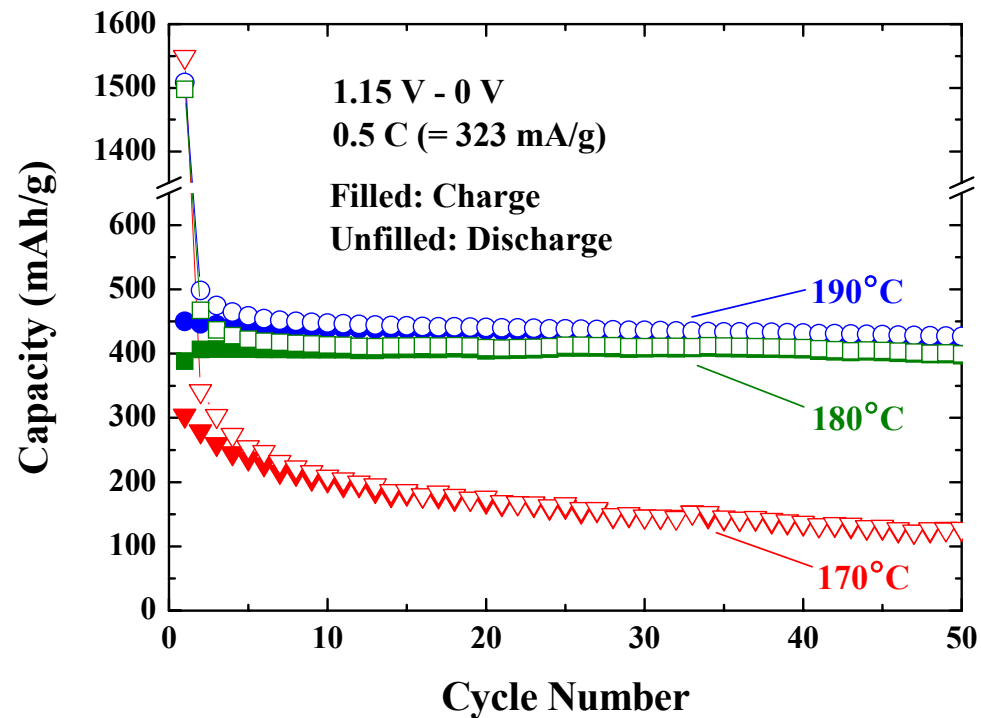
Long Layer-Rolled and Wiggled Sheets



Charge-Discharge Experiments

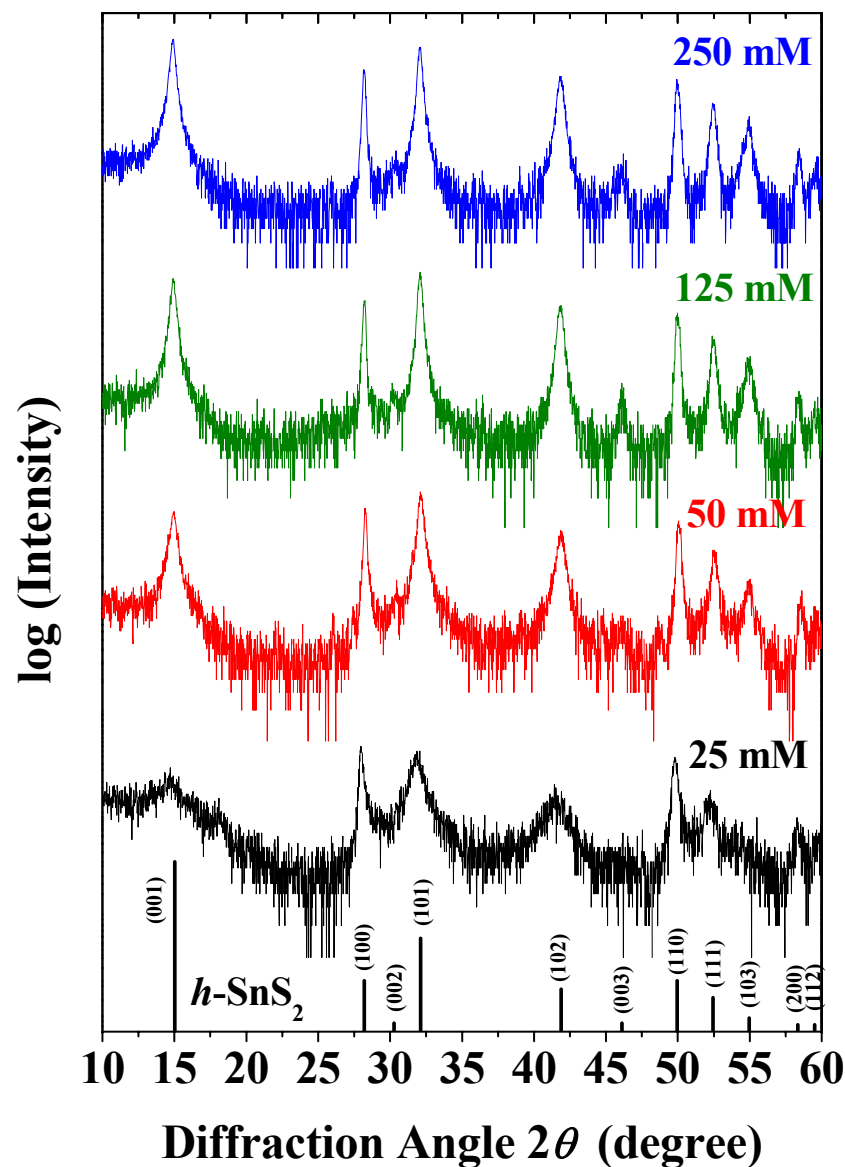


Electrochemical Cycling Test



SnS₂-nanosheet anodes synthesized at 180°C and 190°C exhibit excellent capacity retention.

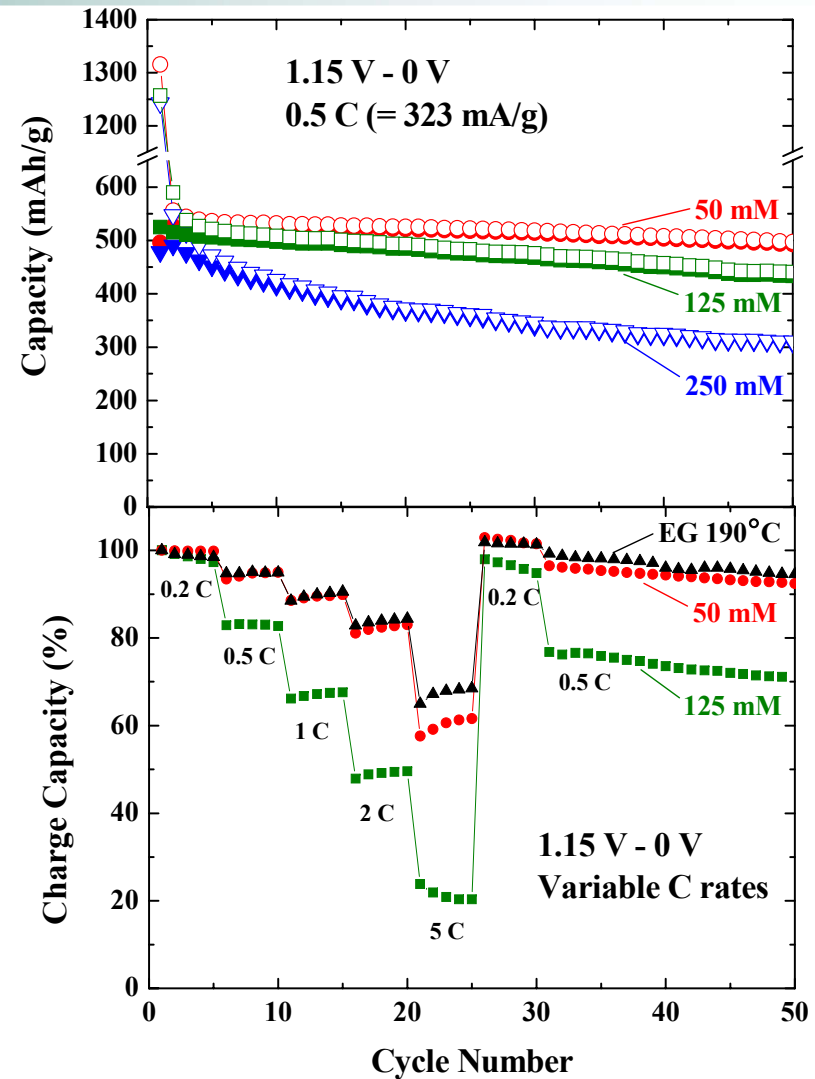
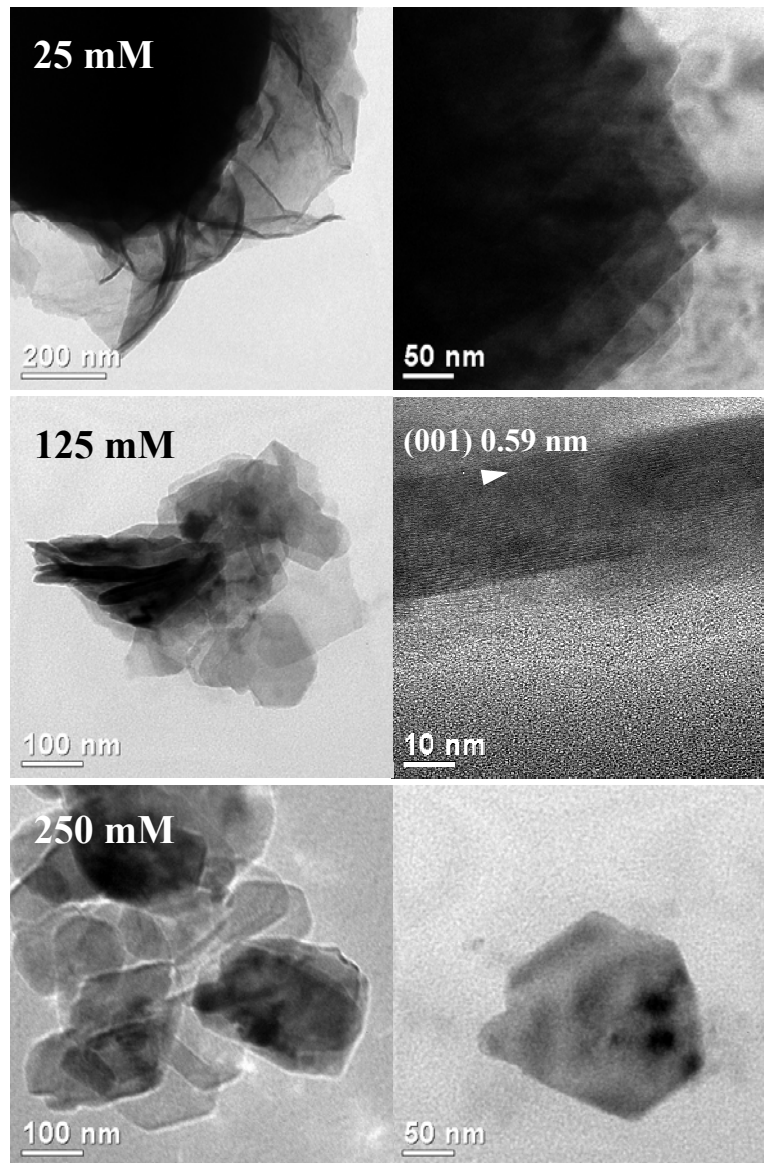
Size Variation of SnS₂ Nanosheets



Control of Source Concentration
 SnCl₂·2H₂O + thiourea (NH₂)₂CS

Synthesis Condition	[001] Direction	[100] Direction
25 mM	3.2 ± 0.5 nm	41.3 ± 4.3 nm
50 mM	10.4 ± 0.2 nm	42.5 ± 1.9 nm
125 mM	17.5 ± 0.3 nm	48.9 ± 2.2 nm
250 mM	25.6 ± 0.2 nm	70.4 ± 1.7 nm

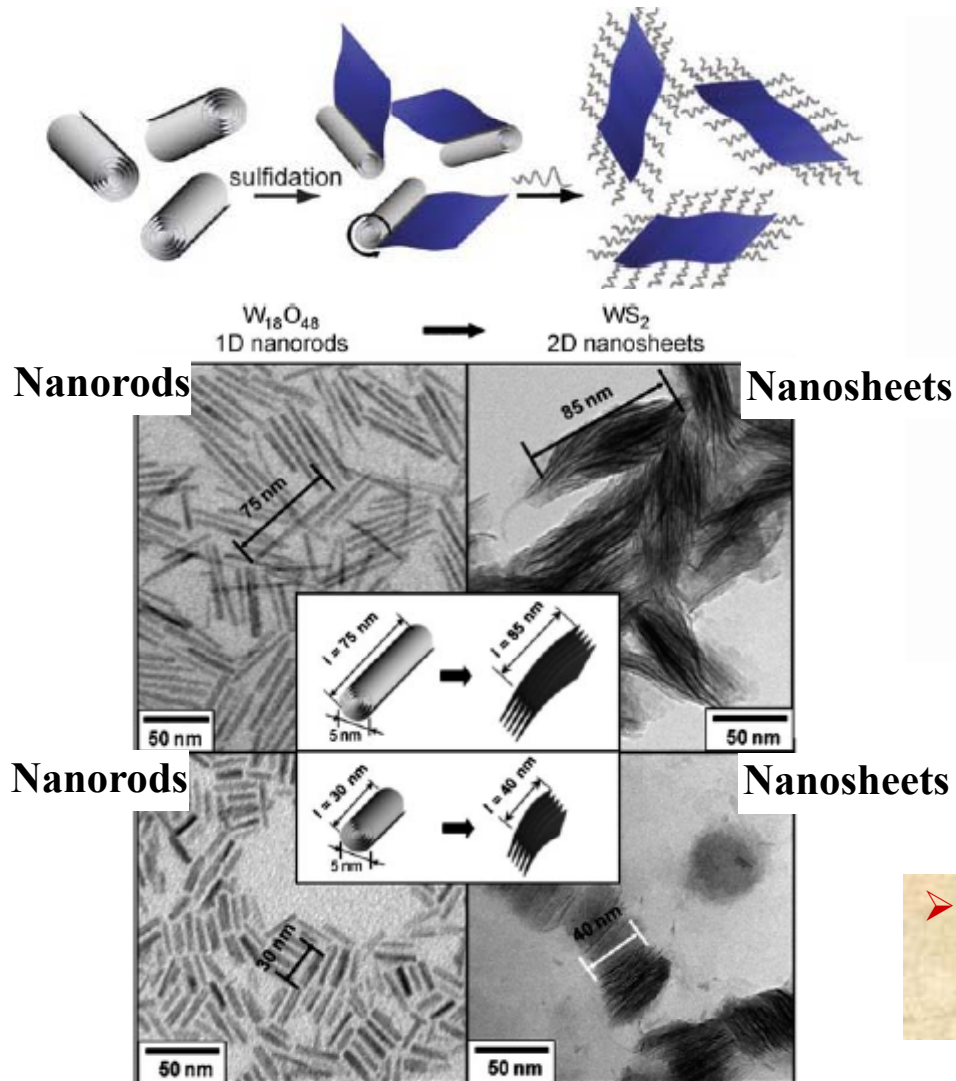
Size Variation of SnS₂ Nanosheets



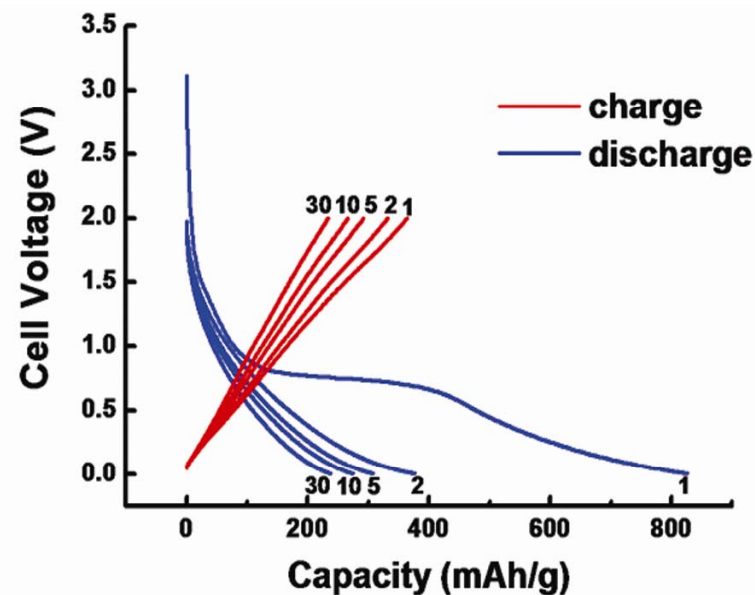
Nanosheets with a smaller thickness show improved electrochemical properties.

WS₂ Nanosheets

Synthesis by J. Cheon's Group



Electrochemical Tests

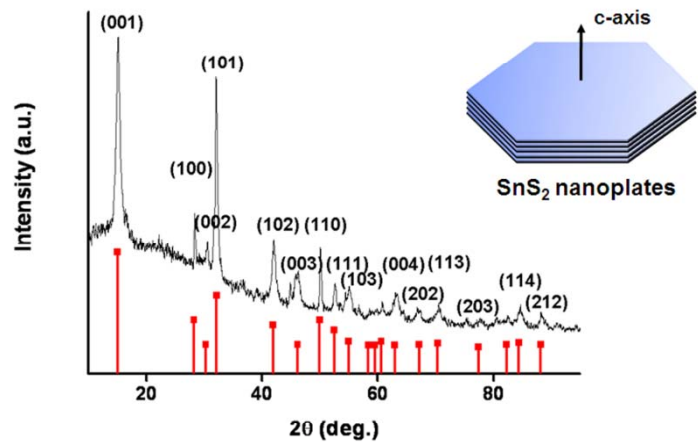
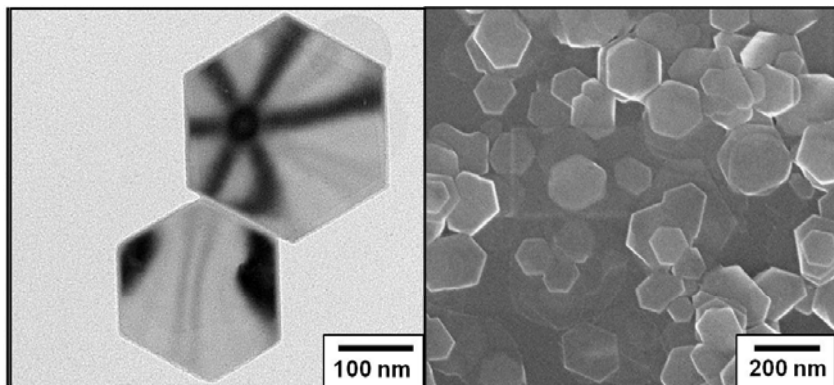


Various Nanostructures for High-Capacity Anode

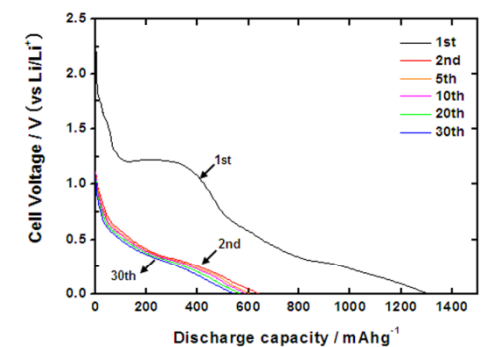
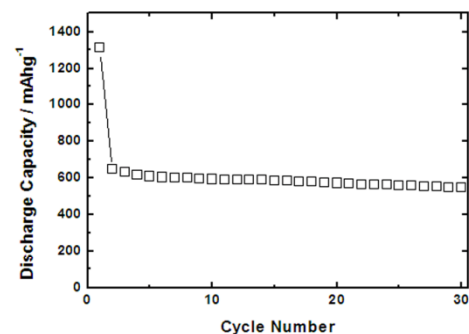
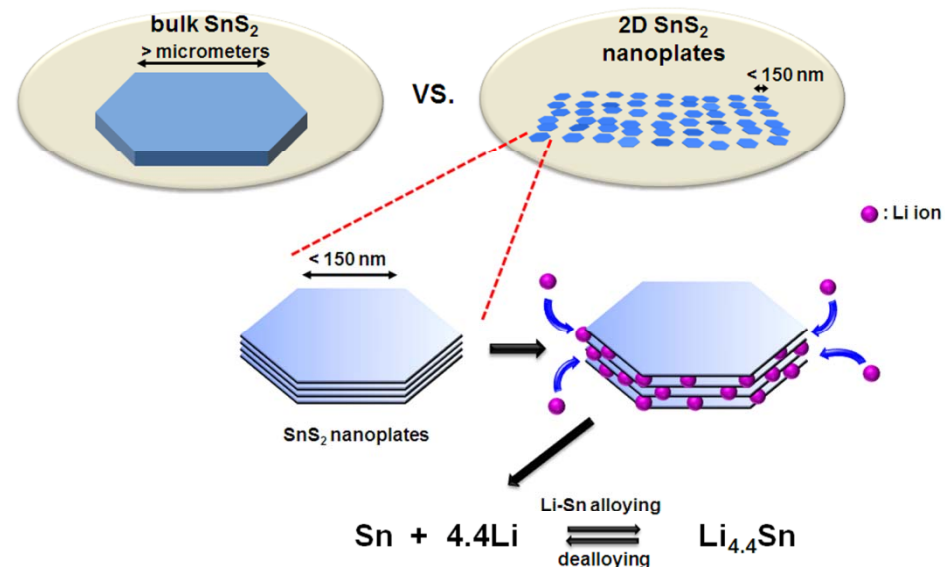
- J.-W. Seo, Y.-W. Jun, S.-W. Park, H. Nah, T. Moon, B. Park, J.-G. Kim, Y. J. Kim, and J. Cheon *Angew. Chem. Int. Ed.* **46**, 8828 (2007).

Two-Dimensional SnS₂ Nanoplates

Synthesis by J. Cheon's Group



Enhanced electrochemical properties by 2-D layered SnS₂ nanoplates.



➤ J.-W. Seo, J.-T. Jang, S.-W. Park, C. Kim, B. Park, and J. Cheon *Adv. Mater.* **20**, 4269 (2008).

Nanoscale Interface Control

- Compositions?
- Nanostructures?
- Mechanisms?

<http://bp.snu.ac.kr>

Your Goal for ~80 Years?



- 2009-11-24